

# Improving the Photo-Stability of Polymers Using Graphene

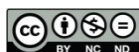
by

Samira KARIMI

MANUSCRIPT-BASED THESIS PRESENTED TO ÉCOLE DE  
TECHNOLOGIE SUPÉRIEURE IN PARTIAL FULFILLEMENT FOR THE  
DEGREE OF DOCTOR OF PHILOSOPHY  
PH.D.

MONTREAL, MARCH 13, 2024

ÉCOLE DE TECHNOLOGIE SUPÉRIEURE  
UNIVERSITÉ DU QUÉBEC



Samira Karimi, 2024



This Creative Commons licence allows readers to download this work and share it with others as long as the author is credited. The content of this work can't be modified in any way or used commercially.

**BOARD OF EXAMINERS (THESIS PH.D.)**  
**THIS THESIS HAS BEEN EVALUATED**  
**BY THE FOLLOWING BOARD OF EXAMINERS**

Mrs. Nicole R. Demarquette, Thesis Supervisor  
Department of Mechanical Engineering, École de Technologie Supérieure

Mr. Éric David, Thesis Co-supervisor  
Department of Mechanical Engineering, École de Technologie Supérieure

Mr. Sylvain G. Cloutier, President of the Board of Examiners  
Department of Electrical Engineering, École de Technologie Supérieure

Mr. Ricardo J. Zednik, Member of the jury  
Department of Mechanical Engineering, École de Technologie Supérieure

Mr. Ricardo JE. Andrade, External Evaluator  
Graphene and Nanomaterials Research Center - MackGraphe,  
Mackenzie Presbyterian University, Brazil

**THIS THESIS WAS PRESENTED AND DEFENDED**  
**IN THE PRESENCE OF A BOARD OF EXAMINERS AND PUBLIC**  
**ON MARCH 11, 2024**  
**AT ÉCOLE DE TECHNOLOGIE SUPÉRIEURE**



## ACKNOWLEDGMENT

I would like to express my deepest gratitude to those who have played a crucial role in the completion of this journey.

I am profoundly grateful to my PhD thesis directors, Prof. Nicole Demarquette and Prof. Eric David, for their unconditional support and invaluable insights throughout the entire research process. Their encouragement and guidance have been a crucial factor in my successful completion of this thesis.

I express my gratitude to the members of my thesis committee, Prof. Sylvain Cloutier and Prof. Ricardo Zednik from École de Technologie Supérieure, as well as Prof. Ricardo Andrade from Mackenzie Presbyterian University, for consenting to evaluate this work during the defense.

I extend my appreciation to the researchers, research staff, and technicians at École de Technologie Supérieure. I am specially thankful to Mazen Samara for his invaluable assistance in reviewing my articles. Additionally, I would like to express my gratitude to Nabil Mazeghrane, Mohammad Saadati, Radu Romanica, Simon Laflamme, and all the staff in the Mechanical Engineering Department for their consistent and practical support.

I would like to deeply thank the individuals at NanoXplore company, our esteemed industrial partner, with special appreciation for Nima Moghimian and Giovanna Gutiérrez. Their unwavering support and valuable insights have significantly contributed to the success of my PhD thesis.

I would like to give my special thanks to Emna Helal for her exceptional support and invaluable insights during my PhD journey. Her unconditional assistance has been instrumental in achieving this success.

I would like to thank my friends and colleagues whose unwavering support and encouragement have made this accomplishment possible.

Finally, I would like to express my deepest appreciation to my family, whose belief in my abilities has always been a constant source of strength. Their boundless love, encouragement, support, and sacrifices have always been behind my determination and successes.

# AMÉLIORATION DE LA PHOTO-STABILITÉ DES POLYMÈRES EN UTILISANT LE GRAPHÈNE

Samira KARIMI

## RESUME

Cette thèse visait à obtenir des polymères stabilisés aux UV en incorporant du graphène à quelques couches (FLG), à évaluer les mécanismes d'action dominants du FLG, et optimiser son rôle en tant que photo-stabilisateur. Les performances du FLG en tant que photo-stabilisateur et son effet sur les changements macro et microstructuraux des composites en polyéthylène haute densité (HDPE) survenant lors de la photo-dégradation, ont été étudiés.

Des composites HDPE contenant différentes concentrations de FLG (0, 0.1, 0.25 et 0.5 % en poids) ont été préparés par mélange à l'état fondu à l'aide d'une extrudeuse à double vis, suivie d'une exposition à l'irradiation UV-A pendant plusieurs durées. Les propriétés rhéologiques et mécaniques ont été évaluées en fonction du temps d'exposition aux UV. Pour déterminer les mécanismes de photo-stabilisation du FLG, un test contrôlé spécifique impliquant le processus d'exposition aux UV du mélange de peroxyde d'hydrogène ( $H_2O_2$ ) et des suspensions aqueuses de FLG a été réalisé. Ensuite, la quantité de radicaux libres créés a été mesurée à l'aide d'un test de résonance paramagnétique électronique (EPR). Enfin, l'effet de l'ajout de FLG sur la pénétration de la photo-dégradation dans le HDPE, et la corrélation entre la profondeur de la photo-dégradation à laquelle la chimie-cristallisation se produit, et l'allongement à la rupture, ont été étudiés à l'aide de la microscopie Raman.

Il a été constaté que l'ajout de seulement 0.25 % en poids de FLG dans le HDPE résultait en une résistance notable aux UV pendant une durée d'exposition de 672 heures, comme en témoigne la rétention soutenue des propriétés rhéologiques et mécaniques. De plus, il a été démontré que 57 % de la réduction observée des signaux EPR, indiquant la réduction de la quantité de radicaux libres créés, est due à l'absorption/réflexion des UV et 43 % à la capacité de piégeage des radicaux libres du FLG. Il a été démontré que les mécanismes d'absorption/réflexion des UV et de piégeage des radicaux libres sont dominants parmi les trois mécanismes de photo-stabilisation du FLG (absorption/réflexion des UV, piégeage des radicaux libres et barrière physique à l'oxygène).

Enfin, il a été constaté que la fragilisation se produisait dans le HDPE pur lorsque la profondeur de la photo-dégradation atteignait environ 10 % de l'épaisseur de l'échantillon. En revanche, les échantillons contenant 0,5 % en poids de FLG conservaient un comportement de rupture ductile, malgré une profondeur notable de 12,5 % de photo-dégradation à l'intérieur de l'échantillon et malgré la présence de fissures de surface. La persistance du comportement ductile a été attribuée à l'effet de photo-stabilisation du FLG, ainsi qu'à la tendance de la couche dégradée à se détacher du cœur ductile du composite. La capacité des composites contenant du FLG à maintenir la ductilité par le mécanisme de détachement a conduit à l'écart par rapport

## VIII

au principe de superposition observé dans le HDPE pur, entre l'épaisseur de l'échantillon, le temps d'exposition aux UV et les dommages UV.

**Mots-clés:** Photo-dégradation, Graphène, Photo-stabilisant, Barrière physique, Piégeur de radicaux, Absorption/réflexion des UV, Fragilisation, Ductilité, Chimie-cristallisation, Profondeur de la photo-dégradation



# IMPROVING THE PHOTO-STABILITY OF POLYMERS USING GRAPHENE

Samira KARIMI

## ABSTRACT

This thesis aimed at achieving UV-stabilized polymers, using the incorporation of few-layer graphene (FLG), and to evaluate the dominant action mechanisms of FLG, and optimize its role, as a photo-stabilizer. The FLG performance as a photo-stabilizer and its effect on both macro and microstructural changes of High-Density Polyethylene (HDPE) composites, occurring during photo-degradation, were investigated. HDPE composites containing different FLG concentrations (0, 0.1, 0.25, and 0.5 wt%) were prepared through melt mixing using a twin-screw extruder, followed by exposure to UV-A irradiation for several durations. Rheological and mechanical properties were evaluated as a function of UV exposure time. To determine FLG's photo-stabilizing mechanisms, a specific controlled test, involving the UV exposure process of the mixture of hydrogen peroxide ( $H_2O_2$ ) and the FLG aqueous suspensions, was conducted. Then, the amount of created free radicals was measured using an Electron Paramagnetic Resonance (EPR) test. Finally, the effect of the FLG addition on the penetration of photo-degradation within HDPE, and the correlation between photo-degradation depth at which chemi-crystallization occurs, and elongation at break, were investigated using Raman microscopy.

It was found that the addition of only 0.25 wt% FLG into HDPE showed a notable UV resistance for an exposure time of 672 hours, evident from sustained retention of rheological and mechanical properties.

Additionally, it was shown that 57% of the observed reduction in EPR signals, indicating the reduction in the amount of created free radicals, is due to UV absorption/reflection and 43% due to the free radical scavenging abilities of FLG. It is demonstrated that UV absorption/reflection and free radical scavenging mechanisms are the dominant ones among the three FLG photo-stabilizing mechanisms (UV absorption/reflection, free radical scavenging, and physical barrier to oxygen).

Finally, it was found that embrittlement occurred in neat HDPE when photo-degradation depth reached around 10 % of the sample thickness. Conversely, the samples containing 0.5 wt% FLG maintained a ductile failure behavior, despite a notable 12.5% depth of photo-degradation within the sample, and in the presence of surface cracks. The persistence of ductile behavior was attributed to the photo-stabilizing effect of FLG, as well as, to the tendency of the degraded layer to detach from the ductile core of the composite. The ability of the FLG-containing composites to maintain ductility through the detaching mechanism led to the deviation from the superposition principle observed in neat HDPE, between sample thickness, UV exposure time, and UV damage.

**Keywords:** Photo-degradation, Graphene, Photo-stabilizer, Physical barrier, Radical scavenger, UV absorption/ reflection, Embrittlement, Ductility, Chemi-crystallization, Photo-degradation depth

## TABLE OF CONTENTS

	Page
INTRODUCTION.....	1
01. Context of research.....	1
02. Objectives and research steps.....	2
03. Approach and methodology.....	3
04. Organization of thesis.....	4
<b>CHAPTER 1 THEORITICAL BACKGROUND</b>	<b>7</b>
1.1 Introduction.....	7
1.2 Photophysical and Photochemical reactions.....	8
1.3 Photo-degradation steps.....	9
1.4 Photo-degradation mechanism of HDPE.....	11
1.5 Chemi-crystallization during polymer photo-degradation.....	12
1.6 Embrittlement in HDPE.....	13
<b>CHAPTER 2 A REVIEW ON GRAPHENE'S LIGHT STABILIZING EFFECTS FOR REDUCED PHOTODEGRADATION OF POLYMERS</b>	<b>17</b>
2.1 Introduction.....	18
2.2 Physical and Chemical Aspects of Polymer Photodegradation.....	20
2.2.1 Introduction.....	20
2.2.2 How Does Light Affect Polymers?.....	21
2.2.2.1 Photodegradation.....	21
2.2.2.2 Photo-Oxidative Degradation.....	24
2.2.2.3 Mechanisms of Actions of Photostabilizers.....	25
2.3 Graphene.....	33
2.3.1 Types of Graphene.....	33
<b>2.3.2</b> Structure of Graphene.....	33
2.3.3 Graphene Derivatives.....	34
2.4 How Graphene Slows down Photodegradation in Polymers.....	35
2.4.1 UV absorbers and screeners.....	35
2.4.2 Radical scavengers.....	36
2.4.3 Quenchers.....	37
2.4.4 Physical barrier.....	38
2.4.5 Photodegradation reduction through changes in crystallinity, glass transition temperature (T <sub>g</sub> ), polymer mobility, and free volume upon the addition of graphene.....	39
2.5 Discussion.....	51
2.6 Conclusions.....	51

CHAPTER 3	PHOTO-STABILIZATION MECHANISMS OF HDPE BY A COMMERCIAL FEW-LAYER GRAPHENE	55
3.1	Introduction.....	56
3.2	Materials and Methods.....	58
3.2.1	Materials .....	58
3.2.2	Composites Preparation .....	59
3.2.3	Photo-degradation Process.....	59
3.2.4	Sample Preparation for EPR.....	60
3.3	Characterization .....	61
3.4	Results.....	63
3.4.1	Dispersion of FLG .....	63
3.4.2	Chemical Properties .....	63
3.4.3	Rheology .....	66
3.4.4	Surface Morphology .....	67
3.4.5	Mechanical Properties.....	68
3.4.6	Photo-stabilization Mechanism of FLG.....	70
3.5	Discussion.....	72
3.6	Conclusion .....	75
CHAPTER 4	Effect of Few-Layer Graphene (FLG) and Thickness on the Photo- Degradation Behavior of High-Density Polyethylene	77
4.1	Introduction.....	78
4.2	Materials and Methods.....	80
4.2.1	Materials .....	80
4.2.2	Composites Preparation .....	81
4.2.3	Photo-degradation Process.....	81
4.2.4	UV Dosage Calculation .....	82
4.2.5	Characterization .....	84
4.3	Results.....	86
4.3.1	Cross-Section Morphology .....	86
4.3.2	Surface Morphology .....	87
4.3.3	Mechanical Properties.....	89
4.3.4	Photo-Degradation Depth .....	95
4.3.5	Failure Zone based on "Normalized photodegradation depth", D/T .....	99
4.4	Discussion.....	100
4.5	Conclusion .....	104
CONCLUSION	.....	105
RECOMMENDATIONS.....	.....	109
LIST OF BIBLIOGRAPHICAL REFERENCES.....	.....	113

## LIST OF TABLES

	Page
Table 2.1	Intensity of sunlight absorption in different polymers.....23
Table 2.2	Common photostabilizers based on their chemical structure .....32
Table 2.3	Results obtained from photodegradation of polymer/graphene nanocomposites.....43
Table 3.1.	Physical Properties of HDPE.....58
Table 3.2.	Physical Properties of FLG from the supplier’s datasheet.....58
Table 3.3.	Photo-degradation procedure .....59
Table 3.4	Mechanical properties of HDPE, HDPE01, HDPE025, and HDPE05 before and after 672 hours of UV exposure.....70
Table 4.1	Physical Properties of HDPE .....80
Table 4.2	Physical Properties of FLG from product Technical Data Sheet (TDS) provided by NanoXplore Inc .....80
Table 4.3.	Effective UV dosage corresponding to different UV exposure times .....84
Table 4.4	The observed crack depth in HDPE and HDPE05.....89
Table 4.5.	Different zones in stress-strain curves of HDPE .....90
Table 4.6.	The calculated $t_{50}$ for neat HDPE and its composites.....93
Table 4.7.	photo-degradation depth and normalized photo-degradation depth values of neat HDPE and its composites. ....98



## LIST OF FIGURES

		Page
Figure 1.1	Solar spectrum at the top of the atmosphere and at sea level .....	8
Figure 1.2	(a) Potential energy diagram of a diatomic molecule: 1)absorption; 2)vibrational relaxation; 3)emission, (b) Photodissociation of a molecule .	9
Figure 1.3	Photo-degradation steps .....	10
Figure 1.4	Nurrish reactions .....	12
Figure 1.5	Schematic of UV-induced chemi-crystallization and cracking .....	13
Figure 1.6	Schematic of stress-strain curve of HDPE.....	14
Figure 1.7	Microstructural deformation during the tensile test: (a) lamellae orientation and interlamellar shear; (b) lamellae slip in the crystals; (c) initiation of lamellae fragmentation; (d) fibrillar state .....	15
Figure 2.1	General pathways of photodegradation and stabilization mechanisms .....	26
Figure 2.2	Example of UV absorbers .....	28
Figure 2.3	Mechanism of action of phenolic antioxidants .....	30
Figure 2.4	(a) Structure of graphene with pi orbitals, (b) sp <sup>2</sup> configuration in graphene .....	34
Figure 2.5	Radical adduct formation at the sp <sup>2</sup> carbon sites and H-donation from hydroxyl groups .....	37
Figure 2.6	Pathway of oxygen diffusion in neat polymer and graphene nanocomposite .....	39
Figure 3.1	Schematic of sample preparation for EPR .....	60
Figure 3.2	SEM image of HDPE05UV0 .....	63
Figure 3.3	(a) FTIR absorption spectra of HDPE with different exposure times, b) CI of HDPE and composites as a function of exposure time.....	65
Figure 3.4	Complex viscosity of (a) HDPE, (b) HDPE01, (c) HDPE025, (d) HDPE05 for different exposure times.....	67

Figure 3.5	SEM images of exposed surface of (a-b) HDPEUV672h, (c-d) HDPE01UV672h, and (e-f) HDPE05UV672h .....68
Figure 3.6	(a) Stress-strain curves of HDPE, HDPE01, HDPE025, and HDPE05, before and after 672h of exposure, (b) properties retention after 672h of exposure for HDPE, HDPE01, HDPE025, and HDPE05 .....69
Figure 3.7	(a)Uv-vis Spectroscopy of HDPE and the composites, (b) transmittance at 340nm as a function of graphene concentration .....71
Figure 3.8	EPR spectra.....72
Figure 3.9	Photo-oxidative degradation in polymers and different mechanisms of action of graphene.....74
Figure 4.1	Schematic of different sides of the samples.....85
Figure 4.2.	FLG dispersion across the cross-section of HDPE05 .....87
Figure 4.3.	SEM images of the exposed surfaces of neat HDPE and HDPE05 with sample thicknesses of 2 and 3 mm.....88
Figure 4.4.	SEM images of the side surfaces of neat HDPE and HDPE05 with sample thicknesses of 2 and 3mm.....89
Figure 4.5.	Stress-strain curves of neat HDPE with a thickness of: a) 3 mm and b) 2 mm and HDPE05 with a thickness of: c) 3 mm and d) 2 mm with different UV exposure times .....91
Figure 4.6	Retention of elongation at break of neat HDPE, HDPE01, and HDPE05 with thicknesses of 3 and 2 mm as a function of exposure time and corresponding "effective UV dosage" .....92
Figure 4.7.	Retention of elongation at break of neat HDPE, and HDPE05 as a function of UV dosage per sample volume. The arrows indicate the deviation from the superposition principle. ....94
Figure 4.8.	Raman spectrum of neat HDPE exposed surface with different UV exposure times .....95
Figure 4.9.	Schematic of chemi-crystallization evolution with UV exposure time .....96
Figure 4.10.	Crystal band intensity of: a-b) neat HDPE, c-d) HDPE05, with thicknesses of 3 and 2 mm as a function of sample depth, for different UV exposure times.....97



Figure 4.11. Failure behavior of neat HDPE and its composites as a function of UV dosage and normalized photo-degradation depth. The green color represents ductile behavior (Zone III and IV), and the red color indicates brittle behavior (Zone I and II). .....100



## LIST OF ABBREVIATIONS

CA	Cellulose acetate
Ch	Chromophore group
DI	Deionized water
DMPO	5,5-Dimethyl-1-pyrroline N-oxide
DSC	Differential scanning calorimetry
EPR	Electron paramagnetic resonance
FESEM	Field emission scanning electron microscope
FLG	Few layers graphene
FTIR-ATR	Fourier transform infrared spectroscopy – Attenuated total reflectance
GO	Graphene oxide
GPC	Gel permeation chromatography
HALS	Hindered amine light stabilizer
HCl	Hydrogen chloride
HDPE	High density polyethylene
MEH-PPV	Poly(2-methoxy-5-(2-ethylhexyloxy)-1,4-phenylenevinylene)
OM	Optical microscopy
PAH	Polycyclic aromatic hydrocarbons
PP	Polypropylene
PS	Polystyrene
PU	Polyurethane
PVA	Poly vinyl alcohol
PVC	Poly vinyl chloride
rGO	Reduced graphene oxide
SEM	Scanning electron microscopy
TPU	Thermoplastic polyurethane



## LIST OF SYMBOLS

$A$	Absorbance spectrum of the material
$E_0$	UV irradiance
$\lambda$	UV wavelength
$\Gamma$	Spectral distribution
$\phi$	Quasi-quantum yield function
$\delta(\lambda)$	Dirac function
$\tau$	Time
$D_{\text{eff}}$	Effective UV dosage
$Q$	Quencher
$T_g$	Glass transition temperature
$RH$	Polymer chain
$R^\circ$	Alkyl radical
$ROOH$	Hydroperoxide
$ROO^\circ$	Peroxy radicals
$COOH$	Carboxylic acid
$OH$	Hydroxyl
$^\circ OH$	Hydroxyl radical
$H_2O_2$	Hydrogen peroxide
$HO_2^\circ$	Hydroperoxy radical
$TiO_2$	Titanium dioxide
$ZnO$	Zinc oxide
$Fe_2O_3$	Iron(III) oxide
$Cr_2O_3$	Chromium(III) oxide
$CI$	Carbonyl index
$\pi$	Pi bond
$s, p_x, p_y$	Sigma bonds
$A_i$	FTIR peak areas of i group



## INTRODUCTION

### 01. Context of research

Polymers find extensive application across various industries due to their inherent properties. However, their vulnerability to sunlight poses a significant concern, leading to photo-degradation upon exposure to sunlight and UV irradiation. This degradation causes irreversible alterations in polymer properties, ultimately resulting in product failure (Claudé et al. 2001; Yousif and Haddad 2013a; Rånby 1989; Geuskens 1975). Consequently, there's a critical need to enhance polymers' stability against UV and sunlight. To achieve this, additives known as photo-stabilizers are commonly incorporated into polymer matrices (Wiles and Carlsson 1980). These stabilizers can be categorized into three primary groups based on their mechanisms of action: UV absorbers/reflectors (Strobel and Catino 1962; Padrón 1989; Kockler et al. 2014), free radical scavengers (Allen et al. 2004), and fillers/nucleating agents (Yousif and Haddad 2013a). However, use of the traditional photo-stabilizers is associated with challenges, including compatibility issues with polymers, migration concerns (Allen et al. 2004; Nikafshar et al. 2017), toxicity and health related problems (Tipton and Lewis 2008; Chaudhuri et al. 2018; Alotaibi et al. 2015c), and a decline in effectiveness over time (Asimakopoulos et al. 2013).

Recently, graphene, a two-dimensional carbon-based material, has emerged as a promising alternative to conventional photo-stabilizers (de Oliveira et al. 2019; Tayouri et al. 2022; Mistretta et al. 2019; Amrollahi et al. 2019; Uran, Alhani, and Silva 2017; Goodwin Jr, Shen, et al. 2020). Notably, graphene presents a more sustainable and safer option compared to traditional photo-stabilizers (Moghimian and Nazarpour 2020). Additionally, the presence of  $\pi$  bonds in graphene structure, enables it to function both as an electron acceptor and donor, serving as a potential free radical scavenger. Moreover, graphene's capability to absorb UV light through  $\pi \rightarrow \pi^*$  transitions and its 2D structure act as a physical barrier, impeding the diffusion of low molecular weight substances, like oxygen, into the polymer, all which prevent polymer photo-degradation (Dash, Pattanaik, and Behera 2014; Johra, Lee, and Jung 2014;

Yoo et al. 2014; Cui, Kundalwal, and Kumar 2016; Qu et al. 2014). Furthermore, graphene derivatives (Graphene Oxide (GO), reduced Graphene Oxide (rGO)) have also been used as a photo-stabilizer in different polymers, and their mechanism of action, are poorly understood. More insight into its photo-stabilization mechanism of graphene and its derivatives is essential to optimize its use. In addition, the performance of graphene as a photo-stabilizer depends on different factors including product thickness, graphene concentration, and UV exposure time, all of which influence the extent of degradation in a given sample. These issues also deserve to be fully understood.

It is well known that photo-degradation in polymers induces microstructural changes, including alterations in molecular weight and crystallinity (Rabello and White 1997a; Fayolle et al. 2007; Deshoulles et al. 2021), which vary in depth within the sample (Shyichuk et al. 2005). These changes directly impact macroscopic properties and eventual product failure. Notably, the depth of photo-degradation within a sample and the portion affected by UV exposure contribute to product failure. However, there exists limited data on the depth of photo-degradation in composites containing graphene and the correlation between microstructural changes and macro properties, necessitating further investigation.

As a conclusion, graphene presents a promising avenue for enhancing polymer stability against UV-induced degradation. However, a comprehensive understanding of its photo-stabilizing mechanisms and its interplay with microstructural alterations and macro properties is imperative for maximizing its potential in safeguarding polymers against UV-induced deterioration.

## **02. Objectives and research steps**

The primary objective of this work was to enhance the UV-stability of High Density Polyethylene (HDPE) using the addition of a commercial 6-10 layers graphene (FLG), and to assess its dominant action mechanism, and optimize its role, as a photo-stabilizer.



To achieve this goal, in a first step, the efficiency of FLG to photo-stabilize High Density Polyethylene (HDPE) was investigated through a comprehensive analysis of chemical, rheological, and mechanical properties of HDPE composites as a function of UV exposure time. Then the mechanism behind FLG's photo-stabilizing effect was investigated and the contribution of different FLG's photo-stabilizing mechanisms, specifically, UV absorption capacity and free radical scavenging ability was separated. The results of these studies are presented in Chapter 3 of the thesis and were published in *Polymer Engineering and Science* journal.

In addition, this study aimed at optimizing FLG role as a photo-stabilizer, and to find out the FLG impact on photo-degradation depth within HDPE and its correlation with macroscopic properties alteration, particularly mechanical properties, during photo-degradation. The results of this part are reported in Chapter 4 of the thesis, and in the manuscript submitted to *Polymer Degradation and Stability* journal.

### **03. Approach and methodology**

This PhD project, based on the above-mentioned objectives, is divided in two main parts.

In the first step, HDPE composites with different FLG concentrations (0, 0.1, 0.25, and 0.5 wt%) were prepared through melt mixing using a twin-screw extruder. To analyse the performance of FLG, as a photo-stabilizer, the change in chemical, rheological, and mechanical properties of the prepared composites, after exposure to different UV exposure times, were evaluated.

Once photo-stabilization achieved by incorporating FLG into HDPE, the contributions of UV absorption/reflection and free radical scavenging to the FLG photo-stabilizing effect were separated through a specific controlled test. Electron Paramagnetic Resonance (EPR) was conducted on UV exposed hydrogen peroxide ( $H_2O_2$ ) solutions with and without FLG, to

measure the amount of created free radicals. This test enabled us to quantify the contribution of UV absorption/reflection and free radical scavenging mechanism separately.

To optimize FLG use as a photo-stabilizer, it is required to understand the failure behavior (transition from ductile to brittle behavior) of the samples. It can be said that the failure is a function of degradation depth. To relate the failure behavior to photo-degradation depth, in the last step, the impact of FLG addition on the penetration (depth) of photodegradation into HDPE was investigated. For that, neat HDPE and two corresponding composites containing 0.1 and 0.5 wt% FLG, with two different thicknesses, 3 and 2 mm, were exposed to UV irradiation for several exposure times. The elongation at break was assessed as a function of UV exposure time and correlated to the photo-degradation depth at which chemi-crystallization occurs, using Raman microscopy.

#### **04. Organization of thesis**

This thesis is organized in four main chapters. Following this introduction, Chapter 1: theoretical background of photo-degradation in HDPE is reviewed.

Chapter 2 includes the published review paper in *crystal* journal. This chapter explains the concepts of polymer photo-degradation, and describes different types of photo-stabilizers, based on their action mechanisms. Also, the possible photo-stabilizing mechanisms of graphene are discussed in details.

In Chapter 3, the paper entitled " Photo-Stabilization Mechanisms of HDPE by a Commercial Few-Layer Graphene", published in *Polymer Engineering and Science* journal, is presented. This paper focuses on the first part of the project, which studies the performance of FLG as a photo-stabilizer and the main mechanism behind its photo-stabilizing effect.

Chapter 4 includes the paper entitled " Effect of Few-Layer Graphene (FLG) and Thickness on the Photo-Degradation Behavior of High-Density Polyethylene" submitted to *Polymer*

*Degradation and Stability* journal. This paper presents the last step of this project which aims at investigating the effect of FLG addition on photo-degradation depth within HDPE and relate microstructural alternation to macro properties changes and failure behavior after UV exposure.

In the conclusion chapter, the conclusions of the whole project are presented. This chapter highlights the research discoveries and limitations and provide suggestions for future works.



## CHAPTER 1

### THEORITICAL BACKGROUND

High-Density Polyethylene (HDPE), a versatile thermoplastic polymer, is one of the most widely used polymers in numerous applications thanks to its exceptional properties and ease of processing. A high degree of crystallinity, due to its simple chemical structure, makes it resistant to moisture and chemicals. Furthermore, HDPE finds various applications in packaging, as well as construction, due to its flexibility, excellent electrical insulation properties, and low cost.

Despite its widespread applications, HDPE's poor resistance against sunlight and UV irradiation remains a notable challenge. It is well known that when HDPE is used in outdoor applications and subjected to UV exposure, it undergoes photo-degradation, resulting in molecular structural changes, reduced mechanical properties, embrittlement, discoloration, and product failure. Consequently, while HDPE remains a preferred choice for various applications, its poor resistance to sunlight emphasizes the importance of incorporating photo-stabilizers to mitigate degradation and prolong its lifetime in outdoor applications.

In this chapter, theoretical backgrounds on photo-degradation concepts, HDPE photo-degradation mechanisms, chemi-crystallization, and embrittlement in HDPE are reviewed.

#### 1.1 Introduction

Polymers undergo photo-degradation during prolonged exposure to solar radiation, regardless of their inherent resistance. The solar spectrum ranges from 200 nm to 2500 nm, with 50% of the energy in the visible range, 40% in the infrared, and 10% in the ultraviolet. The Ozone atmosphere filters out radiation below 295 nm, which corresponds to UV-C, so sunlight reaching Earth follows a specific spectrum, as shown in Figure 1.1. The solar ultraviolet, ranging from 400 to 280 nm, UV-A and UV-B, comprises only about 6% of total solar radiation but is the main cause of degradation in polymers (Wu et al. 2011).

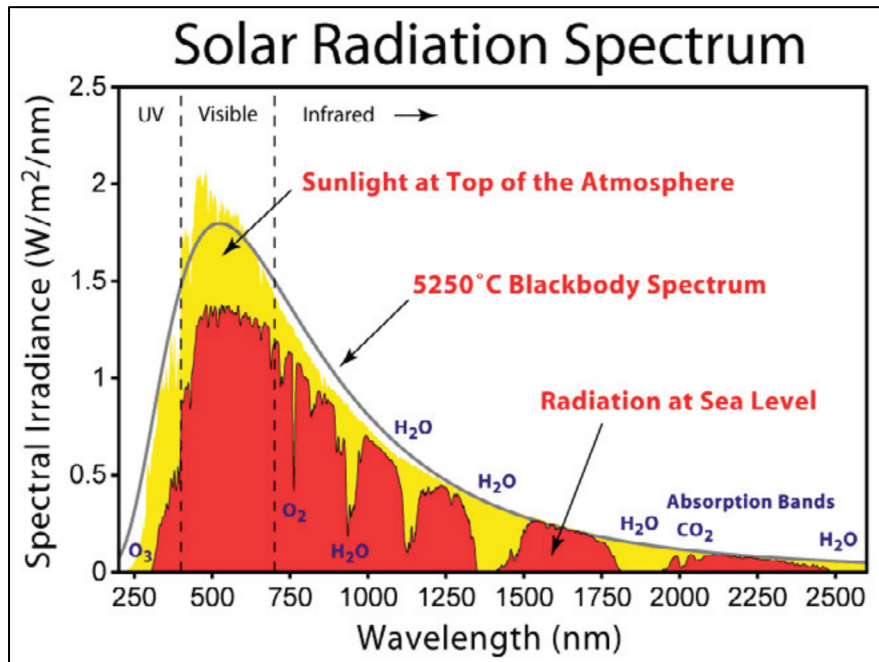


Figure 1.1 Solar spectrum at the top of the atmosphere and at sea level

Taken from Wu et al. (2011, p.528)

Exposure to sunlight and UV irradiation cause photophysical and photochemical reactions in polymers which can lead to photo-degradation. These two reactions are described in the following:

## 1.2 Photophysical and Photochemical reactions

Photophysical and photochemical processes include light absorption from UV or visible spectrum by polymer chains and electron transition, and excited state creation. During photophysical process the created excited electron returns back to the ground state through various mechanisms including radiative deactivation, radiationless transitions such as internal conversion and intersystem crossing, and energy transfer, as presented in Figure 1.2(a). It is worth mentioning that in this process chemical properties of materials remain unchanged (Geuskens 1975).

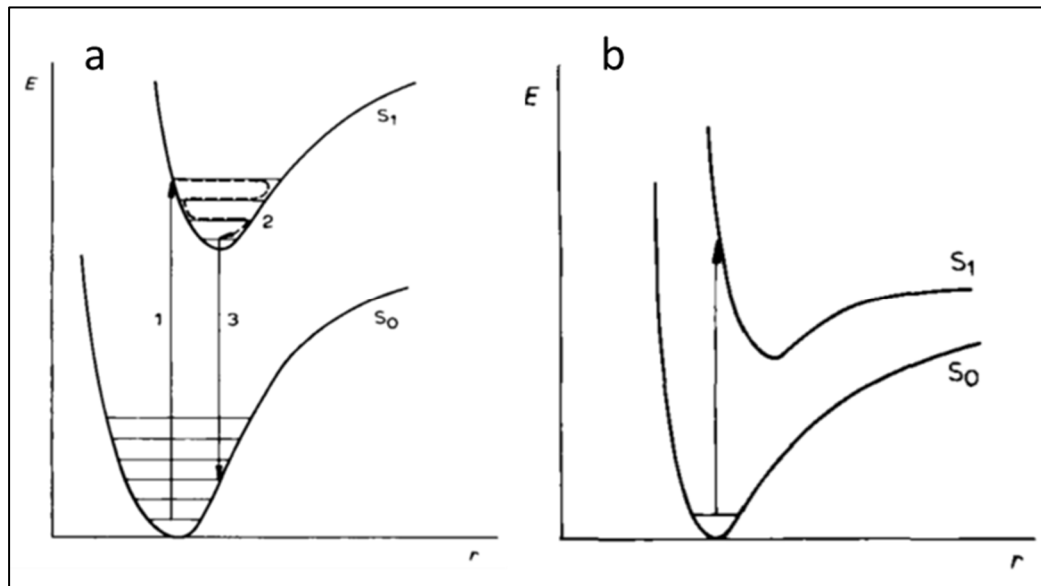


Figure 1.2 (a) Potential energy diagram of a diatomic molecule: 1)absorption; 2)vibrational relaxation; 3)emission, (b) Photodissociation of a molecule  
Taken from Geuskens (1975, p.333)

Conversely, during photochemical processes, electron transition leads to molecule decomposition or dissociation. In this process, a stable excited state is reached, but the absorption energy is beyond the dissociation limit, leading to molecule decomposition, as shown in Figure 1.2(b)(Geuskens 1975). This process leads to changes in the chemical structure of polymer chains, and the formation of free radicals which is the start of photo-degradation in polymers. The following section will describe photo-degradation steps in polymers.

### 1.3 Photo-degradation steps

Photo-degradation of polymers consists of three different steps including initiation, propagation, and termination. Each step is defined in the following, and schematically shown in Figure 1.3.

### Initiation step

This step involves a photochemical reaction and the creation of the first primary radical following the UV absorption. This initiation normally requires the presence of specific chemical groups within polymer structure, called chromophore groups, presented as CH in Figure 1.3, which have the ability to absorb UV wavelengths.

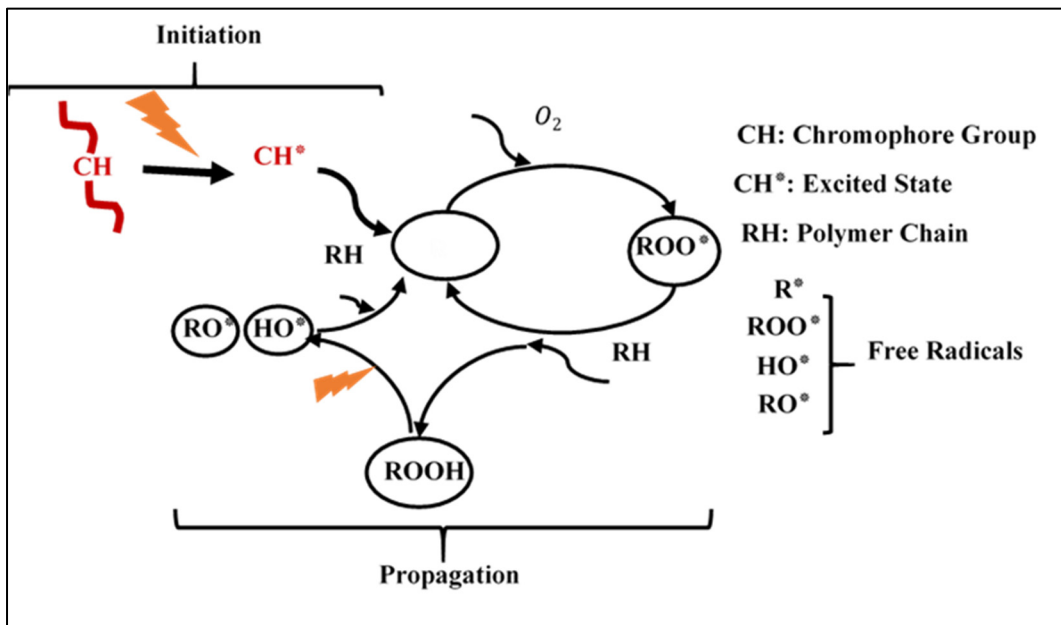


Figure 1.3 Photo-degradation steps

### Propagation step

As presented in Figure 1.3, in propagation step, the created radicals react with oxygen and attack to the neighboring molecules, RH, resulting in generating an increasing number of radicals. Additionally, the presence of oxygen accelerates the photo-degradation, leading to photo-oxidative degradation. This step leads to chain scission or crosslinking in polymers.



## Termination step

This step is associated with the combination of two active free radicals and the creation of non-active species.

### 1.4 Photo-degradation mechanism of HDPE

Photo-degradation in polyolefins, including HDPE, involves a photochemical process. HDPE undergoes photo-oxidative degradation when exposed to air or oxygen, which is a combination of photo-degradation and oxidation process. Despite the initial expectation of stability against UV irradiation, HDPE exhibits susceptibility to UV degradation over time. The UV wavelengths reaching the Earth, typically in the range of 290-400 nm, possess insufficient energy to break alkane bonds in the HDPE structure, as these chemical groups lack absorption spectrum beyond 200 nm. However, prolonged exposure to UV irradiation renders HDPE brittle.

Furthermore, studies have revealed that even pure HDPE contains some degree of vinyl (C=C) and carbonyl (C=O) unsaturation. With the maximum wavelength sensitivity of HDPE being around 300 nm, carbonyl groups found in commercial HDPE are likely responsible for its photo-degradation under sunlight through  $\pi \rightarrow n^*$  transition. The presence of ketone structures in HDPE, resulting from carbonyl impurities, reduces the band gap from about 8 eV for ideal HDPE to 4.3 eV, rendering it sensitive to UV radiation.

The interaction of ketones with UV irradiation can initiate two distinct reactions: Norrish I and Norrish II, as described in Figure 1.4. These two reactions are considered as main photo-degradation mechanism in HDPE. Norrish I reaction results in creation of one acyl and one alkyl radical, which can potentially combine with a hydroxyl radical to form carboxylic acid or release carbon monoxide. Conversely, the Norrish II reaction involves a hydrogen transfer

from the polymer chain to the carbonyl group, resulting in polymer chain  $\beta$ -scission and the formation of a methyl ketone and a polymer fragment with a vinyl end-group. During HDPE weathering, Norrish II reaction contributes to brittleness due to excessive chain scission (Grause, Chien, and Inoue 2020).

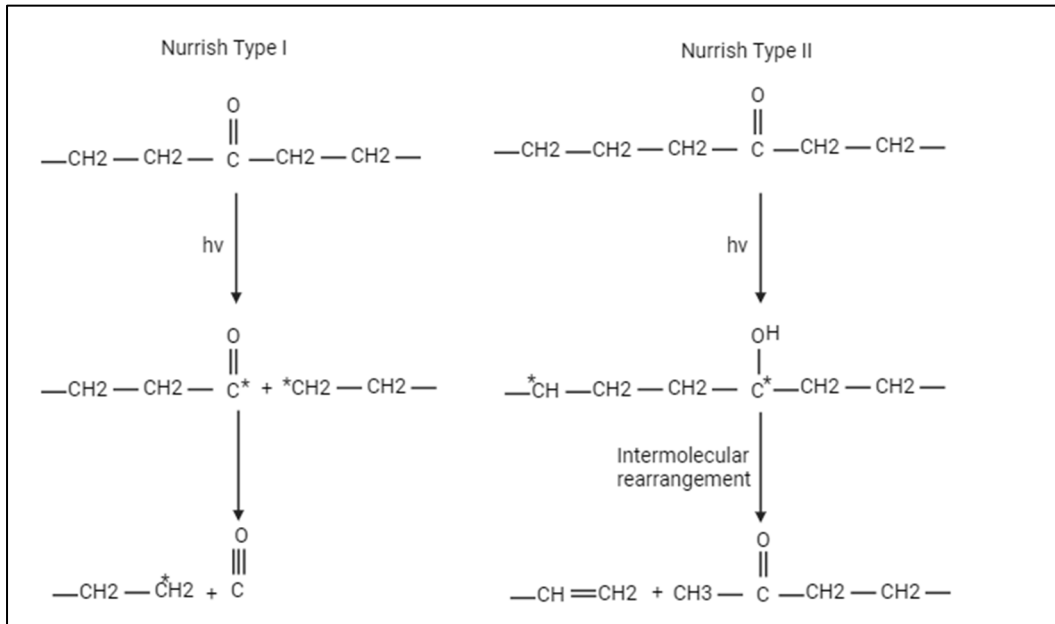


Figure 1.4 Norrish reactions  
Adapted from Grause et al. (2020, p.7)

## 1.5 Chemi-crystallization during polymer photo-degradation

In semi-crystalline polymers like HDPE, photo-degradation predominantly takes place within the amorphous phase due to the limited penetration of oxygen and radicals into the densely packed crystal structure. This process is associated with structural changes, including chain scission within the amorphous regions, which disrupt non-crystallizable segments, such as entanglements, and enhance chain mobility. As a result, a phenomenon known as chemi-crystallization occurs, wherein increased chain mobility promotes recrystallization, facilitating the formation of new crystalline structures within the polymer matrix. Figure 1.5 schematically presents chemi-crystallization process during UV exposure in the semi-crystalline polymer (Rodriguez et al. 2020).

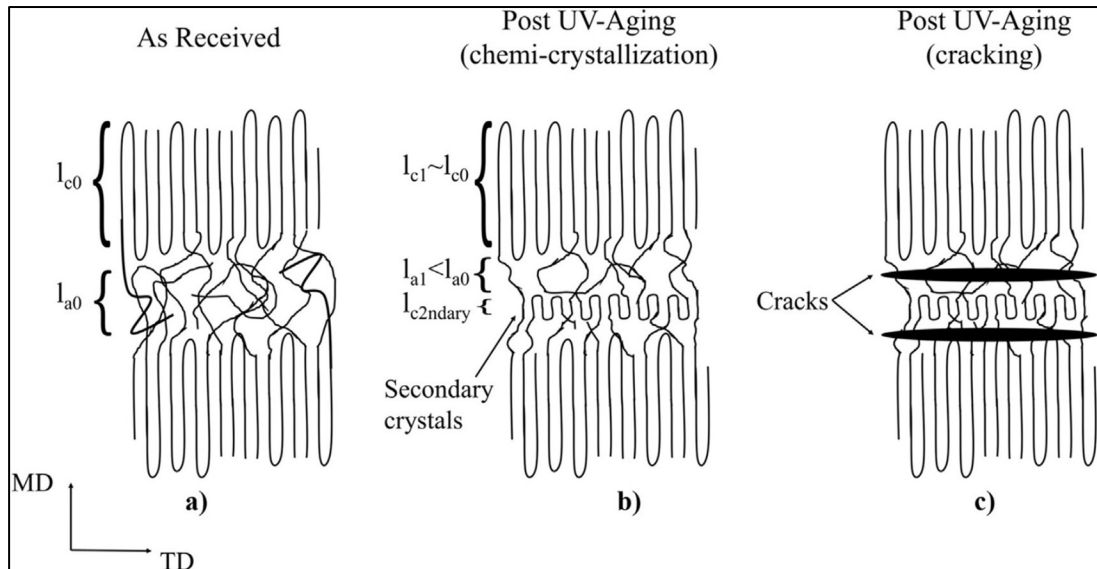


Figure 1.5 Schematic of UV-induced chemi-crystallization and cracking

Taken from Rodriguez et al. (2020, p.12)

Chemi-crystallization results in a higher density of crystals compared to the amorphous regions. This phenomenon induces shrinkage and establishes a gradient of density within the material. Under UV irradiation, chain scission and subsequent chemi-crystallization exhibit variation based on the distance from the exposed surface. Consequently, this non-uniform distribution of crystallization density and residual stresses within the sample promotes the creation of cracks, as shown in Figure 1.5(c)(Rodriguez et al. 2020). This phenomenon contributes to the embrittlement and eventual failure of the HDPE materials, a topic that will be further described in the following section.

## 1.6 Embrittlement in HDPE

HDPE exhibits a ductile behavior under tension, characterized by plastic deformation and distinctive stress-strain curves featuring double yield points. The stress-strain curve presents four distinct zones, as schematically shown in Figure 1.6, each corresponding to a specific microstructural deformation. These zones delineate the microstructural evolution of HDPE under tension, a phenomenon crucial for understanding its mechanical properties. The microstructural deformations during the tensile test are presented in Figure 1.7(a-d).

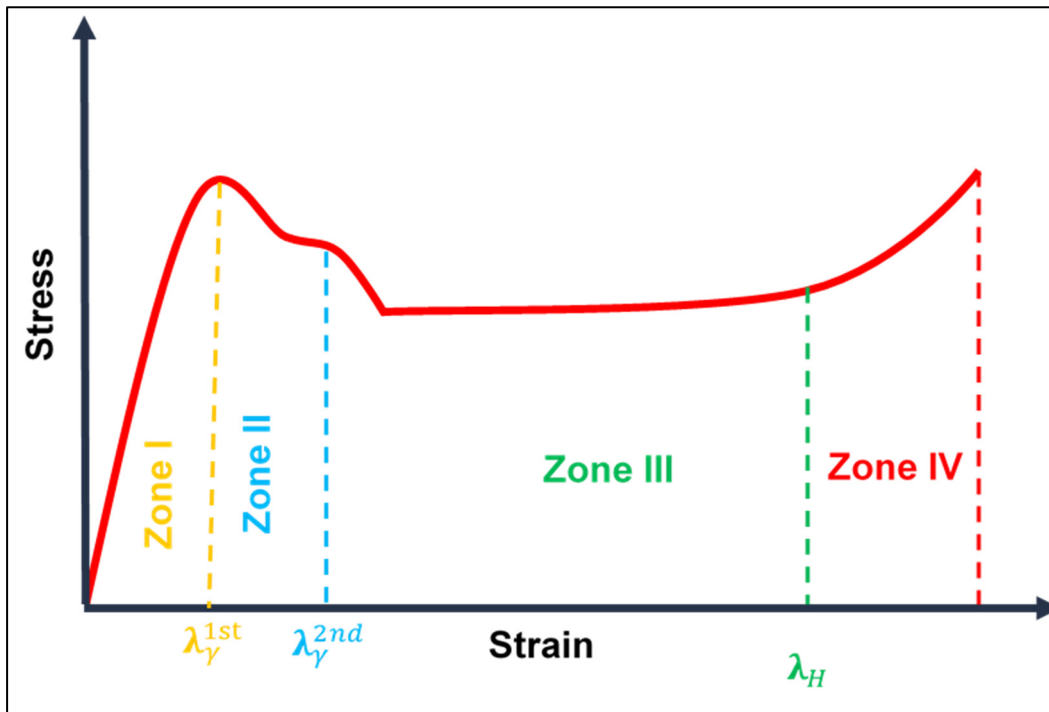


Figure 1.6 Schematic of stress-strain curve of HDPE

The initial segment in Stress-Strain curve, known as zone I or the elastic zone, precedes the first yield point, corresponding to reversible orientation of lamellae in the direction of tensile and interlamellar shear, Figure 1.7(a). Zone II follows as strain accumulates between the first and second yield points, signifying the onset of plastic deformation and irreversible lamella orientation and slipping, Figure 1.7(b). Upon surpassing the second yield point, zone III initiates, indicating the onset of lamella fragmentation and progressing into a necking development process, Figure 1.7(c). Beyond the hardening point lies zone IV, representing the fibrillar state, Figure 1.7(d) (Nikolov, Lebensohn, and Raabe 2006).

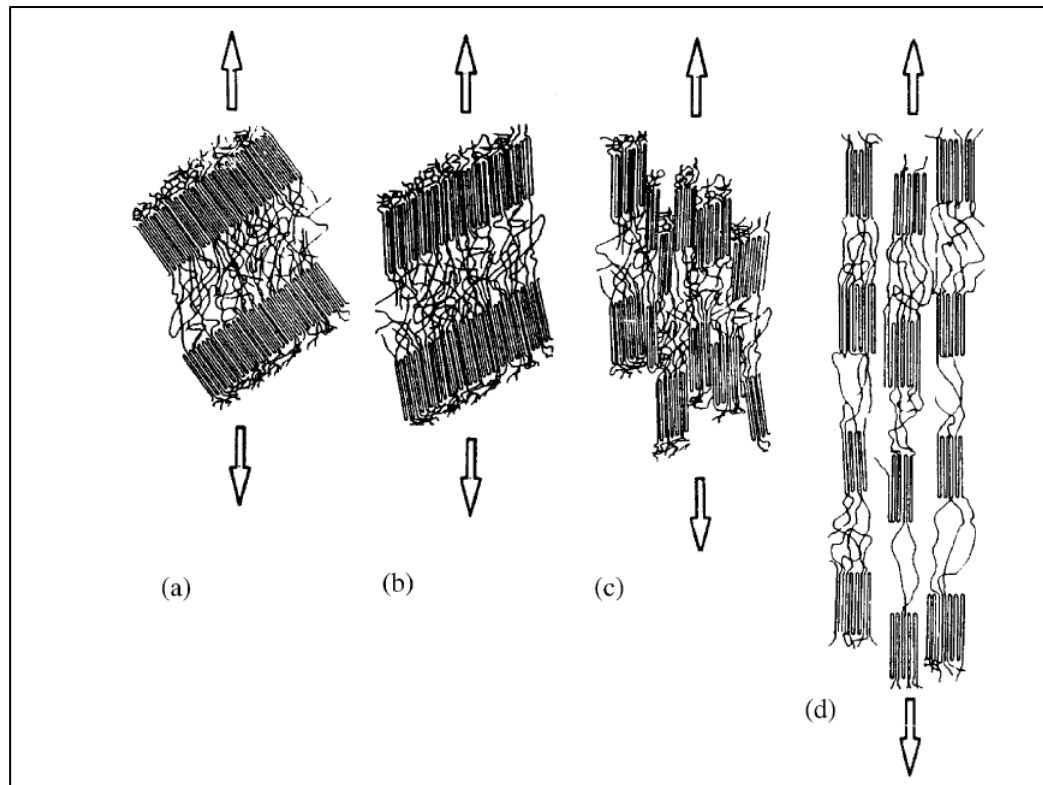


Figure 1.7 Microstructural deformation during the tensile test: (a) lamellae orientation and interlamellar shear; (b) lamellae slip in the crystals; (c) initiation of lamellae fragmentation; (d) fibrillar state  
Taken from Nikolov et al. (2006, p.1351)

In HDPE, significant plastic deformation under tension predominantly begins after surpassing the second yield point. At this critical point, tie molecules play a pivotal role in transferring the load to crystal structures, thereby initiating plastic deformation via lamellae slipping and fragmentation. However, if the material fails to progress beyond the second yield point and efficiently transfer the load to the crystal structures, embrittlement occurs.

Photo-degradation, followed by chain scission and subsequent chemi-crystallization, disrupts this transition process, resulting in reduced plasticity and a heightened susceptibility to failure in HDPE materials. So it is critical to address the susceptibility of HDPE to UV degradation.

To mitigate the deleterious effects of UV exposure on HDPE, it becomes imperative to stabilize the material against such environmental factors. Enhancing the UV stability of polymers often

involves the incorporation of additives known as photo-stabilizers. These compounds, each with its unique photo-stabilizing mechanism, intervene at various stages of the photo-degradation process. The next chapter includes a comprehensive review of different photo-stabilizers and their mechanisms of action, shedding light on their efficacy in safeguarding polymers against UV degradation. Furthermore, the potential of graphene as a promising photo-stabilizer is explored, along with its proposed mechanisms for enhancing photo-stability, offering insights into novel approaches for bolstering the UV resistance of polymers like HDPE.

## CHAPTER 2

### A REVIEW ON GRAPHENE'S LIGHT STABILIZING EFFECTS FOR REDUCED PHOTODEGRADATION OF POLYMERS

Samira Karimi <sup>1</sup>, Emna Helal <sup>2,\*</sup>, Giovanna Gutierrez <sup>2</sup>, Nima Moghimian <sup>2</sup>, Milad Madinehei <sup>1</sup>, Eric David <sup>1</sup>, Mazen Samara <sup>1</sup> and Nicole Demarquette <sup>1,\*</sup>

<sup>1</sup> Mechanical Engineering Department, École de Technologie Supérieure, 1100 Notre-Dame St W, Montreal, Canada QC H3C 1K3

<sup>2</sup> NanoXplore Inc., 4500 Thimens Boulevard, Saint-Laurent, QC, Canada H4R 2P2

Paper published in *Crystal*<sup>1</sup>, December 2020

#### Abstract

Graphene, the newest member of the carbon's family, has proven its efficiency in improving polymers' resistance against photodegradation, even at low loadings equal to 1 wt% or lower. This protective role involves a multitude of complementary mechanisms associated with graphene's unique geometry and chemistry. In this review, these mechanisms, taking place during both the initiation and propagation steps of photodegradation, are discussed concerning graphene and graphene derivatives, i.e., graphene oxide (GO) and reduced graphene oxide (rGO). In particular, graphene displays important UV absorption, free radical scavenging, and quenching capabilities thanks to the abundant  $\pi$ -bonds and  $sp^2$  carbon sites in its hexagonal lattice structure. The free radical scavenging effect is also partially linked with functional hydroxyl groups on the surface. However, the  $sp^2$  sites remain the predominant player, which makes graphene's antioxidant effect potentially stronger than rGO and GO. Besides, UV screening and oxygen barriers are active protective mechanisms attributed to graphene's high surface area and 2D geometry. Moreover, the way that graphene, as a nucleating agent, can

---

<sup>1</sup> Crystals 2021, 11(1), 3

improve the photostability of polymers, have been explored as well. These include the potential effect of graphene on increasing polymer's glass transition temperature and crystallinity.

**Keywords:** graphene; polymer photodegradation; photostabilization; UV absorption; UV screening; free radical scavenging; antioxidant; quenching effect; oxygen diffusion; polymer nanocomposites

## 2.1 Introduction

Polymeric materials are widely used for outdoor applications, such as construction, transportation, recreation, protective paints, and coatings, mainly due to their high strength and modulus to weight ratios. A key challenge in using polymers for outdoor applications is their light sensitivity that results in photodegradation accelerated by humidity and temperature. Polymer photodegradation may induce irreversible changes in physical, chemical, and mechanical properties, such as cracking, chalking, yellowing, and glossy loss. A car's exterior paint offers a perfect example of polymer photodegradation. As the polymers degrade, they begin fading in color and losing their glossy appearance. After extended exposure, the coating becomes fragile, loses strength and flexibility, and begins to crack (Claudé et al. 2001).

Photodegradation is a process in which the polymer properties are irreversibly altered due to the absorption of photons from the sunlight that reaches the earth's surface. The incident radiation consists of three different ranges (ultraviolet, visible, and infrared), each with different energy levels. Although UV radiation represents only 8% of total sunlight, it has the most energy, and it is the primary cause of degradation in polymers and other materials (Wu et al. 2011). This degradation causes irreversible effects on polymer properties, such as a change in molecular weight, deterioration of mechanical properties, as well as loss of color and surface finish, leading to lower performance of the materials (Yousif and Haddad 2013a). Therefore, the study of the effects of photodegradation is key to improving polymers' resistance to sunlight and environmental factors that would extend the materials' lifetime. For this purpose, "stabilizers" are commonly added to the polymer matrix. These additives usually



offer an adequate protection from light and UV in particular. Six main groups have been widely used to boost polymers' UV protection: pigments, metal chelates, phenolic and nonphenolic UV absorbers, hindered amine light stabilizer (HALS), and phenolic antioxidants (Kumar et al. 2009).

However, it is worth noting that sustainability and health and safety risks have been associated with many conventional UV stabilizers and are well documented according to the existing standard regulations. These risks represent a concern for materials manufacturers and users (Tipton and Lewis 2008; Chaudhuri et al. 2018).

Recently, graphene, which consists of  $sp^2$ -hybridized networks of carbon atoms in two dimensional hexagonal structures with one atom thickness, started gaining interest as a novel multifunctional additive that may effectively replace conventional light stabilizers, which are mostly specific in their action (Kolanthai et al. 2015; Hasani et al. 2018). In addition to its excellent photostabilizing properties, which will be discussed in details in this article, graphene features promising electrical, mechanical, thermal, and chemical properties (Soldano, Mahmood, and Dujardin 2010; Helal et al. 2019; Batista et al. 2019; Serenari et al. 2020) attracting worldwide attention in the academic and industrial fields as a promising candidate for various applications (Bae et al. 2012; Fu et al. 2019; Reiß, Hjelt, and Ferrari 2019). Furthermore, the recent progress in large-volume and cost-effective manufacturing of few-layer graphene has made it an economically viable choice for the plastics industry.

In terms of health and safety concerns, graphene has lately shown promising results as well. In fact, a recent study published by Moghimian et al. discussed the dermal, inhalation, and gene toxicity tests of an industrial few-layer graphene (which has 6–10 layers and a predominant particle size of 0.5–2 microns and  $\sim 1$  wt.% oxygen content) (Moghimian and Nazarpour 2020). This study has been specifically performed in accordance with the standard regulatory guidelines in place and has concluded no dermal and inhalation toxicity and no gene mutation induced by the studied graphene type, adverse effects repeatedly reported for conventional UV additives. It is worth noting however that the biological behavior of graphene-based materials

depends on their structure (number of layers, average, lateral dimensions, carbon-to-oxygen atomic ratio, surface functionalization), and therefore different toxicological effects might be associated with different types of graphene derivatives (Sanchez et al. 2012; Fadeel et al. 2018).

Besides, most graphene manufacturing methods do not involve high temperatures or incomplete combustion processes, which are required for the production of some conventional carbon-based materials, such as carbon black. As a consequence, it does not induce the formation of polycyclic aromatic hydrocarbons (PAH), which are substances with carcinogenic and mutagenic properties occurring during incomplete combustion (Tsai et al. 2001). Industrial graphene manufacturing is rather based on more sustainable processes, such as the mechanochemical exfoliation of graphite.

In this paper, the role of graphene as an additive to inhibit or reduce polymer photodegradation is reviewed. In the following section the latest advancements reported in the literature regarding the photodegradation phenomena, as well as the strategies currently used to cope with that problem are reviewed and discussed. The third part of this manuscript is focused on how graphene can be used as a UV additive and its potential benefits to prevent and counteract the photodegradation of polymers. Before going into the subject, a summary of the photodegradation phenomena will be presented using the excellent monograph book of Rabek as a primary source (Rabek 2012).

## **2.2 Physical and Chemical Aspects of Polymer Photodegradation**

### **2.2.1 Introduction**

Photodegradation takes place when polymers are exposed to sunlight radiation, which consists of three ranges of the electromagnetic spectrum: ultraviolet (100–400 nm), visible (400–700 nm), and infrared (700 nm–1000 nm). The ultraviolet radiation, which has the highest energy, is responsible for photodegradation. Ultraviolet radiation is divided into three wavelength ranges: UV-A (320–400 nm), UV-B (280–320 nm), and UV-C (100–280 nm). The

stratospheric ozone mostly absorbs UV-C wavelength, and only UV-A and UV-B can reach the earth's surface (Wu et al. 2011). In the next part, the UV radiation mechanisms acting on polymers will be described in detail.

### **2.2.2 How Does Light Affect Polymers?**

Photodegradation is triggered when materials are exposed to sunlight, particularly in the UV region (290–400 nm). Rabek has written a comprehensive review of the photodegradation mechanisms in polymers (Rabek 2012). In this section, some important aspects of photodegradation mechanisms will be briefly presented.

Photodegradation can occur in two types of atmospheres: in an inert atmosphere (without oxygen) or in the presence of oxygen (air), and in this case the process is called photo-oxidative degradation (Bateman and Gee 1948). Below, general phenomena concerning photodegradation mechanisms are presented; afterward, the photo-oxidative degradation will be discussed.

#### **2.2.2.1 Photodegradation**

Photodegradation starts with the absorption of photons by polymer chains. After absorption, the molecules' energy increases and they assume an excited state, which leads to the breakup of bonds and the formation of free radicals. Such production of free radicals is the first step for photodegradation to occur (Rabek 2012). The essential condition to start photodegradation is the presence of chemical groups in the polymer that can absorb particular wavelengths from the sunlight (280–400 nm) called chromophore groups (Ch). Chromophores are divided into two categories:


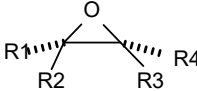
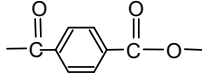
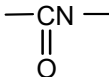
(1) Internal/external impurities, which do not form part of the polymer structure. The impurities can be external compounds (traces of catalyst, solvents, additives, etc.) or functional groups in polymer chains (in-chain or end-chain). They initiate photodegradation and produce active free

radicals. PVC is a good example of this category. Its polymer chains are formed by C-C, C-H, and C-Cl bonds, which do not have any absorption peak wavelength longer than 190–220 nm. However, the impurities added during polymerization and processing initiate photodegradation and produce primary radicals. These reactions lead to dehydrochlorination and production of hydrogen chloride—HCl. The presence of HCl then strongly accelerates PVC's photodegradation, which leads to its low photostability (Rabek 2012; Yousif and Hasan 2015). Poly(ethylene) (PE) and poly(propylene) (PP) also degrade due to the presence of impurities (Rånby 1989). During polymerization and processing, such as extrusion, ketone and hydroperoxide groups, which are chromophore groups, are formed in polymer chains. These groups absorb UV and make polymer chains sensitive to sunlight (Rabek 2012).

(2) Chromophores integrated in the polymer chains. The chromophore group's presence in the polymer structure increases light absorption, leading to lower photostability. For example, poly(styrene) (PS) presents aromatic groups frequently repeated through the polymer chains. This group acts as a chromophore group, absorbing UV wavelengths. It is responsible for the yellowing of PS over time, which is a sign of photodegradation.

Table 2.1 shows the different polymers' absorption characteristics when exposed to the solar spectrum and their resistance to photodegradation. It is worth mentioning that even polymers with high photostability, such as PP and PE, need to be photostabilized in order to meet the requirements for long term exposure, especially for outdoor applications.

Table 2.1 Intensity of sunlight absorption in different polymers

Polymer	Groups Triggered by UV	Absorption Peak (nm)	Absorptivity to Solar Spectrum	Overall Photostability	Cause of Degradation
Poly(ethylene)	-	300–310, 340 (Kamweru et al. 2014)	Low	High	1
Poly(propylene)	-	290–300, 330, 370	Low	High	1
Poly(styrene)		290 (Li, Zhou, and Jiang 1991)	Moderate	Moderate	2
Poly(vinyl chloride)	-	210 (Hasan et al. 2015)	Low	Low	1
Poly(methyl acrylates)	-	700, 1030 (Das et al. 2014)	Low	High	1
Epoxy resins		240–300 (Durmus et al. 2011)	High	Moderate	2
Poly(ethylene terephthalate)		240, 300 (Ouchi et al. 1999)	High	Low	2
Nylon 6,6		290 (Allen and Parkinson 1982)	High	Moderate	2

1—Degradation initiated by impurities. 2—Absorption by chromophore group in the polymer chain.

### 2.2.2.2 Photo-Oxidative Degradation

The polymer suffers a photo-oxidative degradation in air or oxygen, a combination of photodegradation and oxidation processes. Photodegradation and photo-oxidative reactions consist of three steps (Jan.F. Rabek 1995; Rånby 1989):

(1) Initiation step: in this step, light-absorbing groups (chromophore groups or impurities) produce primary radicals under UV or visible light irradiation according to reaction (2.1) (Jan.F. Rabek 1995):



where  $R^\circ$  and  $HO_2^\circ$  are polymer alkyl radical and hydroperoxy radical.

(2) Propagation step: after producing primary radicals, these radicals attack the polymer chains and produce more and more polymer radicals leading to crosslinking or chain scission. The presence of oxygen accelerates the production of polymer radicals. At first, polymer peroxy radicals ( $ROO^\circ$ ) are formed by the reaction of polymer alkyl radicals ( $R^\circ$ ) with oxygen. This reaction is the key reaction in the propagation step, a fast but diffusion-controlled reaction (2.2).

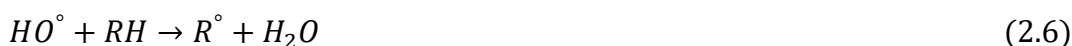


The next reaction in the propagation step is hydrogen abstraction from polymer chains, leading to the formation of a new polymer alkyl radical ( $R^\circ$ ) and hydroperoxide (ROOH), which decompose into polymer oxy radicals ( $RO^\circ$ ) and hydroxyl radicals ( $HO^\circ$ ), reactions (2.3) and (2.4).





These new radicals ( $RO^\circ$  and  $HO^\circ$ ) can react with polymer chains and generate more polymer alkyl radicals ( $R^\circ$ ) (Jan.F. Rabek 1995), reactions (2.5) and (2.6).



(3) Termination step: the termination step occurs when different radicals recombine together and form nonradical products (Jan.F. Rabek 1995).

According to the points mentioned above, photodegradation is a complex problem that is always present in the polymer industry. To limit the photodegradation's harmful effects, photostabilizers are widely added to polymers to improve their durability. In the next part, the mechanisms of action of the most commonly used photostabilizers are reviewed.

### 2.2.2.3 Mechanisms of Actions of Photostabilizers

To determine the mechanisms of graphene action as a photostabilizer, it is essential to mention conventionally used photostabilizers and their action mechanisms. In this section, a summary of different photostabilizers and their mechanisms will be presented.

Figure 2.1 presents the general pathway of photodegradation, the photostabilization mechanisms, and the step at which each type of photostabilizer takes action during the photodegradation process to stabilize the polymer. As shown in Figure 2.1, photodegradation starts by absorbing UV radiation by chromophore groups, converting polymer to an excited state ( $Ch^*$ ), which leads to breaking the bonds (occurs in bonds with lower energy) and the formation of primary radicals ( $R^\circ$ ), i.e., the initiation step. Then, the formed free radicals, in the presence of oxygen, produce peroxy radicals ( $ROO^\circ$ ). Peroxy radicals attack the polymer

chain (RH), leading to the formation of a new alkyl radical and hydroperoxide. Subsequently, hydroperoxide decomposes to new free radicals (oxy radicals ( $RO^\circ$ ) and hydroxyl radicals ( $HO^\circ$ )) that support the propagation step described in Section 2.2.2.2.

Photostabilizers can be classified based on their chemical structure or their mechanism of action (Yousif and Haddad 2013b; Mohamed 2015). Based on the latter criteria, five main classes of photostabilizers can be distinguished: UV absorber, UV screener, quenchers, antioxidants, nucleating agents, and fillers.

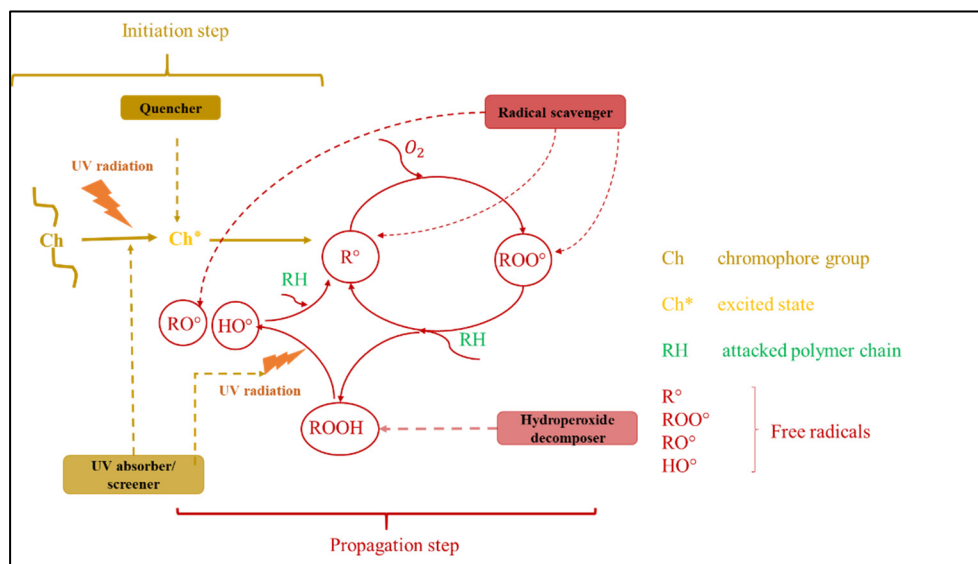


Figure 2.1 General pathways of photodegradation and stabilization mechanisms

According to their mechanism of action, the different additives act at different stages of the photodegradation, while UV absorber, UV screener, and quencher interact at the initiation step, antioxidants react with free radicals and slow down the propagation step. The details of the mechanisms for each type of photostabilizer are reviewed below.



### (1) UV absorber

This type of UV stabilizer has an absorption peak in the UV wavelength range. This property allows it to absorb UV, preventing it from reaching the polymer chains (Wiles and Carlsson 1980; Mohamed 2015). UV stabilizers interfere with the initiation step and postpone or eliminate the primary radicals' formation, as illustrated in Figure 2.1. The most commonly used UV absorbers are organic compounds, such as phenolic UV absorbers (Kumar et al. 2009). Benzotriazoles, dihydroxybenzophenones, and organic nickel compounds are the best examples of this kind of stabilizers. Two typical examples are illustrated in Figure 2.2. Their chemical structure gives them the ability to absorb energy and dissipate it as heat through a reversible chemical rearrangement (Mohamed 2015). The main drawback concerning the organic UV absorber is their temporary protection. In fact, organic UV absorbers tend to decompose due to their mechanism of action, which is based on a chemical rearrangement. Also these types of photostabilizers are more likely to migrate to the polymer surface over time, which leads to gradual loss of their stabilization efficiency (Allen et al. 2004; Nikafshar et al. 2017). Besides, it is worth mentioning that their efficiency significantly depends on the protected material thickness (Pascal Xanthopoulos 2019) and its chemical structure. In fact, UV absorbers tend to show large differences in effectiveness with different resins (Ashton 1970).

Besides the technical limitations, it is worth mentioning that decomposition products of the UV absorbers also migrate from the bulk of the polymer to the surface, where they are washed out. Thus, environmental and health issues become another relevant aspect to consider due to their toxicity and bioaccumulation nature, as well as their role as pollutants in aquatic environments (Alotaibi et al. 2015a; Asimakopoulos et al. 2013; Kusk, Avdolli, and Wollenberger 2011; Tipton and Lewis 2008).

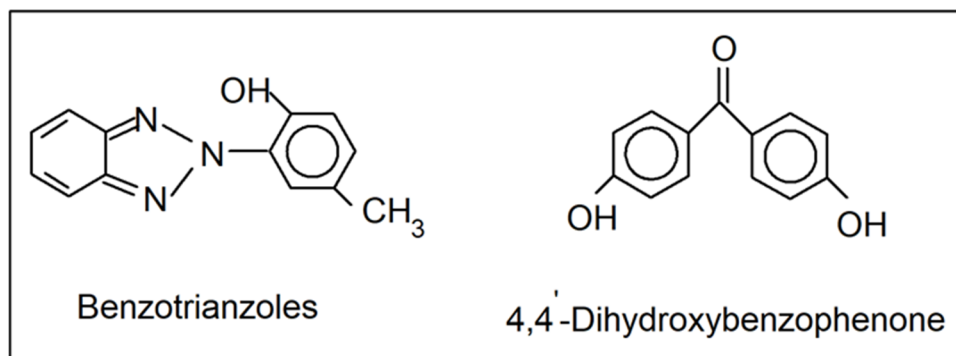


Figure 2.2 Example of UV absorbers

Apart from organic UV absorbers, carbon black is also a well-known UV absorber, widely used to protect polyolefins and elastomers from light. Simultaneously, it acts as a pigment (Han et al. 2011). As discussed in a later section, carbon black can also act as UV screener and free radical scavenger.

## (2) UV screener

A UV screener stops the light from reaching the polymer by reflecting it. As shown in Figure 2.1, UV screeners take action during the initiation step and avoid/reduce the UV absorption by chromophore groups. Metal oxide pigments like  $\text{TiO}_2$ ,  $\text{ZnO}$ ,  $\text{Fe}_2\text{O}_3$ , and  $\text{Cr}_2\text{O}_3$ , among others, have a remarkable ability to reflect light and act as screeners for polymers (Padrón 1989). Some pigments can also absorb UV and act as a UV absorber, such as  $\text{TiO}_2$ . Their performance is strongly related to the size of their crystals (Kockler et al. 2014). The main problem associated with the use of pigments is that the photostabilization process is limited to the surface (Yousif and Haddad 2013b) and also the use of color pigments cause discoloration in polymers, which make them impractical in many applications and white pigments like nanosized  $\text{TiO}_2$  and  $\text{ZnO}$  may be toxic for humans (Smijns and Pavel 2011).

## (3) Quenchers

These stabilizers have no absorption peak in UV wavelengths, but can accept energy from excited state molecules (Wiles and Carlsson 1980; Yousif and Haddad 2013b). Quenchers act

during the initial step, as illustrated in Figure 2.1. Quenchers react with the excited state molecules and convert them to the nonreactive state through an energy transfer process (Yousif and Haddad 2013b). Quenchers can release the transferred energy through less harmful energy-like heat. Reaction (2.7) describes such a mechanism, where Ch and Q are chromophore groups and quenchers, respectively.



\* shows the excited state

Equation (2.7) illustrates how quenchers hinder primary radical formation after UV absorption by chromophore groups. As a result, the photodegradation rate is decreased. Metal chelates are a good example of this group (Kumar et al. 2009). Nickel quenchers are the most common type, usually used for agricultural film purposes. Their main setback is the presence of heavy metals in their structure and the toxicity associated to it (Abdel-Bary 2003). Also, some aesthetic limitations exist due to the greenish pigmentations developed or to color distortion in the final products.

#### (4) Antioxidants

Unlike above-mentioned UV stabilizers, this kind of stabilizer intervenes during the propagation step. This group consists of two main classes—free radical scavengers and hydroperoxide decomposers (Fondriest Environmental 2014).

##### (4.1) Radical scavengers

The materials from this class, also called primary antioxidants, react with the propagating radicals such as peroxy, alkoxy, and hydroxyl radicals, and through hydrogen and H-donation processes at wavelengths below 250 nm, converting them to nonreactive components, as illustrated in Figure 2.1. Hindered phenols and hindered amine light stabilizers—HALS—are the most used commercial antioxidants (Fondriest Environmental 2014). The main problems

associated with this kind of stabilizer are their compatibility with polymer chains in high molecular weight and migration in low molecular weights, in addition to the environmental, health, and safety risks related to their high toxicity (Tipton and Lewis 2008). Figure 2.3 shows the general mechanism of action of hindered phenolic radical scavengers. This type of antioxidant can react with two peroxy radicals. It means that the intrinsic mechanism of the photostabilization process leads to the consumption of the phenolic antioxidants, thus their efficiency decreases over time (Zweifel 1999).

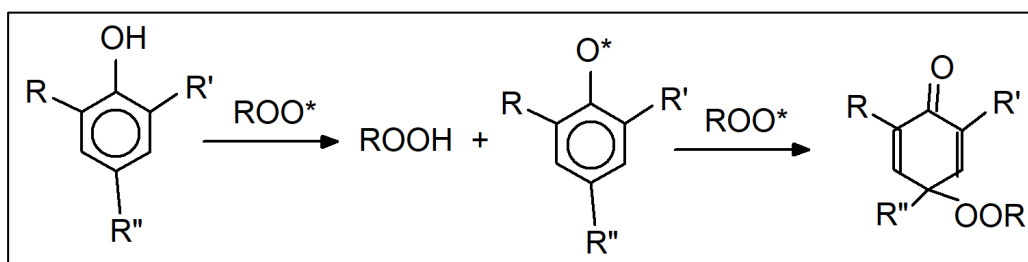


Figure 2.3 Mechanism of action of phenolic antioxidants

#### (4.2) Peroxide decomposers

This group, also called secondary antioxidants, reacts with hydroperoxides, as illustrated in Figure 2.1 To be more specific, they decompose the hydroperoxides (ROOH) into nonreactive products and prevent the formation of extremely active alkoxy and hydroxy radicals. Trivalent phosphorus compounds (phosphites) and thioethers sulfides are the most common secondary antioxidants. Secondary antioxidants are widely used to achieve higher efficiency in combination with primary antioxidants (Fondriest Environmental 2014).

#### (5) Nucleating agents and fillers

These materials have no direct effect on the photodegradation process, but they can change some properties of the polymer matrix, and have a secondary impact on photodegradation. For instance, fillers can act as nucleating agents in the polymer matrix, increasing crystallinity and glass transition temperature by reducing chain mobility. This reduction in chain mobility leads

to less diffusivity of radicals, making it harder to attack the neighboring polymer chains resulting in lower photodegradation rates (Kumar et al. 2009; Jan.F. Rabek 1995).

It is worth mentioning that, in many cases, effective protection is obtained only if UV stabilizers of different mechanisms (screeners, UV absorbers, quenchers, and antioxidants) are combined and exhibit a synergistic effect (Horrocks and Liu 2003). Besides, the probability of encountering problems of compatibility with polymer chains, migration, evaporation and immobility is higher in the presence of one type of photostabilizer, which decreases the final performance (Kumar et al. 2009). The probable issue concerning the combination of different photostabilizers is the increment in final costs.

Table 2.2 summarizes the above-discussed categories of photostabilizers, their mechanisms of action, as well as some examples. Besides the traditional photostabilizers, it has been established that carbon-based materials, such as carbon black can efficiently stabilize polymers. Such stabilization against sunlight can be achieved through different mechanisms, by acting simultaneously as a UV absorber, UV screener, and free radical scavenger (Horrocks et al. 1999; Javadi, Hosseini, and Aghjeh 2014; Liu and Horrocks 2002; Bigger and Delatycki 1989c). The carbon black performance as a photostabilizer is related to a wide range of parameters, including concentration and dispersion into the polymer matrix, structure, and primary particle size (Peña et al. 2000; Ghasemi-Kahrizangi et al. 2015). In particular, it has been observed that the protection efficiency of carbon black decreases with increasing particle size, with the best performance achieved with particles < 20 nm (Liu and Horrocks 2002). A limitation associated with the use of carbon black is related to its manufacturing process, associated with environmental and health issues, since it implies partial combustion of fossil fuels and generation of greenhouse gas byproducts and polycyclic hydrocarbons (Chaudhuri et al. 2018; Moghimian and Nazarpour 2020). Carbon nanotubes (CNT) are another example of carbon-based materials that have shown a photostabilizing effect in polymer matrices. The main mechanisms associated with CNT for photo stabilization are UV absorption and radical scavenging (Najafi and Shin 2005; Morlat-Therias et al. 2007; Martínez and Galano 2010).

Table 2.2 Common photostabilizers based on their chemical structure

<b>Type</b>	<b>Example</b>	<b>Role</b>
Pigments	$TiO_2$ , , $ZnO$ , $Fe_2O_3$ , $Cr_2O_3$	UV screener, UV absorber
Phenolic and nonphenolic UV absorbers	Hydroxyphenyl benzoate Hydroxyphenyl benzotriazoles	UV absorber
Hindered amine light stabilizer	Derivatives of Tetramethylpiperidine	Radical scavenger Quencher
Phenolic antioxidants	Calixarene	Radical scavenger
Metal chelates	Nickel chelates	Quencher
Carbon-based materials	Carbon black CNT	UV absorber UV screener Radical scavenger

Graphene, a new carbon-based material, has a high potential as a UV stabilizer thanks to its unique combination of physical and chemical photostabilizing mechanisms. Besides the mechanisms for UV absorption, screening, and radical scavenging (Mistretta et al. 2019; Kolanthai et al. 2015), graphene displays a huge specific surface area that enables it to act as a physical barrier against diffusion of low molecular compounds or gases like oxygen into the polymers (Yoo et al. 2014).

Graphene-based nanocomposites have been widely studied (Allen, Tung, and Kaner 2010). However, the field of knowledge concerning their photodegradation remains barely adequate. In the next two sections, graphene properties and their action mechanisms as a photostabilizer will be respectively discussed.

## 2.3 Graphene

Graphene is a two-dimensional material that consists of carbon atoms organized in a hexagonal lattice with  $sp^2$  bonds. Single-layer graphene is theoretically stronger than steel (Terrones et al. 2011; Lee et al. 2008). Owing to its excellent electrical, thermal, and optical properties, graphene-based composites find various applications in different fields, including electrostatic discharge protection (ESD), automotive, sensors, solar cells, and drug delivery systems (Fan and Wang 2015; Chowdhury et al. 2015).

### 2.3.1 Types of Graphene

Graphene is mainly known as a single layer or bilayer of carbon atoms arranged in a honeycomb, hexagonal structure that is usually produced in a highly controlled laboratory environment. This type of graphene is mainly known as research-grade or laboratory-grade graphene. For industrial use, however, there are two major categories of graphene: electronic-grade graphene, which is mainly produced by chemical vapor deposition (CVD), and commercial-grade or bulk powder graphene. The latter is most suitable for bulk industrial applications, such as UV protection, due to its ease of manufacturing and cost-effectiveness. Commercial-grade, also known as few-layer graphene, is typically made of five to ten atomic layers of  $sp^2$ -hybridized sheets of carbon and can be prepared through a sustainable process based on mechanochemical exfoliation of graphite (Moghimian et al. 2017; Batista et al. 2019; Moghimian and Nazarpour 2020). Furthermore, it has been demonstrated recently that few-layer graphene is rather a safer alternative to conventional UV additives (Alotaibi et al. 2015a; Asimakopoulos et al. 2013; Kusk, Avdolli, and Wollenberger 2011; Tipton and Lewis 2008; Chaudhuri et al. 2018; Moghimian and Nazarpour 2020).

### 2.3.2 Structure of Graphene

The outstanding properties of graphene are associated with the configuration of carbon's valence electrons. Carbon has four valence electrons located at four different orbitals (s,  $p_x$ ,  $p_y$ ,

and  $p_z$ ). In graphene, each carbon is connected with three other carbons, as illustrated in Figure 2.4(a). In this structure, carbon has a  $sp^2$  configuration, in which three orbitals, called sigma orbitals, ( $s$ ,  $p_x$ , and  $p_y$ ) take place at the molecule plane and the  $p_z$  orbital,  $\pi$  orbital, is located perpendicular to the molecule plane. This configuration allows carbon to form sigma bonds, with three neighbor carbons (with an angle of  $120^\circ$  degree), and  $\pi$  bonds through  $\pi$  orbital, as illustrated in Figure 2.4(b). Sigma bonds are responsible for the strong mechanical properties of graphene, and  $\pi$  bonds provide high electrical conductivity for graphene (Mak et al. 2012). Also, the presence of conjugated bonds ( $\pi$  bonds) on the structure of graphene introduce other interesting properties including strong electron donor and acceptor capability, and great ability to absorb UV wavelengths through  $\pi \rightarrow \pi^*$  transitions (Dash, Pattanaik, and Behera 2014).

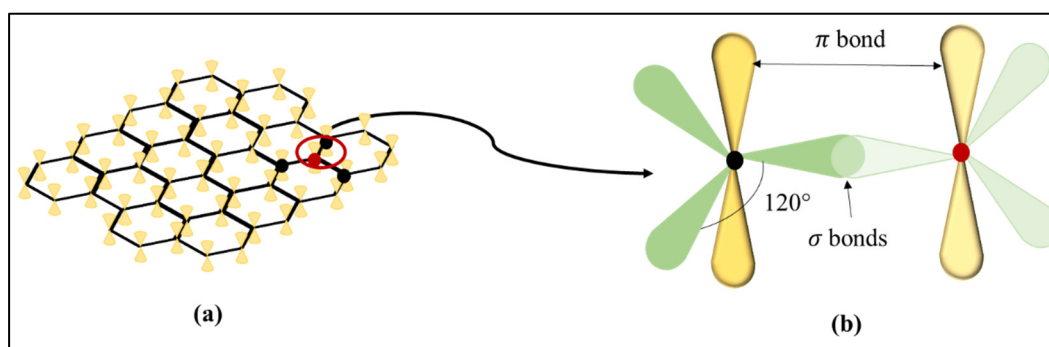


Figure 2.4 (a) Structure of graphene with pi orbitals, (b)  $sp^2$  configuration in graphene

### 2.3.3 Graphene Derivatives

Graphite is composed of graphene layers. Graphene's surface chemistry can be tuned by treating graphite in the presence of strong oxidizers such as sulfuric acid. This treatment results in a compound called graphene oxide, which consists of one layer, or graphite oxide (GO), which consists of several layers. GO has oxygen-containing functional groups such as carboxylic acid (COOH), hydroxyl (OH), and epoxide located on the basal plane or the edges (Shams et al. 2019; Du et al. 2018). Reduced graphene oxide (rGO) is another class of graphene derivatives produced by chemical and thermal treatment of GO to decrease the oxygen content (Tarcan et al. 2020).



Along with graphene, GO and rGO are also used as photostabilizers. However, the change in their surface chemistry and the disappearance of a portion of the conjugated bonds play an essential role, affecting several properties, including mechanical, electrical, optical, and even photostabilization properties (Fondriest Environmental 2014). The differences between graphene, GO, and rGO as UV stabilizers will be discussed in the next sections.

## **2.4 How Graphene Slows down Photodegradation in Polymers**

Several mechanisms contribute to the photostabilizing effect of graphene, including UV absorbers and screeners, radical scavengers, quenchers, and physical barriers. These mechanisms will be discussed in detail in this section.

### **2.4.1 UV absorbers and screeners**

As described in Section 2.2.2.3, UV absorbers and screeners mainly affect the initiation step and prevent the formation of primary radicals.

In some studies, UV absorption and reflection have been considered as the most dominant mechanisms of actions of graphene (Mistretta et al. 2019; Hasani et al. 2018; de Moraes et al. 2015). The UV blocking mechanism of graphene is governed by absorption in the range 100–280 nm, and by reflection at longer wavelengths.

Thanks to the high amount of conjugated bonds in its structure, graphene features strong UV absorption, attributed to  $\pi \rightarrow \pi^*$  transitions. As a result, it exhibits a broad absorption peak between 230–320 nm with the maximum around 280 nm (Johra, Lee, and Jung 2014; Demchenko 2019). In fact, graphene absorbs UV radiation and prevents it from reaching polymer chains, limiting the initiation step of photodegradation.

Also, graphene can reflect UV radiation due to its 2D structure. When UV or sunlight hits particles, a portion of radiation reflects in different directions. In this way, graphene blocks UV and protects the polymer chains. De Oliveria et al. (de Oliveira et al. 2019) investigated the role of GO in photostability of polypropylene -PP. In this study, UV reflection was suggested as the mechanism of action for GO. In the same context, Qu et al. (Qu et al. 2014) studied the photostability of cotton fabrics modified with waterborne polyurethane/graphene hybrid composites and concluded that the main UV blocking mechanism of graphene is governed by absorption at wavelengths  $<281$  nm and reflection at longer wavelengths.

As a general effect, and considering that the critical parameter in the initiation step is the UV absorption, graphene presence will result in a more photostabilized polymer.

#### **2.4.2 Radical scavengers**

Radical scavengers mostly attenuate the propagation step by reacting with the propagating radicals and making them inactive, as illustrated in Section 2.2.2.3.

Radical scavenging is another mechanism of action that is widely suggested for graphene (Prosheva et al. 2019; Hasani et al. 2018). In fact, it has been proven that graphene has an antioxidant effect when exposed to sunlight and can protect polymers against oxidation and trap free radicals (Kolanthai et al. 2015; Qiu et al. 2014).

As discussed above, the key reaction in the propagation step is the abstraction of a hydrogen from the polymer chain by peroxy radicals ( $\text{ROO}^\circ$ ) to produce a new polymer alkyl radical ( $\text{R}^\circ$ ), as illustrated in reaction (3).

Graphene has a remarkable ability to deactivate free radicals, i.e., peroxy radicals, through radical adduct formation at the  $\text{sp}^2$  carbon sites and H-donation from hydroxyl groups, preventing polymer chains from being attacked by peroxy radicals, as shown in Figure 2.5. As a result, it leads to photostability.

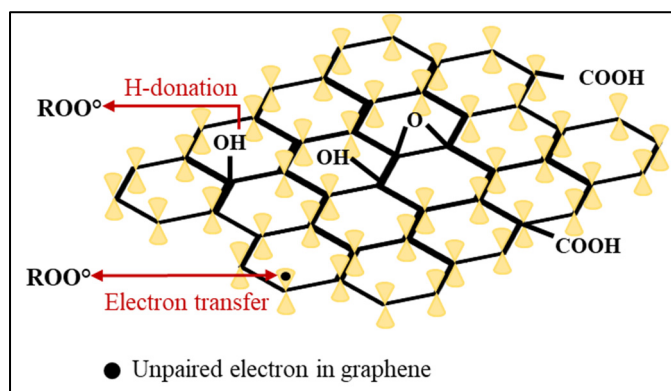


Figure 2.5 Radical adduct formation at the  $sp^2$  carbon sites and H-donation from hydroxyl groups

The effect of graphene chemistry on this free radical scavenging activity has been investigated (Qiu et al. 2014). Three different graphene modifications, including GO, reduced graphene oxide -rGO, and few-layer graphene (FLG), were selected to determine what part is responsible for it. The results showed that graphene's antioxidant activity is in the following order: FLG > rGO > GO. It has been concluded that free radical scavenging activity is strongly associated with  $sp^2$  carbons on basal surfaces rather than H-donation from hydroxyl groups. In fact, conjugated bonds are highly reactive toward free radicals because they form more stable radicals by resonance structure. Thus, the protection mechanism mainly occurs through  $sp^2$  carbon sites instead of functional groups or defects at the edges.

### 2.4.3 Quenchers

Another suggested mechanism to explain graphene's role as a photostabilizer is the quenching effect (Ran et al. 2012). As mentioned before, quenchers interact with excited state molecules, receive their energy, and make them nonreactive species. It has been proven that graphene is a great electron acceptor (Dash, Pattanaik, and Behera 2014). This property makes it an excellent candidate to protect polymer chains from photodegradation through a high-speed energy transfer.

Polymer chains go to the excited state by absorbing UV radiation. In the presence of rGO, the excited electrons in the polymer transfer rapidly onto rGO. As a result, this process eliminates the photodegradation and protects polymers against UV (Qiu et al.). Since graphene, rGO, and GO have the same structural base ( $sp^2$  bonds), this mechanism is valid for all graphene derivatives.

#### **2.4.4 Physical barrier**

Besides the properties mentioned above, graphene and graphene derivatives act also as a physical barrier against the diffusion of low molecular compounds, namely oxygen, into polymers, thanks to graphene's 2D geometry, enormous specific surface area, and high aspect ratio (Yoo et al. 2014; Cui, Kundalwal, and Kumar 2016). More specifically, the presence of graphene in a polymer matrix creates tortuous pathways that make it difficult for oxygen and free radicals to diffuse into the polymer bulk. As a result, the first reaction rate in the propagation step (which is diffusion-controlled (Equation (2.2)) decreases and, consequently, the photodegradation rate is slowed down. Figure 2.6 illustrates oxygen diffusion in a pure polymer vs. a polymer containing graphene. It depicts how the diffusion pathway of oxygen is longer in the presence of graphene sheets leading to less diffusion (Chang et al. 2014). It is worth noting that due to lower aspect ratio, this protective mechanism is less or not effective when isotropic particles such as carbon black are used for photostabilization (Kalaitzidou, Fukushima, and Drzal 2007).

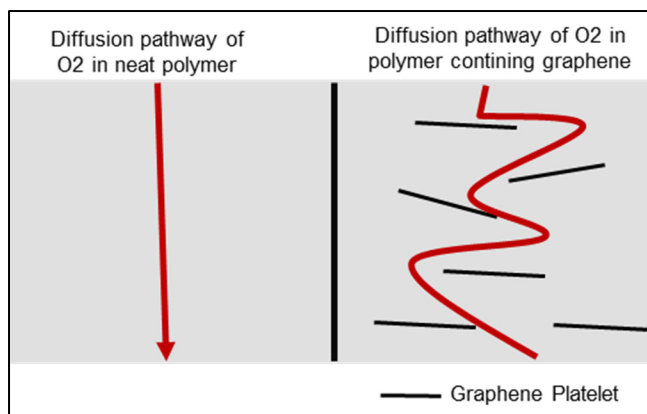


Figure 2.6 Pathway of oxygen diffusion in neat polymer and graphene nanocomposite

#### 2.4.5 Photodegradation reduction through changes in crystallinity, glass transition temperature (T<sub>g</sub>), polymer mobility, and free volume upon the addition of graphene

When graphene is added to a polymer matrix, T<sub>g</sub>, polymer mobility, free volume, and crystallinity may change. How these changes can affect the polymer photodegradation is explained below.

##### (1) Free volume, polymer mobility, and glass transition temperature

The fraction of free volume and T<sub>g</sub> determine the mobility of the polymer segments (Jan.F. Rabek 1995). The increase of free volume and polymer mobility accelerates photodegradation and makes it easier for radicals to separate and attack the neighboring polymer chains. The presence of graphene usually increases the glass transition temperature (Xue et al. 2013; Mahendia et al. 2016), decreases free volume, and restricts polymer chains' motion (Klonos et al. 2015). These changes can lead to a decrease in radical separation and an overall decrease in photodegradation.

## (2) Crystallinity

It has been reported that graphene acts as a nucleating agent when added to polymer matrices, which leads to an increased crystallinity (Lee, Hong, and Jang 2013; Zhao et al. 2014; Karimi, Ghasemi, and Abbassi-Sourki 2019). Since photodegradation usually occurs in the amorphous phase of polymers (Jan.F. Rabek 1995), the improvement of the crystallinity of a polymer matrix leads to a decrease in polymer photodegradation.

Accordingly, in addition to UV absorption, UV screening and reflection, radical scavenging, quenching, and physical barrier mechanisms, graphene can also alter fundamental polymer properties (such as T<sub>g</sub> and crystallinity). All these effects are translated into a further increase in the material's stability against UV radiation.

Table 2.3 presents a summary of some studies that investigated the effect of graphene and graphene derivatives on polymers photodegradation. The Table shows the polymer matrices, type of graphene derivatives used (GO, rGO, or graphene), graphene concentration, the details of UV-degradation process (device, UV wavelength, exposure time, cycle), and a sum up of the results. As we can see, the presence of different graphene derivatives in polymer matrices significantly improved their resistance against photodegradation, at loadings as low as 0.1 wt% in several reported studies. It has been also reported that graphene derivatives present a better performance compared to organic UV absorbers. The roughness increment, which is a sign of photodegradation, after 700 h exposure, decreased from 195% in neat sample to 180% in the presence of organic UV absorber and 65% in the presence of 0.1 wt% GO. Moreover, graphene derivatives exhibited lasting photostabilizing effects, while organic UV absorbers, especially those with low molecular weight, decomposed or migrated to the surface and lost their protective effect after a while. This feature makes graphene and graphene derivatives suitable for long-term protection of polymers (Hasani et al. 2018). The release of some organic UV absorbers represents an environmental concern as some of them, for instance the benzotriazole absorbers, are classified as very persistent and very bio accumulative (European chemicals agency 2020) It is worth mentioning that graphene derivatives may accumulate at degraded

nanocomposite surfaces and release during the photodegradation process as well (Zepp et al. 2020). Their release is dependent on the exposure conditions. A recent study by Goodwin Jr et al. (Goodwin Jr, Shen, et al. 2020; Goodwin Jr, Lai, et al. 2020), which investigated the release potential of graphene derivatives, revealed that the release of graphene is limited under dry UV conditions but can be promoted under humid UV conditions with small mechanical forces. In the context of humid UV conditions, the migration to the surface and release of graphene oxide might be more significant than the release of graphene because of its hydrophilic nature leading to a reduction in its UV protection efficiency (Goodwin Jr, Lai, et al. 2020).

A key parameter that strongly affects the protective role of graphene derivatives is their concentration and the quality of dispersion and exfoliation in the polymer matrix. In general, more efficient protection is associated with higher concentration and better graphene dispersion and exfoliation (Moon et al. 2011).

In terms of comparison between graphene and the rest of the graphene derivatives (rGO and GO), it seems that graphene exhibits stronger free radical scavenging activity, as discussed earlier (Qiu et al. 2014), and an overall better protection when UV exposure is accompanied by high humidity levels, as the hydrophilic nature of GO may lead to water absorption and further degradation (Goodwin Jr, Lai, et al. 2020), while graphene has shown a 10 times reduction in photodegradation rate in both dry and wet conditions (Goodwin Jr, Shen, et al. 2020). It was also shown that carbon-based materials could be more interesting than other stabilizers. For example Bussière et al. (Bussière et al. 2013) showed that TiO<sub>2</sub> and ZnO could have a negative effect on the photostability of polymers depending on their concentration and polymer matrix, while CNT as a carbon-based material presented a positive effect on the improving the stability of polymers against sunlight. Furthermore, it was shown that graphene presents a better performance as a photostabilizer compared to carbon black, which is widely used to protect polymer against UV (Frasca et al. 2016). In their study Frasca et al. showed that graphene presents higher UV absorption peak around 270 nm, indicating more UV absorption when compared to the one of carbon black, even in lower concentrations. Moreover,

graphene showed stronger ability to trap radicals with a scavenging efficiency improving upon increase of graphene concentration (Frasca et al. 2016).

It should be noted that photodegradation of polymers is usually investigated using accelerated weathering chambers. These chambers allow the simulation of photodegradation in outdoor and indoor conditions at accelerated exposure times compared to real sunlight exposure periods. UV/VIS lamps commonly used in the chambers differ depending on their emission spectra (high, medium, and low-pressure lamps), radiation intensity, size, lifetime, and the source of UV or visible radiation (mercury, xenon, and fluorescent lamps). When UV degradation occurs, it is essential to consider the effect of environmental factors on polymer UV degradation. Weathering chambers are equipped to simulate the outdoor conditions, mainly the humidity and temperature. In these devices, samples can be exposed to simulated sunlight, various temperatures (for day and night simulation), humidity, rainfall conditions, and sometimes atmospheric contaminations (ozone, nitrogen oxide, etc.) (Jan.F. Rabek 1995).



Table 2.3 Results obtained from photodegradation of polymer/graphene nanocomposites

Matrix	Graphene Derivatives	Concentration (Wt%)	Process/Characterization	UV Test Conditions	Assessment of Photostabilization	Ref.
PP	Graphene nanoplatelets	0.5 1 2	Twin-screw extruder Rheology Mechanical ATR-FTIR	Device: Q-UV chamber Wavelength: UV-B region Exposure period: 144 h Cycle: 8 h of light at T = 50 °C followed by 4 h condensation at T = 40 °C and RH 40% ± 3.	<ul style="list-style-type: none"> <li>• Reported mechanism: UV absorber and radical scavenger</li> <li>• Optimal grapher content: 2 wt% performance improve by increasing grapher content</li> <li>• Molecular weight loss decreased from 75% in neat PP after 48 h exposure to less than 10% in the presence of 2%wt graphene.</li> <li>• Time to reach 50% loss of elongation at break increased from 16.5 h for neat PP to 60 h in the presence of 2 wt% graphene (specimen thickness: 200 μm)</li> <li>• Carbonyl index showed a rapid increase in neat PP while nanocomposites containing graphene presented a very slow rise</li> </ul>	(Mistretta et al. 2019)

Matrix	Graphene Derivatives	Concentration (Wt%)	Process/Characterization	UV Test Conditions	Assessment of Photostabilization	Ref.
PP	GO	0.1 0.5 1 2	Mini-lab extruder FTIR	Device: QUV chamber Intensity: 0.89 W/m <sup>2</sup> Wavelength: UV-B region Exposure period: 4 weeks. Cycle: (a) 8 h exposure at T = 50 °C (b) 4 h cooling with DI water	<ul style="list-style-type: none"> <li>• Reported mechanisms: UV screening and decrease of oxygen diffusion due to crystallinity enhancement</li> <li>• Optimal GO content: 2 wt%, photostability improved by increasing GO content</li> <li>• Specimen thickness: 70–100 μm</li> <li>• Carbonyl index of neat PP increased 12 times during the UV exposure, while in the presence of 2% wt GO it increased only 3 times.</li> </ul>	(de Oliveira et al. 2019)

Matrix	Graphene Derivatives	Concentration (Wt%)	Process/ Characterization	UV Test Conditions	Assessment of Photostabilization	Ref.
Polyurethane (PU)	GO vs. organic UV absorber	0.1	Solution mixing Surface roughness Surface hardness Contact angle FTIR	Device: Weathering chamber Intensity: 0.71 W/m <sup>2</sup> Wavelength: UV-A region Exposure period: 700 h Cycle: 8 h of UV radiation followed by 4 h humidity at T = 50 °C	<ul style="list-style-type: none"> <li>• Reported mechanism: UV screener and radical scavenger</li> <li>• Reduction of protection efficiency of organic UV absorber by time (after around 400 h)</li> <li>• GO maintains its performance during 700 h exposure</li> <li>• Tested specimen thickness: 50–60 μm</li> <li>• Roughness increment after 700 h decreased from 195% in neat sample to 180% in the presence of organic UV absorber and 65% in the presence of 0.1 wt% GO</li> <li>• Hardness retention after 700 h UV exposure increased from 55% in neat PU to 61% in the presence of organic UV absorber and 75% by adding 0.1 wt% GO to PU</li> </ul>	(Hasani et al. 2018)

Matrix	Graphene Derivatives	Concentration (Wt%)	Process/ Characterization	UV Test Conditions	Assessment of Photostabilization	Ref.
PU	Graphene	2 4 6	Lay-up technique ATR- FTIR AFM Contact angle	Q-UV chamber Wavelength: UV-A Exposure period: 20 days Cycle: 12 h exposure to UV 12 h salt spray at T = 32 °C	<ul style="list-style-type: none"> <li>• Reported mechanism: UV absorber</li> <li>• Optimal graphene content: 2 wt%, further increase in concentration did not have significant effect on photostability</li> <li>• Tested specimen thickness: 75 μm</li> <li>• Change in contact angle after 20 days of UV exposure decreased from 35% in neat PU to 11% in PU containing 2 wt.% graphene</li> <li>• AFM revealed the reduction of formation of pit and cracks on the surface after UV exposure in the presence of 2 wt% graphene.</li> </ul>	(Nuraje et al. 2013a)

Matrix	Graphene Derivatives	Concentration (Wt%)	Process/ Characterization	UV Test Conditions	Assessment of Photostabilization	Ref.
Poly(vinyl alcohol)(PVA)	GO	1 3 5 10	Solution Calculating the amount of soluble gel	Device: mercury vapor lamp intensity:500, 1000, 1500, 2000 KJ/m <sup>2</sup> Wavelength: 254 nm Temperature: room temperature	<ul style="list-style-type: none"> <li>•Optimal content: 5 wt% GO</li> <li>•The amount of soluble gel after UV radiation decreased from 65% to 53% in the presence of 5 wt% of GO indicating lower rate of molecular weight reduction</li> </ul>	(Moon et al. 2011)
Poly(2-methoxy-5-(2-ethylhexyloxy)-1,4-phenylenevinylene) (MEH-PPV)	rGO	0.05, 0.1, 0.15, 0.2, 0.25, 0.3, 0.4, 0.5	Solution UV absorption peak before and after exposure	Device: 365 nm UV lamp Intensity: 0.978 mW/cm <sup>2</sup> , Exposure period: 4, 8, 12, 16 h Temperature: room temperature	<ul style="list-style-type: none"> <li>•Reported mechanism: Quencher</li> <li>•Optimal rGO content: 0.5 wt%, photostabilizing effect improved by rGO content</li> <li>•UV absorption peak keep constant after UV exposure in the presence of rGO, which is a sign of photostability</li> </ul>	(Ran et al. 2012)

Matrix	Graphene Derivatives	Concentration (Wt%)	Process/Characterization	UV Test Conditions	Assessment of Photostabilization	Ref.
Cellulose Acetate (CA)	GO	0.1 0.25 0.5	Solution	Ultraviolet-visible (UV-vis) spectroscopy (200–800 nm) On an Agilent/Varian Cary 50 UV-vis spectrophotometer.	<ul style="list-style-type: none"> <li>• Reported mechanism: UV screener/absorber</li> <li>• Optimal GO content: 0.5 wt%, UV shielding effect increased by GO content</li> <li>• Specimens thickness: 20 <math>\mu\text{m}</math></li> <li>• CA films containing 0.5% GO shielded 57% of UV</li> </ul>	(de Moraes et al. 2015)
PU	Graphene/CNT	1 (different ratios)	Solution ATR-FTIR	Device: UV lamp Intensity: 550 mW/cm <sup>2</sup> Wavelength: 366 nm Exposure period: 400 h T = 55 °C	<ul style="list-style-type: none"> <li>• Reported mechanism: radical scavenger</li> <li>• Optimal ratio: best performance at 10:1 (graphene/CNT) ratio, which led to better exfoliation of graphene</li> <li>• Hydroxyl index (indicative of degradation in FTIR test) increased in neat polymer to 10 while in the presence of 1 wt% of graphene and CNT, it showed a smaller increment of 1.5.</li> </ul>	(Prosheva et al. 2019)

Matrix	Graphene Derivatives	Concentration (Wt%)	Process/Characterization	UV Test Conditions	Assessment of Photostabilization	Ref.
Polyamide 6 filaments coated with PU	rGO	1 2 4	Solution Tensile strength	Device: UV lamp Power: 125 w Wavelength: 365 nm Exposure time: 4, 10, 20, 40, 60, 100 h	<ul style="list-style-type: none"> <li>• Optimal rGO content: 4 wt%, stabilizing action improved by rGO content</li> <li>• The tensile strength loss rate after 100 h exposure decreased from 85% to 46% in the presence of 4% r-GO</li> </ul>	(Tian et al. 2018)
PU	GO	0.4 1.2	Solution ATR-FTIR	Device: weathering chamber Intensity: 140 W/m <sup>2</sup> Wavelength: 295–400 nm Exposure period: ranging from 15 d–140 d Temperature: 55 °C Humidity: 0 and 75%	<ul style="list-style-type: none"> <li>• Reported mechanism: UV screener/absorber</li> <li>• Optimal GO content: 0.4 wt%,</li> <li>• Under dry UV conditions: the presence of GO increased the durability</li> <li>• Under humid UV conditions: the presence of GO did not improve the durability</li> <li>• Degradation decreased by 35% compared to neat matrix based on growth in carboxylic acid peak in FTIR</li> </ul>	(Goodwin Jr, Lai, et al. 2020)

Matrix	Graphene Derivatives	Concentration (Wt%)	Process/Characterization	UV Test Conditions	Assessment of Photostabilization	Ref.
TPU	Graphene	3	Twin-screw extruder FTIR	Device: weathering chamber Intensity: 140 W/m <sup>2</sup> Wavelength: 295–400 nm Exposure period: ranging from 0–60 d Temperature: 55 °C Humidity: 0 and 75%	<ul style="list-style-type: none"> <li>• Reported mechanisms: UV absorber, radical scavenger, increased cross-linking in graphene/TPU nanocomposites</li> <li>• Under both weathering conditions (dry and humid), 3% graphene decreased photodegradation rate by 10 times, based on FTIR test and thickness loss. (specimens thickness: 2 mm)</li> </ul>	(Goodwin Jr, Shen, et al. 2020)
Epoxy	Graphene	1	FTIR Contact angle	Device: weathering chamber Intensity: 60 W/m <sup>2</sup> Wavelength: 300–400 nm Exposure period: 500, 1000, 2500 h Temperature: 65 °C	<ul style="list-style-type: none"> <li>• Presence of graphene improve the stability of epoxy against UV</li> </ul>	(Zepp et al. 2020)



## 2.5 Discussion

From Table 2.3, it can be seen that graphene can be used as an efficient photostabilizer. However, the actual reasons for its efficiency are barely understood, and studies regarding a clearer understanding of the role of graphene as a photostabilizer should be carried out. In particular, the influence of graphene chemical modification should be studied. Also, the contribution of the different mechanisms of action (UV absorbers, UV screeners, quenchers, radical scavengers, physical barriers, and changes in crystallinity) should be better understood. It is necessary to find out the role of  $sp^2$  bonds and oxygen-containing groups on the performance of graphene as a photostabilizer. To investigate the above mentioned factors, UV absorption and radical scavenging effect of graphene and GO should be compared using appropriate techniques such as UV-vis spectroscopy and electron paramagnetic resonance (EPR). Moreover, the final photodegradation rate of polymers in the presence of graphene with different chemical structures should be compared. To separate the contribution of different mechanism of actions, samples containing graphene or GO should be prepared with different morphology and dispersion rates of graphene into the polymer matrix (highly oriented or randomly dispersed) and should be exposed to the same weathering conditions. Different morphologies and dispersions of graphene have different physical barrier effects against oxygen diffusion into polymer matrix, which provide good information about the contribution of the physical barrier effect of graphene on photostabilization of polymers.

## 2.6 Conclusions

In this review, the role of graphene and graphene derivatives as a new type of polymer photostabilizer has been discussed in detail. In particular, the protective mechanisms that this class of materials undertake were reviewed and linked to morphological and functional features intrinsic to graphene's unique structure and chemistry.

Five complementary routes of action taking place during the initiation and propagation steps of photodegradation were identified. The first line of defense involves UV screening, UV absorption, and quenching. These three mechanisms occur in the initiation step and are

respectively associated with the high surface area, the presence of  $\pi$ -bonds, and the excellent electron acceptor/donor property of graphene. Besides, radical scavenging and oxygen barrier property ensure antioxidant protection. They act during the propagation step in order to disrupt and slow down the rate of the photodegradation process and are respectively attributed to the presence of  $sp^2$  carbon sites and surface defects, as well as the 2D geometry of graphene. In particular, free radical scavenging occurs through hydrogen donation from hydroxyl groups and radical adduct formation at the  $sp^2$  carbon sites. The latter is predominant, which makes graphene more efficient than GO and rGO in that aspect. In addition to direct mechanisms, graphene-based nanocomposites can benefit from additional indirect effects that may lead to higher photostability, such as potential improvement of crystallinity and glass transition temperature.

The unique synergy between all these mechanisms makes graphene and graphene derivatives promising candidates for industrial applications where high and long-term photostability are needed. Efficient protection can be ensured for a wide range of polymers at low loadings, starting from 0.1–1 wt%. However, higher performance is expected for graphene compared to GO and rGO, thanks to its stronger antioxidant activity and hydrophobic nature, which are more advantageous in weathering conditions with high humidity levels.

Compared to conventional UV stabilizers, the use of an industrial few-layer graphene grade as a UV stabilizer may represent an efficient and cost-effective solution to problems related to long-term stability, release of photodegradation products, and toxicity aspects, which have been widely reported for HALS, organic UV absorbers, and carbon black, for instance. Furthermore, graphene's physical barrier properties set it apart from other low aspect ratio fillers used for photostabilization, including carbon black.

Finally, the diversity of the functional properties that can be tuned and enhanced by the addition of graphene to polymer matrices, including electrical, mechanical, thermal, and processability, which represents another strong argument supporting its use in industrial applications where

improved performance is required along with durability and weathering resistance. These applications include recycled, automotive, and coating materials, among others.



## CHAPTER 3

### PHOTO-STABILIZATION MECHANISMS OF HDPE BY A COMMERCIAL FEW-LAYER GRAPHENE

Samira Karimi<sup>1</sup>, Emna Helal<sup>1,2</sup>, Giovanna Gutierrez<sup>2</sup>, Nima Moghimian<sup>2</sup>, Eric David<sup>1</sup>,  
Mazen Samara<sup>1</sup> and Nicole Demarquette<sup>1\*</sup>

<sup>1</sup> Mechanical Engineering Department, École de Technologie Supérieure, 1100 Notre-Dame St W, Montréal, QC, Canada H3C 1K3

<sup>2</sup> NanoXplore Inc., 4500 Thimens Boulevard, Saint-Laurent, QC, Canada H4R 2P2

Published in *Polymer Engineering and Science*<sup>2</sup>, October 2023

#### Abstract

This work studied few-layer graphene (FLG) dominant action mechanisms as a photo-stabilizer. High-density polyethylene (HDPE) containing 0 to 0.5 wt% FLG were exposed to UVA radiation in a QUV chamber, according to ASTM G154 for different exposure times, ranging from 0 to 672 hours. The chemical, rheological, and mechanical properties were tracked using Attenuated Total Reflection- Fourier Transform Infrared (ATR-FTIR), rheological measurements, and tensile tests. The experimental results showed that the addition of only 0.25 wt% FLG fully stabilized 1-3 mm thick HDPE for an exposure time of 672 hours. Electron Paramagnetic Resonance (EPR) test was performed on the UV-exposed mixture of hydrogen peroxide (H<sub>2</sub>O<sub>2</sub>) and the FLG aqueous suspensions (0, 0.2, 1, and 5 mg/ml), to study the FLG performance and mechanisms as a photo-stabilizer. The results showed that FLG effectively decreased the characteristic EPR signal intensity due to both UV absorption/reflection, and free radical scavenging. 57% of the reduction was found to be due to UV absorption/reflection and 43% due to free radical scavenging. It is demonstrated that UV absorption/reflection and free radical scavenging are the dominant ones among the three

---

<sup>2</sup> Polym Eng Sci.2023;63(11):3879-3890

FLG photo-stabilizing mechanisms (UV absorption/reflection, free radical scavenging, and physical barrier to oxygen).

**Keywords:** Photo-Oxidative degradation, Graphene, Photo-stabilizer, Physical barrier, Radical scavenger, UV absorption/ reflection.

### 3.1 Introduction

Graphene, a two-dimensional carbon-based material, has attracted the attention of both academics and industrialists due to its exceptional chemical and physical properties(Choi et al. 2010; Randviir, Brownson, and Banks 2014; Karimi et al. 2022). In recent years, graphene has emerged as a promising alternative to traditional photo-stabilizers, since the incorporation of traditional stabilizers, such as carbon black(Horrocks et al. 1999), phenolic and nonphenolic UV absorbers(Kumar et al. 2009), hindered amine light stabilizers (HALS)(Horrocks and Liu 2003; Gijssman, Hennekens, and Tummers 1993; Bodur, Bakkal, and Sonmez 2018), and phenolic antioxidants, to the thermoplastics may lead to various issues such as health concerns (Tipton and Lewis 2008; Chaudhuri et al. 2018), toxicity(Alotaibi et al. 2015b; Moghimian and Nazarpour 2020), migration and efficiency decay over time.

Furthermore, graphene offers a more sustainable and safer alternative to most of these traditional photo-stabilizers. For instance, a recent study on the dermal, inhalation, and gene toxicity of 6-10 layer graphene (FLG) confirmed the absence of any adverse effects associated with this FLG(Moghimian and Nazarpour 2020), making it a safe option for photo-stabilization. Additionally, the presence of the  $\pi$  bonds allows graphene to become both a strong electron acceptor and donor(Dash, Pattanaik, and Behera 2014), and enables it to absorb light in the UV region, through  $\pi \rightarrow \pi^*$  transitions(Dash, Pattanaik, and Behera 2014; Johra, Lee, and Jung 2014). Moreover, graphene's 2D structure enhances its ability to act as a physical barrier to the diffusion of low molecular weight substances, such as oxygen, into the polymer(Yoo et al. 2014; Cui, Kundalwal, and Kumar 2016), as well as, augments UV light reflection (Qu et al. 2014).

Consequently, graphene derivatives (Graphene, Graphene Oxide (GO), and reduced GO (rGO)) have been used to photo-stabilize several polymers, such as, Polypropylene (PP)(de Oliveira et al. 2019; Mistretta et al. 2019; Mittal and Patwary 2016), Polyurethane (PU) (Hasani et al. 2018; Nuraje et al. 2013b; Goodwin Jr, Shen, et al. 2020), Poly Vinyl Alcohol (PVA) (Moon et al. 2011), and Cellulose Acetate (CA) films(de Moraes et al. 2015). The polymers' lifetime was, successfully, extended, and their stability against sunlight improved via several mechanisms such as UV absorption/ reflection (Kolanthai et al. 2015; Hasani et al. 2018), free radical scavenging(Prosheva et al. 2019; Qiu et al. 2014; Karimi et al. 2020), and oxygen blocking(Cui, Kundalwal, and Kumar 2016).

The role of graphene, as a photo-stabilizer, however, is poorly understood. More insight into its photo-stabilization mechanism is essential to optimize its use. Most of the published studies in this field have been carried out using GO and rGO. This work aims at exploring the potential use of commercial 6-10 layer graphene (FLG), produced by a mechano-chemical exfoliation process, to photo-stabilize HDPE, and investigating the mechanisms behind its stabilization effect. Such commercial-grade FLG has proven to improve several physical properties of recycled HDPE(Diallo et al. 2022). The potential of this FLG to enhance UV protection would eliminate or significantly reduce the use of traditional photo-stabilizers. The choice of HDPE stems from the fact that polyolefins constitute the predominant category of synthesized polymers employed today, particularly in outdoor applications.

In this context, HDPE containing 0, 0.1, 0.25, and 0.5wt% FLG were investigated. They were exposed to UV in a QUV chamber. Then, changes in chemical, rheological, and mechanical properties were studied as a function of UV exposure time. Subsequently, UV absorption/reflection, and free radical scavenging of graphene were evaluated using UV-vis, and EPR spectroscopy.

## 3.2 Materials and Methods

### 3.2.1 Materials

Injection grade HDPE (Alathon H5618) from LyondellBasell Co. and FLG, GrapheneBlack 3X from NanoXplore Inc. were used in this work. The characteristics of both materials are shown in Tables 3.1 and 3.2.

Table 3.1. Physical Properties of HDPE

Property	Test method	value
Melt flow index(@190°C,2.16kg)	ASTM D 1238	18 g/10min
Melting temperature	ASTM D 3418	130.2°C
Density	ASTM D 1505	0.956 g/cm <sup>3</sup>

Table 3.2. Physical Properties of FLG from the supplier's datasheet.

Property	Value
Primary particle size ( $\mu m$ )	1-2
	D10=5
Agglomerate size ( $\mu m$ )	D50=14
	D90=33
Number of layers	6-10
Bulk density	0.2-0.3 g/cm <sup>3</sup>

Hydrogen peroxide solution (H<sub>2</sub>O<sub>2</sub>, 30 % (w/w)) and 5,5-Dimethyl-1-pyrroline N-oxide (DMPO), purchased from Sigma-Aldrich, were used to prepare the liquid mixtures for the EPR tests.



### 3.2.2 Composites Preparation

HDPE containing 0, 0.1, 0.25, and 0.5 wt% of FLG were prepared by melt mixing using a HAAKE twin-screw extruder, Model Rheomex OS PTW16/40 (L/D =40). The screw speed was set at 100 rpm, and the temperature profile was 180, 180, 180, 180, 190, 200, 200, 190, 190, 180, 180 °C, from the first heating zone to the die. The polymer was fed from a hopper at a rate of 7% of the extruder's screw speed. Each sample was extruded twice to obtain a homogeneous dispersion of FLG within the HDPE matrix.

After extrusion, samples for scanning electron microscopy (SEM), ATR-FTIR, rheological, and UV-vis spectroscopy tests were compression molded. The pellets were pre-heated for 5 minutes at 180 °C. Subsequently, they were pressed at 5 MPa for 5 minutes at that temperature. Finally, the molded specimens were water cooled down at 5 MPa pressure. The dumbbell-shaped specimens for mechanical tests, type I, with a thickness of 3.2 mm and a width of 12 mm, were prepared using an Arburg Allrounder 221K-350-100 Injection molding machine.

### 3.2.3 Photo-degradation Process

The compressed and injected samples were placed in a QUV chamber, an accelerated weathering tester, equipped with lamps type UVA-340. The samples were exposed to UV according to cycle A of ASTM G154 standard, consisting of 8 hours of UV exposure, followed by 4 hours of water condensation, as presented in Table 3.3. The samples were removed after 168, 336, and 672 hours of exposure to evaluate their properties. 672 hours were deemed sufficient to significantly reduce the HDPE mechanical properties.

Table 3.3. Photo-degradation procedure

Step	Function	Irradiance (W/m <sup>2</sup> )	Temperature (°C)	Time (h:m)
1	UV	0.89	60	8:00
2	Condensation	n/a	50	4:00

Each sample was designated as HDPEUV $x$  or HDPE $y$ UV $x$ , where  $x$  refers to exposure time (hours) and  $y$  FLG concentration. For example, HDPE05UV168h corresponds to HDPE containing 0.5 wt% FLG exposed to UV for 168 hours.

### 3.2.4 Sample Preparation for EPR

FLG suspensions in Deionized (DI) water with a concentration of 0, 0.2, 1, and 5 mg/ml, were prepared using an ultrasonic bath with a frequency of 60 kHz for a duration of 40 minutes. Then, 2 ml of the prepared FLG suspensions was added into a mixture of 3 ml H<sub>2</sub>O<sub>2</sub> (50 mM), and 0.5 ml 5,5-Dimethyl-1-pyrroline N-oxide (DMPO) (50 mM) (as spin trapper). The final mixture was exposed to UV using LED UV lamps (20V, 700mA) with a wavelength of 365nm for 15 minutes. Finally, a small amount of the exposed mixtures was extracted into a glass capillary tube for the EPR test. It should be mentioned that UV exposure of the mixture leads to photolysis of H<sub>2</sub>O<sub>2</sub> and creation of  $^{\circ}OH$  radicals, which can form DMPO-OH adduct. These adducts are detectable via EPR (Grela, Coronel, and Colussi 1996).

To separate the contributions of UV absorption/reflection and free radical scavenging to the FLG photo-stabilizing effect, a specific control test was designed, as shown schematically in Figure 3.1.

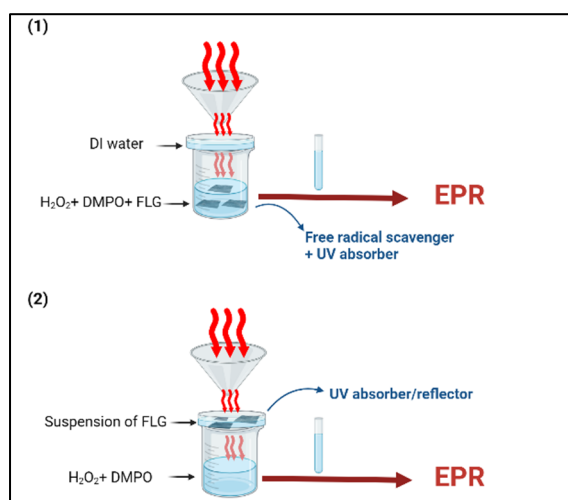


Figure 3.1 Schematic of sample preparation for EPR

A petri dish was placed on the top of the beaker containing H<sub>2</sub>O<sub>2</sub>/DMPO, and the UV radiation was directed towards the center using a funnel, as shown in Figure 3.1.

In the first test, 2 ml of FLG suspensions (1mg/ml) were added to H<sub>2</sub>O<sub>2</sub> inside the beaker. In this way, the presence of FLG would affect the hydroxy radicals through both UV absorption/reflection and free radical scavenging mechanisms.

In the second test, 2 ml of FLG suspensions (1mg/ml) were put in the petri dish on the top of the beaker containing H<sub>2</sub>O<sub>2</sub>/DMPO, and then exposed to the UV, as shown in Figure 3.1. This way, only UV absorption/reflection takes place. No °OH scavenging occurs since FLG is not in contact with H<sub>2</sub>O<sub>2</sub>.

In both cases, a small amount of the exposed mixtures was extracted by a glass capillary tube for the EPR test. The difference between the first and second test yields the radical scavenging contribution.

### 3.3 Characterization

The FLG dispersion within the HDPE matrix was analyzed using a SU-8230 Hitachi ultra-high-resolution field emission scanning electron microscope (FE-SEM), by observing the cross-section of the gold-coated samples.

ATR-FTIR spectra of the samples were obtained using a Perkin-Elmer FTIR spectrometer, Spectrum two™, equipped with a diamond crystal. The tests were carried out on the surface of 1 mm thick samples, over a wave numbers range of 400-4000 cm<sup>-1</sup>, with a resolution of 4 cm<sup>-1</sup> and a number scan of 10. These spectra were used to assess the photo-oxidative degradation of the samples by calculating the carbonyl index (CI) given by equation 3.1:

$$CI = \frac{A_{C=O}}{A_{CH_2}} \quad (3.1)$$

Where  $A_{C=O}$  and  $A_{CH_2}$  are the peak areas of the C=O and CH<sub>2</sub> groups located within 1680-1800 cm<sup>-1</sup> and 680-760 cm<sup>-1</sup> regions, respectively. To ensure the reliability of the reference area in the study, the ratio of the absorbance peaks' intensities located at 730 cm<sup>-1</sup> and 720 cm<sup>-1</sup>,  $I_{730}/I_{720}$  were analyzed. The results revealed that  $I_{730}/I_{720}$  remained constant upon FLG addition and increasing the UV exposure time, confirming the stability of the chosen reference area. The measurements were repeated three times for each sample and the average is reported in the results section.

The gold-coated surfaces of exposed samples were observed using a Scanning Electron Microscope (SEM), Hitachi TM3000 TableTop.

The samples, before and after UV exposure, were subjected to small amplitude oscillatory shear using a MCR 501 Anton Paar rheometer. The experiments were carried out, under a N<sub>2</sub> atmosphere at a temperature of 160°C using parallel plate geometry in the linear viscoelastic region. The diameter and plate gap were 25 mm and 1 mm, respectively.

The samples tensile properties were evaluated according to ASTM D638 at room temperature and a cross-head speed of 50 mm/min on an MTS Alliance RF/200 testing machine. Five specimens with 3.2 mm thickness and 12 mm width were used for each sample and the average value is reported.

UV-vis spectroscopy tests were carried out on non-aged thin samples, using a UV-vis spectrophotometer (Varian Cary 300 Bio), operated in the absorption mode in the wavelength range of 200-800 nm.

Electron Paramagnetic Resonance (EPR) spectroscopy tests were recorded at room temperature using an EPR spectrometer (Bruker; Germany) operating at a power of 20 dB, center field of 3514G, and sweep width of 100G.

## 3.4 Results

### 3.4.1 Dispersion of FLG

Figure 3.2 presents a typical HDPE morphology containing 0.5 wt% FLG, HDPE05UV0. The red arrows are used to indicate the presence of FLG within the HDPE matrix. It is observed that the FLG is uniformly distributed throughout the HDPE matrix. Size analysis was performed using Image J software and the results showed that FLG aggregates exhibit a broad size distribution ranging from a few to approximately 30  $\mu\text{m}$ .

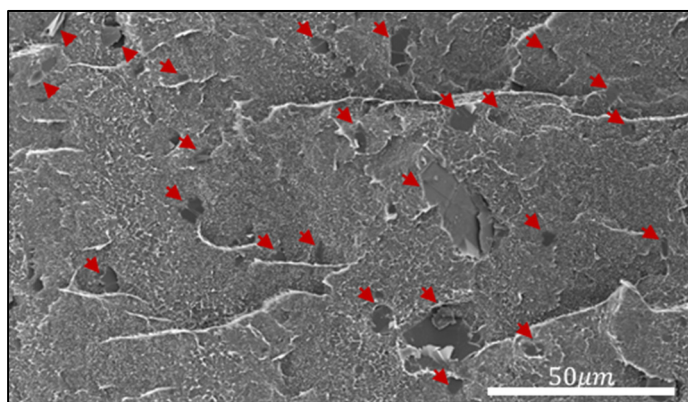


Figure 3.2 SEM image of HDPE05UV0

### 3.4.2 Chemical Properties

Figure 3.3(a) presents HDPE's FTIR absorption spectra at different UV exposure times. It can be seen from Figure 3.3(a) that UV exposure causes the appearance of new absorption peaks at 1715, and 1740  $\text{cm}^{-1}$ , corresponding to internal ketones, and ester groups, respectively (Shehzad, Ahmad, and Al-Harhi 2019; Bertoldo et al. 2003). Moreover, the shape and intensity of these peaks vary as a function of UV exposure time. The calculated CI for HDPE and its composites are shown in Figure 3.3(b), where the error bars indicate the standard deviation for three replicas of one specific sample. As expected (Stark and Matuana 2004; Fairbrother et al. 2019; Rabek 2012), it can be seen that, the CI of HDPE shows a progressive growth, as a function of UV exposure time indicating photo-oxidative degradation.

The addition of as little as 0.1 wt% FLG into HDPE, HDPE01, retards the formation of carbonyl groups, where CI starts to increase only after 168 hours of UV exposure. Furthermore, the rate of that increase is lower than that of neat HDPE. Higher FLG concentrations in HDPE025 and HDPE05, further retard the carbonyl formation and decelerate the CI growth causing it to appear after 336 hours of UV exposure. These results indicate a retardation effect of FLG on HDPE photo-oxidative degradation.

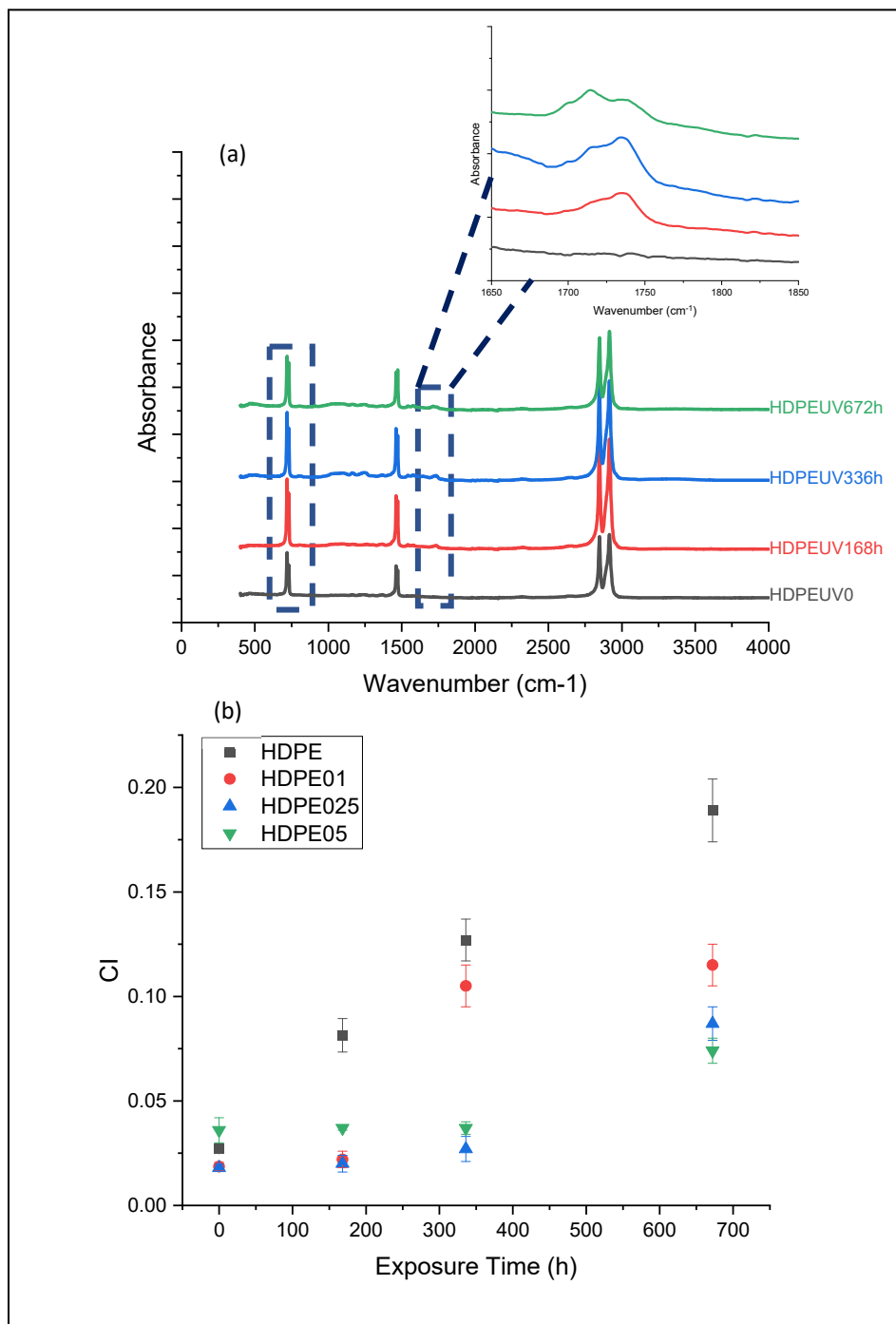


Figure 3.3 (a) FTIR absorption spectra of HDPE with different exposure times, b) CI of HDPE and composites as a function of exposure time

### 3.4.3 Rheology

Figures 3.4(a-d) present the HDPE complex viscosity and corresponding composites which were exposed to UV for different durations. In the case of HDPE composites (Figures 3.4(b-d)), only the complex viscosities before UV and after 672 hours of UV exposure are presented because the viscosity curves for the intermediate exposure times overlapped. It can be seen from Figure 3.4(a) that exposure to UV for a duration of 168 hours results in an increase in the HDPE viscosity at low frequencies. Conversely, when the HDPE sample was exposed for more than 168 hours, its viscosity starts to decrease over the whole range of frequencies.

These results indicate that at the early stage of UV exposure, crosslinking is the dominant mechanism, whereas, at the longer exposure times, chain scission becomes more prominent. Similar conclusions were previously reported for HDPE (Wagner et al. 2017) and LLDPE (Hussein 2007), by analyzing the gel content of samples exposed to UV. In the case of HDPE01, changes in viscosity are only observed after 672 hours of UV exposure. However, once the concentration of FLG becomes equal to or higher than 0.25 wt%, no significant change in viscosity is observed indicating a photo-stabilization plateau.



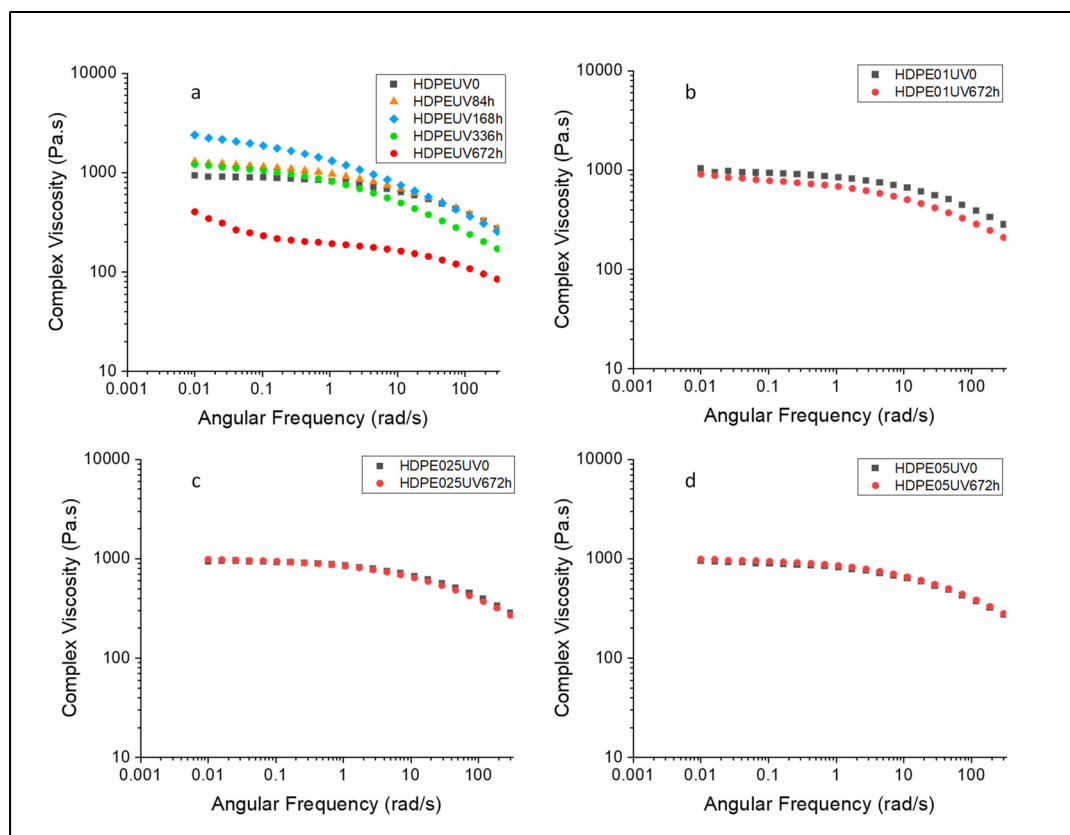


Figure 3.4 Complex viscosity of (a) HDPE, (b) HDPE01, (c) HDPE025, (d) HDPE05 for different exposure times

### 3.4.4 Surface Morphology

Figures 3.5(a-f) present the change in the exposed surfaces of HDPE, HDPE01, and HDPE05, at low and high magnifications, after 672 hours of UV exposure. As we can see in Figures 3.5(a) and (b), deep cracks of up to  $20\mu\text{m}$  in width, can be observed on the surface of HDPE, after 672 hours of UV exposure, indicating surface erosion during photo-oxidative degradation. On the other hand, the surface of both HDPE01 and HDPE05 remained without any cracks, even after 672 hours of exposure. The images of HDPE025 exposed surface, not presented here, were similar to HDPE01 and HDPE05, and showed no cracks.

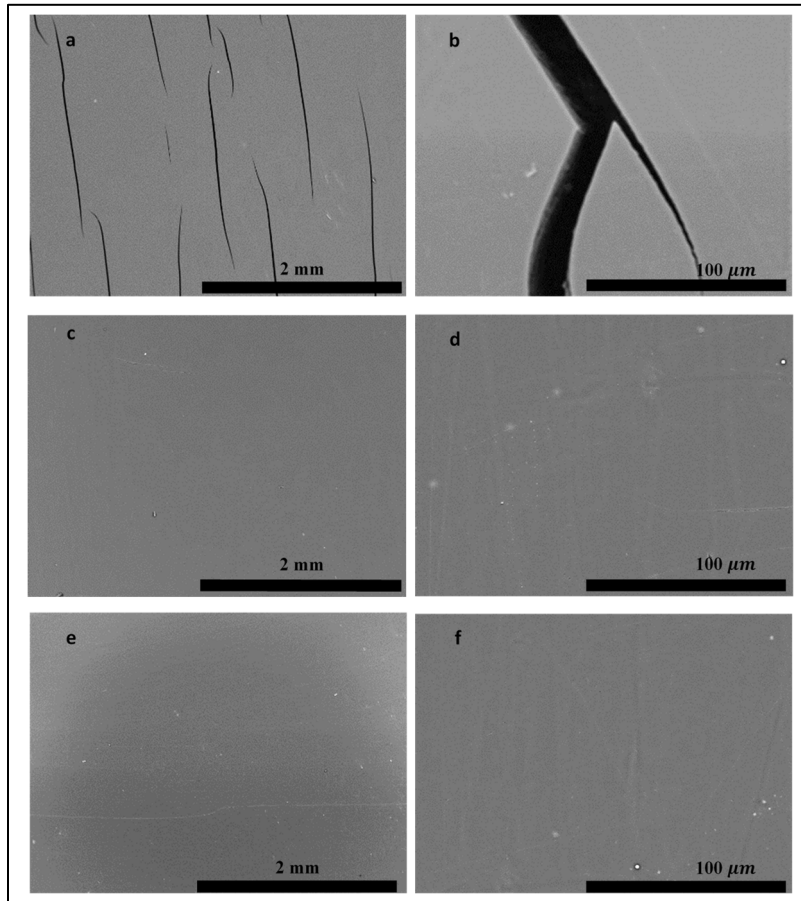


Figure 3.5 SEM images of exposed surface of (a-b) HDPEUV672h, (c-d) HDPE01UV672h, and (e-f) HDPE05UV672h

### 3.4.5 Mechanical Properties

Figure 3.6(a) presents tensile stress-strain curves for HDPE and its composites, prior to and after 672 hours of UV exposure. These curves were used to calculate tensile strength, elongation at break (and its retention), Young modulus, and their changes after 672 hours of UV exposure, presented in Figure 3.6(b) and Table 2.4. It can be seen from Figure 3.6(b) and Table 2.4 that there is a significant reduction in tensile strength and elongation at break in HDPE and HDPE01 after 672 hours of UV exposure, while there is no significant change in the Young modulus. The more stable behavior of the Young modulus in HDPE and HDPE01 could be due to the opposing effects of crosslinking and chain scission on stiffness and modulus(Grigoriadou et al. 2011), which occurred during photo-oxidative degradation as

confirmed by the rheological results. HDPE025 and HDPE05, containing higher concentrations of FLG, however, exhibit a more stable behavior in terms of tensile strength and elongation at break, indicating the photo-stabilizing effect of FLG at those concentrations.

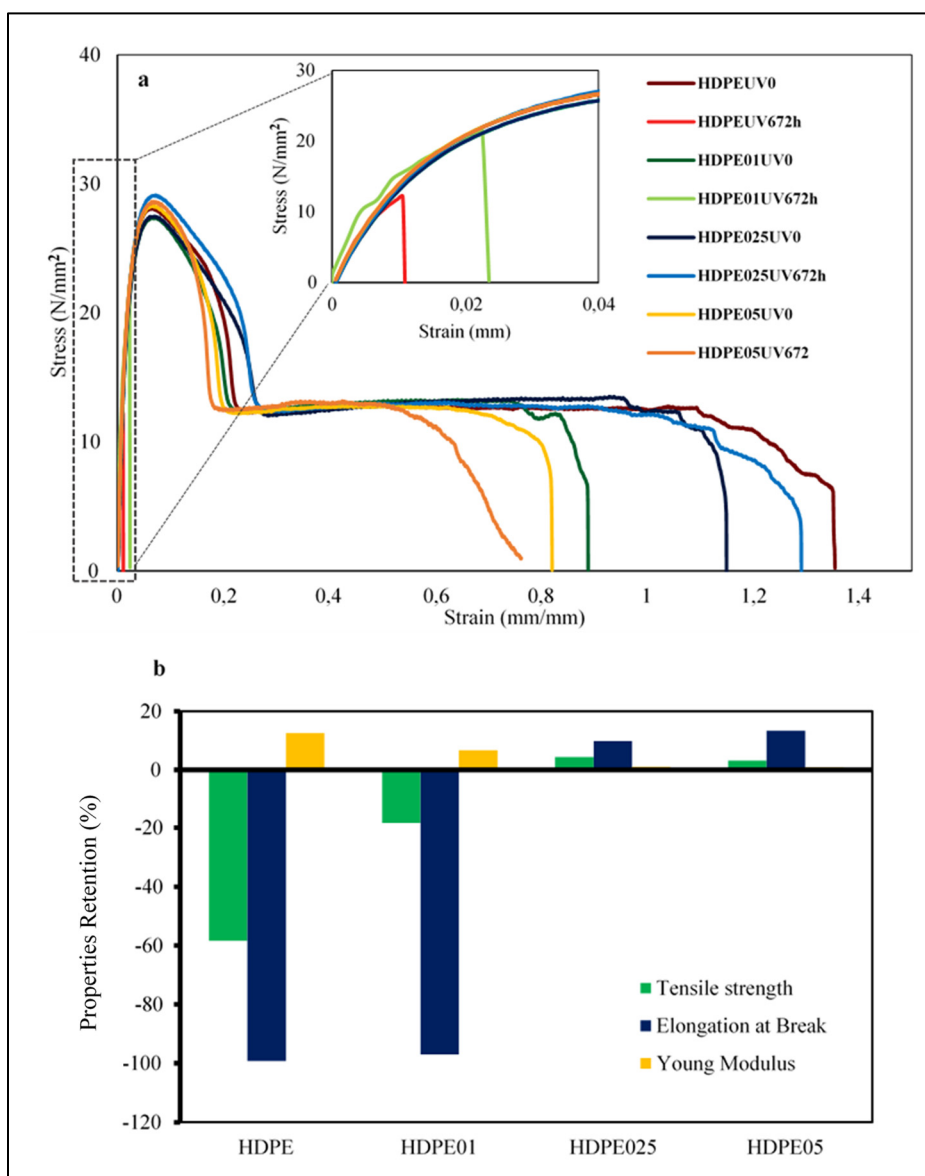


Figure 3.6 (a) Stress-strain curves of HDPE, HDPE01, HDPE025, and HDPE05, before and after 672h of exposure, (b) properties retention after 672h of exposure for HDPE, HDPE01, HDPE025, and HDPE05

Table 3.4 Mechanical properties of HDPE, HDPE01, HDPE025, and HDPE05 before and after 672 hours of UV exposure

Sample	Elongation at Break (%)	Retention of elongation at break (%)	Young Modulus (GPa)	Tensile Strength (MPa)
HDPEUV0	126 ±22	100	1.6 ±0.02	28.1 ± 0.1
HDPEUV672h	1 ±0.8	0.8	1.8 ±0.04	11.7 ±0.6
HDPE01UV0	82 ± 5	100	1.5 ± 0.03	26.7 ± 0.5
HDPE01UV672h	2.4 ± 0.1	3	1.6 ±0.02	21.8 ± 0.4
HDPE025UV0	117 ±12	100	1.6 ± 0.04	27.2 ± 0.5
HDPE025UV672h	128 ±26	109	1.6 ±0.07	28.3 ± 0.6
HDPE05UV0	84 ±13	100	1.7 ± 0.01	28.3 ± 0.2
HDPE05UV672h	96 ±21	114	1.7 ± 0.03	29.2 ± 0.6

The findings presented in the previous sections have demonstrated the FLG ability to stabilize HDPE against photo-oxidative degradation at concentrations equal to and above 0.25 wt%. Although similar behavior has been observed by other authors for other polymers such as PP, PU, and PVA (de Oliveira et al. 2019; Hasani et al. 2018; Moon et al. 2011), the exact mechanism behind this stabilization effect is still unclear to our knowledge. To find out the mechanism behind this stabilization, further analyses were conducted to investigate the FLG ability to act as a UV absorber/reflector, and free radical scavenger. The results of these analyses are presented in the following section to provide a comprehensive understanding of the FLG's photo-stabilizing mechanism in HDPE composites.

#### 3.4.6 Photo-stabilization Mechanism of FLG

Figure 3.7(a) presents the UV-Vis absorbance spectra of HDPE and its composites containing 0.1, 0.25, and 0.5 wt% FLG. It can be seen from Figure 3.7(a) that the FLG addition to HDPE increases the composites' UV absorbance in the studied range of wavelengths, with a new absorption peak appearing at a wavelength of 240 nm. This peak corresponds to  $\pi \rightarrow \pi^*$  transition of aromatic C-C bonds in graphene structure (Çiplak, Yildiz, and Çalimli 2015; Krishnamoorthy, Kim, and Kim 2013), and its intensity increases with FLG concentration. The increase in the composites' UV absorbance, particularly at higher wavelengths, suggests a reduction in UV transmittance compared to that of neat HDPE. To quantify this effect, the UV

absorbance data were used to calculate the UV transmittance for HDPE and its composites, at the wavelength of 340 nm, which corresponds to the wavelength used to study samples degradation, using equation 3.2:

$$\text{Transmittance (\%)} = 10^{2-\text{Absorbance}} \quad (3.2)$$

The calculated UV transmittance results are presented in Figure 3.7(b), where it can be seen that as the concentration of FLG increases in the composites, the UV transmittance decreases, indicating that less UV light passes through the samples. This effect can be attributed to the FLG UV shielding properties, which may be a combination of absorption and reflection. In fact, the presence of  $\pi$  bonds can absorb UV radiation and FLG large surface area can act as an effective UV barrier.

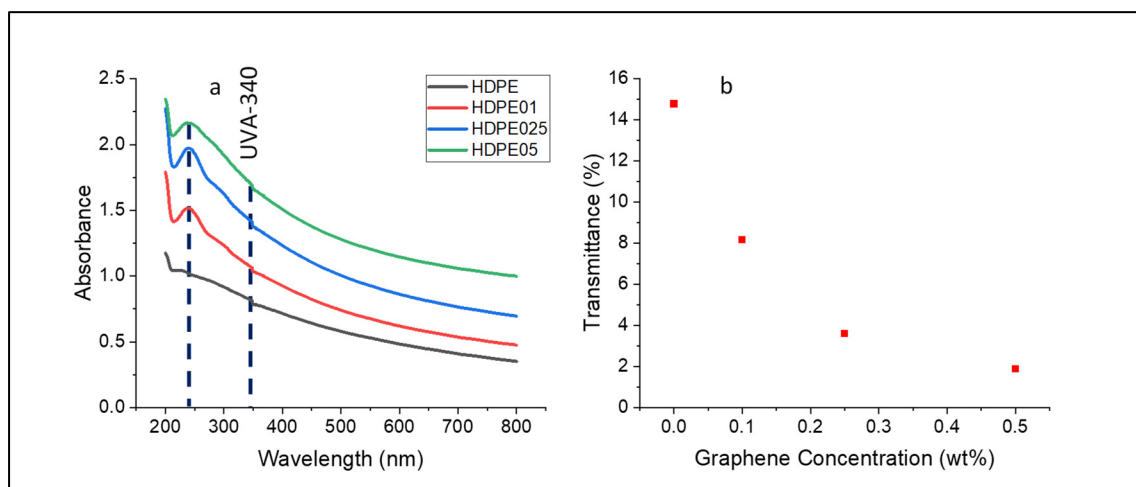


Figure 3.7 (a)Uv-vis Spectroscopy of HDPE and the composites, (b) transmittance at 340nm as a function of graphene concentration

Figure 3.8(a) presents EPR spectra of the UV-exposed  $\text{H}_2\text{O}_2/\text{DMPO}$  mixtures without and with different FLG concentrations. The mixtures were exposed to UV radiation without a petri dish on top of the beaker, and FLG suspensions were added directly to the mixture. The results indicate that UV radiation of  $\text{H}_2\text{O}_2/\text{DMPO}$ , 0 mg/ml-G, leads to the detection of the DMPO-OH adducts' characteristic signal, which stems from the creation of hydroxyl radicals through hydrogen peroxide photolysis. The EPR signal intensity decreases with the addition of even a

small amount of FLG to the mixture (0.2 mg/ml), and further increases in FLG concentration lead to a greater reduction in the signal intensity.

This reduction in the signal intensity may involve both FLG UV absorption/reflection or  $^{\circ}OH$  scavenging effect. To investigate the separate contributions of these two effects, the control procedure mentioned in section 3.2.4 was carried out, where FLG was either placed in the mixture or separate from it, in the path of the UV radiation. The results are presented in Figure 3.8(b). These results show that the EPR signal decreases in both cases, even when FLG was not placed in the mixture. However, the reduction in the EPR signal was more significant when FLG was in the mixture, confirming a contribution of the FLG radical scavenging effect, in addition to the UV absorption/reflection mechanism.

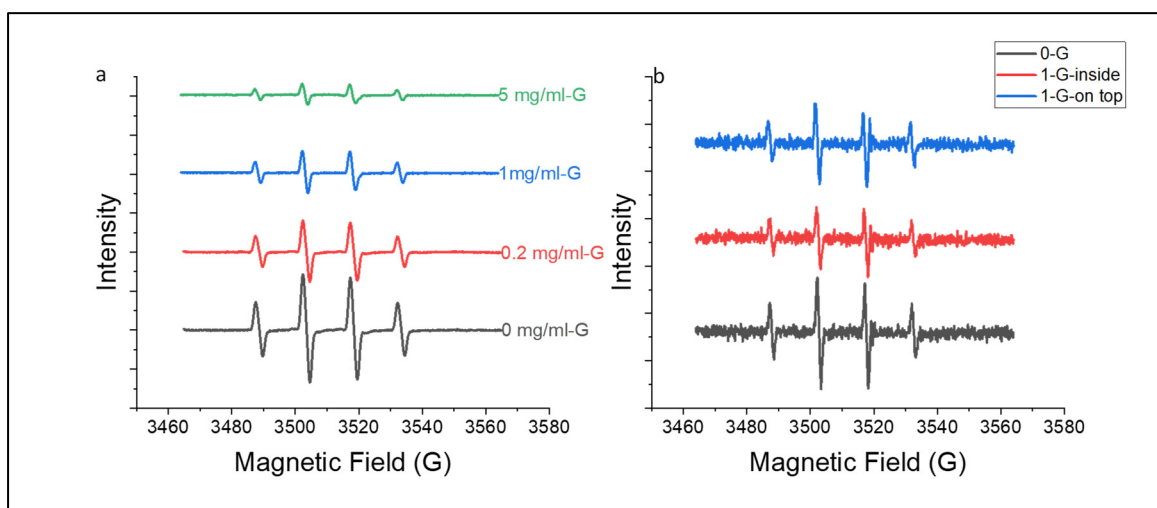


Figure 3.8 EPR spectra

### 3.5 Discussion

The results of this work revealed the efficient role of FLG as a photo-stabilizer for polymers in general, more specifically for HDPE. As expected, HDPE underwent severe photo-oxidative degradation. However, FLG with a concentration equal to or above 0.25 wt% induced pronounced stability for HDPE. This efficient stabilization was reflected in the excellent retention of rheological, and mechanical properties, even after 672 hours of UV exposure.

As highlighted in the introduction, FLG's stabilizing effect originates from its distinct chemical and physical properties. Figure 3.9 schematically shows the photo-oxidative degradation process in polymers and the various mechanisms of countering it by FLG during both the initiation and propagation steps.

Firstly, Graphene's ability to absorb or reflect UV radiation impedes the formation of primary radicals in the polymer, and delay the initiation step. This ability was quantified by calculating the UV transmittance through the samples. The results presented in Figure 3.7 showed that the addition of 0.5 wt% FLG to the HDPE matrix resulted in a, noteworthy, 80% UV transmittance reduction at a wavelength of 340 nm. This finding illustrates the FLG UV shielding effect. The UV shielding effect, whether through absorption or reflection, reduces the absorbance of UV light by polymer chains, which prevents the initiation step, and consequently decreases photo-oxidative degradation. Thus, the FLG UV-absorption/reflection effect can be considered one of the main mechanisms of photo-stabilization in polymer/graphene composites.

Additionally, FLG's unique electronic structure - featuring a network of  $\pi$  bonds- enables it to act as a free radical scavenger, and interact with the created peroxy and hydroxyl radicals, as shown in Figure 3.9, thus impeding their propagation, via adduct formation and electron transfer mechanisms(Wang et al. 2019). In this work, the FLG interactions with hydroxy radicals were investigated.

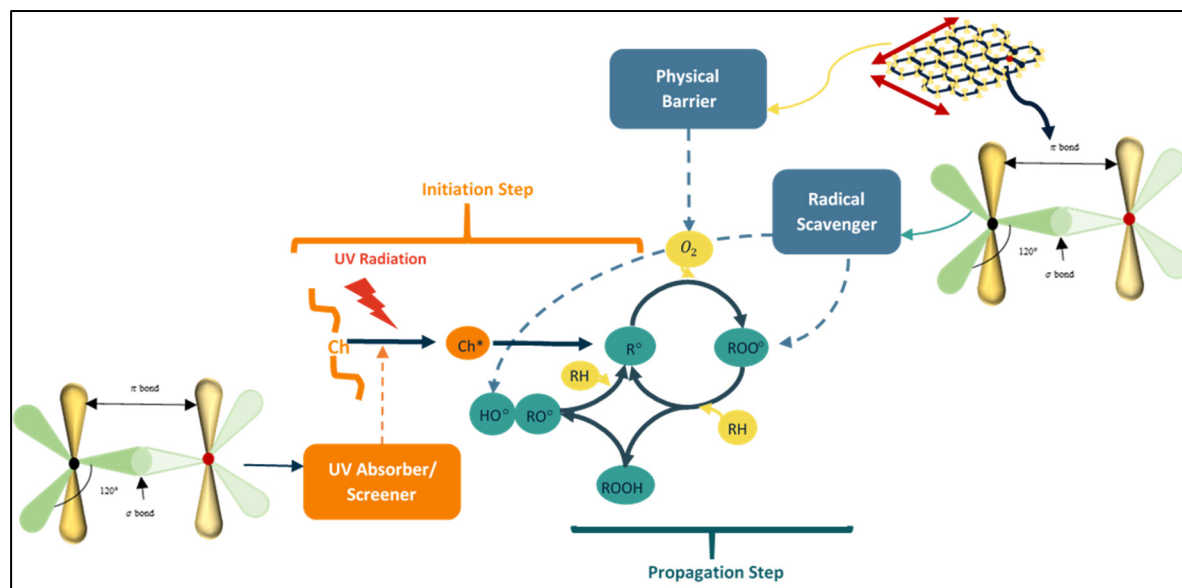


Figure 3.9 Photo-oxidative degradation in polymers and different mechanisms of action of graphene

The EPR spectra presented in Figure 3.8(a) provide evidence of the FLG significant role in reducing DMPO-OH adducts EPR signal, indicating a decrease in the number of available free hydroxyl radicals which can form adducts with DMPO. In more details, this reduction can be explained in two ways. First, FLG UV absorption/reflection ability, as confirmed by UV-vis spectroscopy, leads to a decrease in the amount of created hydroxyl radicals (primary radicals) and consequently, reduces the formation of DMPO-OH adducts. Second, FLG can scavenge and trap the created hydroxyl radicals, reducing their availability to form DMPO-OH adducts.

To determine the contribution of each of these two suggested mechanisms, a specific control experiment was conducted, see section 2.2.4. The results reported in Figure 3.8(b) indicate that when FLG was inside the H<sub>2</sub>O<sub>2</sub>/DMPO mixture, and both UV absorption/reflection and free radical scavenging mechanisms were active, the DMPO-OH signal area showed a more significant reduction of around 40%. However, when FLG was placed on the top of the beaker, and UV absorption/reflection was the only active mechanism, the signal area decreased by approximately 23%. By subtracting the reduction value due to the UV absorption/reflection mechanism (23%) from the total reduction in the signal area (40%), the contribution of the free radical scavenging mechanism was calculated to be around 17%. Therefore, 57%, and 43% of



the total reduction was found to be due to the FLG UV absorption/reflection, and free radical scavenging, respectively. This confirms that the UV absorption/reflection mechanism, is not the only dominant mechanism, as free radical scavenging made a significant contribution.

Furthermore, FLG's two-dimensional structure and high surface area make it a potentially useful material as a physical barrier. FLG ability to slow down the diffusion of oxygen reduces the creation of polymer peroxy radicals, which are key intermediates in the oxidation reaction, and consequently impedes the propagation step. In a recent study, Ferreira et al.(Junior et al. 2022) investigated the effect of adding FLG on the oxygen permeability of a multilayer HDPE composite. They used FLG with a similar lateral size as in this study and found that the addition of just 0.5 wt% FLG resulted in an 18% reduction in the oxygen permeability of the composite material.

In summary, FLG was found to exhibit three mechanisms of action, UV absorption/reflection, free radical scavenging, and acting as a physical barrier to oxygen, towards reducing the HDPE photo-oxidative degradation. However, the results showed that the contributions of UV absorption/reflection and free radical scavenging mechanisms were found to be more significant than the physical barrier effect (80% reduction in UV transmittance vs 18% reduction in oxygen permeability). The importance order of these three mechanisms can be classified as: UV absorption/reflection, free radical scavenging, and physical barrier effect.

### **3.6 Conclusion**

In this work, the FLG performance and the action mechanism, as a photo-stabilizer, were investigated for HDPE photo-oxidative degradation. The obtained results revealed the presence of 0.25wt % FLG, and above, ensured excellent stabilization and inhibited the HDPE photo-oxidative degradation. The study also demonstrated that the main FLG mechanisms were UV absorption/reflection and free radical scavenging, which was confirmed by UV-vis spectroscopy and EPR. Additionally, FLG ability to function as a physical barrier to oxygen further complements its UV absorption/reflection and free radical scavenging mechanisms,

providing a multifaceted approach to photo-stabilization. These findings provide important insights into the potential of graphene-based materials for the development of innovative and high-performance UV stabilizers for various applications.

## CHAPTER 4

### **Effect of Few-Layer Graphene (FLG) and Thickness on the Photo-Degradation Behavior of High-Density Polyethylene**

Samira Karimi<sup>1</sup>, Emna Helal<sup>1,2</sup>, Giovanna Gutierrez<sup>2</sup>, Nima Moghimian<sup>2</sup>, Eric David<sup>1</sup>, Tatiana Parra Vello<sup>3,4</sup>, Guilhermino José Macêdo Fechine<sup>3,4</sup> and Nicole Demarquette<sup>1\*</sup>

<sup>1</sup> Mechanical Engineering Department, École de Technologie Supérieure, 1100 Notre-Dame St W, Montréal, QC, Canada H3C 1K3

<sup>2</sup> NanoXplore Inc., 4500 Thimens Boulevard, Saint-Laurent, QC, Canada H4R 2P2

<sup>3</sup> Engineering School, Mackenzie Presbyterian University, São Paulo, SP, Brazil

<sup>4</sup> Mackenzie Institute of Research in Graphene and Nanotechnologies – MackGraphe, Mackenzie Presbyterian Institute, São Paulo, SP, Brazil

Paper submitted for publication, February 2024

#### **Abstract**

In this study, the effect of the addition of a few-layer graphene (FLG) on the depth of photodegradation into high-density polyethylene (HDPE) was investigated. For that, the samples of neat HDPE and two corresponding composites containing 0.1 and 0.5 wt% FLG, with two different thicknesses, 3 and 2 mm, were exposed to UV irradiation for several durations. The elongation at break was evaluated as a function of UV exposure time and correlated to the photo-degradation depth at which chemi-crystallization occurs, using Raman microscopy. The results showed that in neat HDPE, for 3 and 2mm thicknesses, embrittlement occurs at early exposure times, after 10 and 7 days, respectively, when the photo-degradation depth reached around 10 % of the sample thickness. This embrittlement preceded the appearance of surface cracks on both samples. Conversely, the samples containing 0.5 wt% FLG maintained a ductile failure behavior, even at longer exposure times, up to 45 days. This ductile behavior was observed even at a 12.5% depth of photo-degradation, and in spite of the presence of surface cracks. The persistence of ductile behavior was attributed to the photo-

stabilizing effect of FLG, as well as, to the tendency of the degraded layer to detach from the ductile core of the composite. Furthermore, a master curve was developed to depict the retention of elongation at break in neat HDPE as a function of UV dosage, normalized by the sample thickness, indicating that superposition principle can be applied between thickness and UV exposure time to predict the extent of UV-induced damage in neat HDPE. However, sample containing 0.5 wt% FLG deviated from that principle. This deviation can be explained by the unique ability of the FLG containing composites to maintain ductility through the detaching mechanism.

**Keywords:** Photo-degradation, Embrittlement, Graphene, Photo-stabilizer, Ductility

#### 4.1 Introduction

Research on the photo-stabilization of polymers has been ongoing for several decades, with a particular focus on understanding the mechanisms of photo-degradation and developing methods for photo-stabilization(Allen and McKellar 1975; White and Turnbull 1994; Raad and Abdallh 2022; So 2006; Karimi et al. 2020). Among the potential stabilizers, graphene derivatives have emerged as a promising candidate for specific polymer applications(de Oliveira et al. 2019; Tayouri et al. 2022; Karimi et al. 2023; Mistretta et al. 2019; Amrollahi et al. 2019; Uran, Alhani, and Silva 2017; Goodwin Jr, Shen, et al. 2020). However, the effectiveness of graphene as a stabilizer depends on several critical factors, including the concentration of graphene, UV exposure duration, and thickness of the product to be protected, all of which influence the extent of degradation in a given sample.

Concomitantly, it has been demonstrated that photo-degradation of polymers is associated with structural changes at molecular level, which vary along the thickness of a sample exposed to UV radiation(Shyichuk et al. 2005). In semi-crystalline polymers, chemical alterations during degradation, such as chain scission, lead to chemi-crystallization (Rabello and White 1997a), reduced interlamellar spacing, decreased tie molecule concentration, and ultimately, embrittlement (Fayolle et al. 2007; Deshoulles et al. 2021; Gauthier et al. 2013; Reano et al.

2018; Rodriguez et al. 2020). These result in a transition from ductile to brittle behavior in the material. This transition and product failure are inherently linked to the photo-degradation depth and the proportion of the sample affected by photo-degradation (photo-degradation depth/sample thickness).

It has been demonstrated that photo-degradation depth of a stabilized polymer depends on the efficiency and UV stabilizing mechanism of the photo-stabilizer. In particular, in the case of UV reflectors and screeners, photo-degradation can be confined to the region near the exposed surface (Turton and White 2001). Thus, understanding the photo-degradation depth or microstructural changes beneath the polymer surface exposed to UV degradation, becomes imperative.

The photo-degradation depth in polymers is defined by the depth of the sample which is affected by photo-degradation and undergoes microstructural alteration. It has been studied using various techniques, including DSC (Differential Scanning Calorimetry)(Craig and White 2005), GPC (Gel Permeation Chromatography), and ATR-FTIR (Attenuated Total Reflectance Fourier Transform Infrared Spectroscopy), which involve extracting samples from different depths using a microtome(Gulmine et al. 2003). Gulmine et al. (Gulmine et al. 2003) investigated alterations in crystallinity and chemi-crystallization during photo-degradation of 3 mm thick HDPE and LDPE samples, as a function of the sample depth. The results showed chemi-crystallization remained confined to a depth of 500  $\mu\text{m}$  within the sample thickness, after 6 weeks of UV exposure. However, there is limited data on photo-degradation depth of composites and the relation between microstructural change and macro properties.

This work aimed to investigate the effect of addition of a commercial few-layer graphene (FLG) on photo-degradation depth into HDPE. In this work, the photo-degradation depth of the samples was evaluated and correlated to macroscopic physical properties, specifically, the transition from ductile to brittle behavior. To achieve this, neat HDPE and its composites containing 0.1 and 0.5wt% FLG, with two different thicknesses of 3 and 2 mm, were exposed to UV radiation. The effective UV dosage corresponding to the exposure times was calculated

based on the "Cumulative Damage Model"(Lu et al. 2018). The elongation at break and failure zone were tracked based on the exposure times and corresponding UV dosage. Microstructural change and photo-degradation depth were analyzed using Raman spectroscopy coupled with an optical microscope. This approach provides a higher resolution and non-destructive means of assessing degradation.

## 4.2 Materials and Methods

### 4.2.1 Materials

In this work, injection grade HDPE (Alathon H5618) purchased from LyondellBasell Co. and FLG, GrapheneBlack 3X, provided by NanoXplore Inc., were used as matrix and photo-stabilizer, respectively. Tables 4.1 and 4.2 present the main physical characteristics of these materials.

Table 4.1 Physical Properties of HDPE

Property	Test method	Value
Melt flow index(@190°C,2.16kg)	ASTM D 1238	18 g/10min
Melting temperature	ASTM D 3418	130 °C
Density	ASTM D 1505	0.956 g/cm <sup>3</sup>

Table 4.2 Physical Properties of FLG from product Technical Data Sheet (TDS) provided by NanoXplore Inc

Property	Value
Primary particle size ( $\mu m$ )	1-2
Agglomerate size ( $\mu m$ )	$D_{10} < 10, D_{50} < 30$ $D_{90} < 70$
Number of layers	6-10
Bulk density (g/cm <sup>3</sup> )	0.2-0.3

#### **4.2.2 Composites Preparation**

A HAAKE twin-screw extruder, Model Rheomex OS PTW16/40 (L/D =40), was used to prepare HDPE samples containing 0, 0.1, and 0.5 wt% FLG. The process of HDPE composites involved diluting a 30 wt% Masterbatch of FLG to achieve the desired concentrations. The processing conditions can be found in a previous work (Karimi et al. 2023).

Dumbbell-shaped specimens of type V, with two different thicknesses of 3 and 2 mm, were injected using a microinjection machine (HAAKE MiniJet Pro) under the following conditions: barrel temperature of 160°C, mold temperature of 70°C, injection pressure of 300 bar, injection time of 20 s, holding pressure of 300 bar, and holding time of 15 s.

#### **4.2.3 Photo-degradation Process**

The injected samples were subjected to an accelerated weathering using a QUV chamber equipped with UVA-340 lamps. The samples underwent specific exposure conditions described in our previous work (Karimi et al. 2023). The samples properties were assessed after being exposed to UV for durations of 4, 7, 10, and 15 days. Notably, the HDPE containing 0.5wt% FLG, HDPE05, exhibited greater stability against UV compared to neat HDPE. Consequently, this particular sample remained in the QUV chamber for extended periods of 30 and 45 days.

Each sample was assigned a label in the format HDPEUV<sub>x-z</sub> or HDPE<sub>y</sub>UV<sub>x-z</sub>, where x denotes the exposure time in days, y represents FLG concentration, and z indicates the sample thickness. For example, HDPE05UV30-2 corresponds to HDPE containing 0.5 wt% FLG, with a 30 days exposure to UV and 2 mm thickness.

#### 4.2.4 UV Dosage Calculation

In this study, total effective UV dosage,  $D_{eff}(\frac{J}{m^2})$ , defined by the total effective energy of all the photons received by the sample per unit surface, was estimated based on the "Cumulative Damage Model" described by equation (4.1)(Martin et al. 2002; Lu et al. 2018; Martin 1993):

$$D_{eff}(t) = \int_0^t \int_{\lambda_{min}}^{\lambda_{max}} E_0(\tau) \Gamma(\lambda) (1 - e^{-A(\lambda, \tau)}) \phi(\lambda) d\lambda d\tau \quad (4.1)$$

Where:

$\lambda_{min}$  and  $\lambda_{max}$  = minimum and maximum effective used UV wavelengths (nm)

$A(\lambda, \tau)$  = absorbance spectrum of the material at the wavelength of  $\lambda$

$E_0(\tau)$  = UV irradiance (J/s.m<sup>2</sup>)

$\Gamma(\lambda)$  = spectral distribution (nm<sup>-1</sup>), respecting the condition:  $\int_0^{\infty} \Gamma(\lambda) d\lambda = 1$

t = elapsed time (s)

$\phi(\lambda)$  is a quasi-quantum yield function which describes the relative damage at the wavelength of  $\lambda$ . This function depends on environmental conditions such as temperature and humidity.

In this study, the total effective UV dosage was calculated based on equation (4.1) with the following assumptions:

- Effect of humidity on  $\phi(\lambda)$  is negligible
- Thermal degradation is negligible
- There is no UV radiation transmitted through the sample. So based on Lambert-Beer law, equation (4.2),  $A(\lambda, t)$  is infinity large for the whole duration of the exposure.



- $$\ln \left( \frac{I_0(\lambda)}{I(\lambda)} \right) = A(\lambda) \quad (4.2)$$

Where  $I_0(\lambda)$  and  $I(\lambda)$  are intensities of incident and transmitted light at the wavelength of  $\lambda$ .

- The UV source is a monochromatic source so that  $\Gamma(\lambda) = \delta(\lambda - 340)$ , where  $\delta(\lambda)$  is the Dirac function.

Based on the above-mentioned assumptions, the total effective dosage can be simplified as:

$$D_{eff}(t) = \int_0^t E_0(\tau) \phi(340) d\tau \quad (4.3)$$

The quantum yield for neat HDPE at a wavelength of 340 nm and a temperature of around 40°C has been reported to be  $8.86 \times 10^{-2}$  (Bigger and Delatycki 1989a, 1989b). Considering the fact that quantum yield is an Arrhenius function of temperature (Daglen and Tyler 2010), and the experimental temperature (60°C) is close to 40°C (and both above glass transition temperature of HDPE ( $\approx -120^\circ\text{C}$ )), any significant alteration in quantum yield between 40°C and 60°C was deemed negligible. Consequently, this study employed the quantum yield value of  $8.86 \times 10^{-2}$ . The provided equation, equation (4.3), was employed to calculate the "effective UV dosage",  $D_{eff}(\frac{J}{m^2})$ , corresponding to various UV exposure times of the samples, presented in Table 4.3. To make a meaningful comparison among samples with different thicknesses, the "effective UV dosage" were normalized to the sample thickness. This normalization allowed us to determine the effective UV dosage per sample volume, reported in Table 4.3. In this manuscript, "UV dosage per sample volume" refers to effective UV dosage per sample volume,  $D_{eff}/\text{Thickness}$ .

Table 4.3. Effective UV dosage corresponding to different UV exposure times

Exposure time (UV and condensation ) (day)	Exposure time (UV and condensation ) (hour)	Only UV Exposure time (sec)	$D_{eff}$ ( $J/m^2$ )	$\frac{D_{eff}}{Thickness} (\frac{J}{m^3})$	
				3 mm thick	2 mm thick
0	0	0	0	0	0
4	96	230400	$18.2 \times 10^3$	$60.6 \times 10^5$	$90.8 \times 10^5$
7	168	403200	$31.8 \times 10^3$	$10.6 \times 10^6$	$15.9 \times 10^6$
10	240	576000	$45.4 \times 10^3$	$15.1 \times 10^6$	$22.7 \times 10^6$
15	360	864000	$68.1 \times 10^3$	$22.7 \times 10^6$	$34.1 \times 10^6$
30	720	1728000	$13.6 \times 10^4$	$45.4 \times 10^6$	$68.1 \times 10^6$
45	1080	2592000	$20.4 \times 10^4$	$68.1 \times 10^6$	$10.2 \times 10^7$

#### 4.2.5 Characterization

The dispersion of FLG across the thickness of HDPE matrix was analyzed using an Optical Microscope (OM), Carl Zeiss Jena JENAPOL Instrument, on a thin film with a thickness of  $50 \mu m$ , obtained using a microtome.

A scanning electron microscopy, SEM S3600-N Hitachi, was used to observe the gold-coated surface of the exposed samples. SEM observations were conducted on both the exposed and the side surfaces to analyze the crack density and depth. Figure 4.1 schematically describes the exposed and the side surface, cross-section, as well as the crack depth.

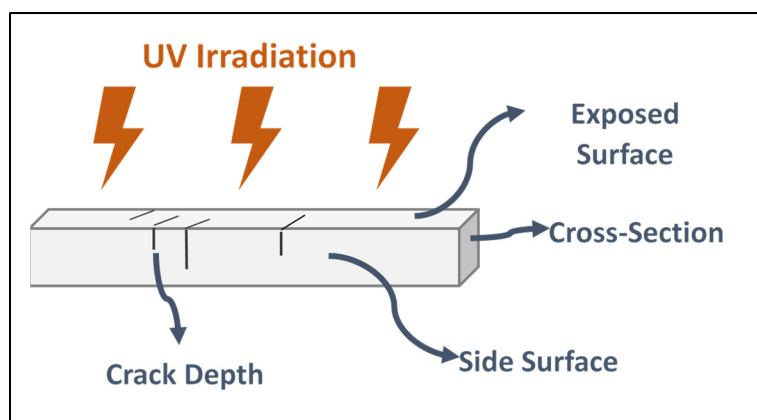


Figure 4.1 Schematic of different sides of the samples

Tensile properties of the samples were assessed at room temperature using an MTS Alliance RF/200 testing machine, following ASTM D638 standard, with a cross-head speed of 50 mm/min. Five specimens of each sample were tested. The reported values are the averages obtained from these measurements.

In order to characterize the change in sample microstructure during photo-degradation, Raman microscopy was conducted using a Witec alpha 300 system equipped with a 532nm laser from Witec with a power of 1 mW, and a grating of 1800 g/mm. A 50x objective lens with a numerical aperture of 0.7 was used for imaging. The integration time for each measurement was set to 10 seconds, and a total of 10 accumulations were performed to enhance the signal-to-noise ratio.

The microstructural change was investigated by tracking the intensity variation of the Raman band at  $1416\text{ cm}^{-1}$ , assigned to the orthorhombic crystalline chains, as a function of UV exposure time and sample depth. To ensure accurate measurements, the intensity of the Raman band at  $1416\text{ cm}^{-1}$  was normalized using the  $\text{CH}_2$  twisting bands at  $1296\text{ cm}^{-1}$  as internal reference, as indicated by equation (4.4):

$$\text{Crystal Band Intensity} = \frac{I_{1416\text{cm}^{-1}} (a.u.)}{I_{1296} (a.u.)} \quad (4.4)$$

Where  $I_{1416}$  and  $I_{1298}$  are the intensities of the Raman bands located at  $1416\text{ cm}^{-1}$ , and  $1296\text{ cm}^{-1}$  respectively.

The corresponding degree of crystallinity was calculated using the following equation (4.5) (Lin et al. 2007):

$$\text{Crystallinity (\%)} = \frac{\text{Crystal Band Intensity}}{0.46} \times 100 \quad (4.5)$$

## 4.3 Results

### 4.3.1 Cross-Section Morphology

Figure 4.2 presents the cross-section dispersion of FLG in HDPE05. It can be seen that FLG concentration is lowest at the region close to the surface. The black arrow indicates the direction from the sample surface toward the bulk and the red arrows point FLG particles.

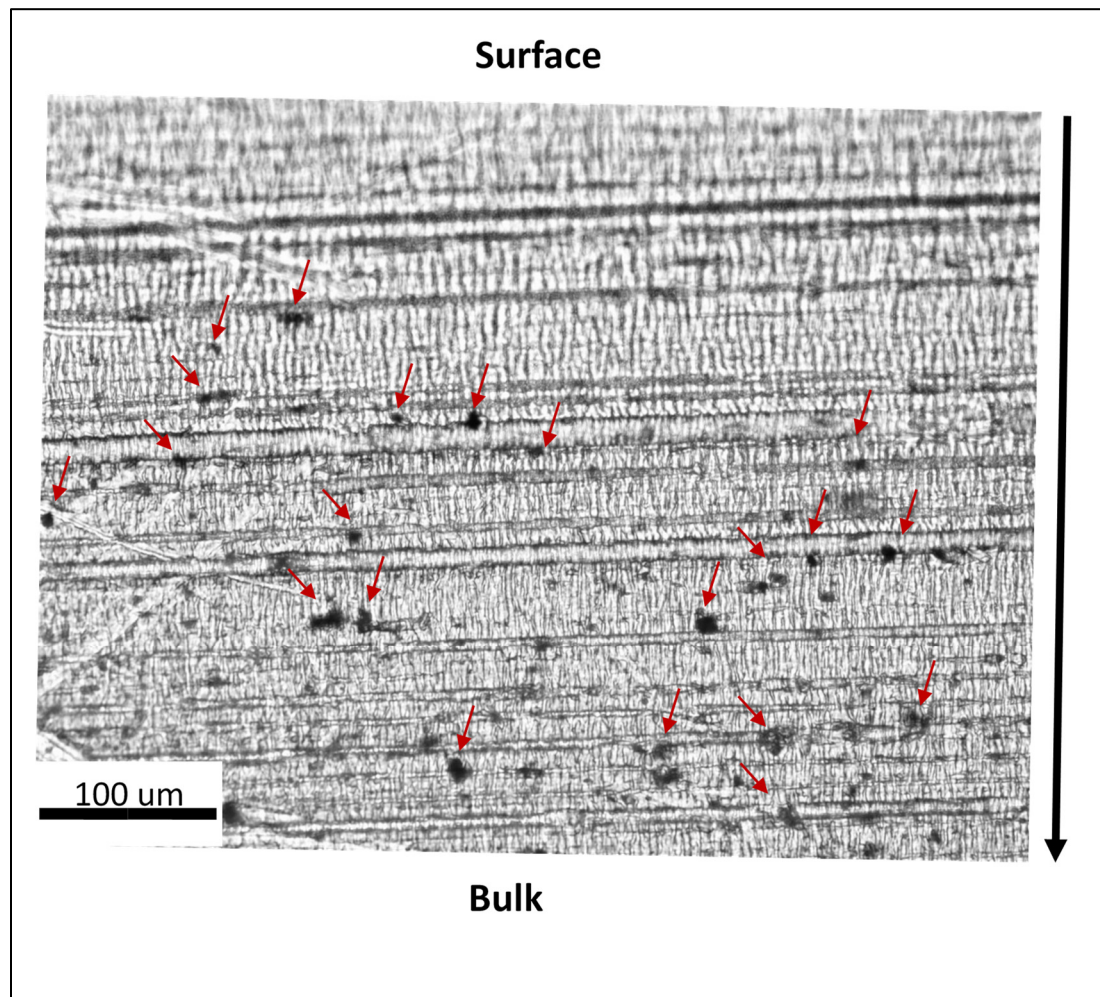


Figure 4.2. FLG dispersion across the cross-section of HDPE05

#### 4.3.2 Surface Morphology

Figures 4.3 and 4.4 show SEM images of UV exposed and side surfaces of neat HDPE and HDPE05, each with two different thicknesses of 2 and 3 mm, for different exposure times. Different scales are used to better illustrate the cracks' size and concentration.

It can be seen that in neat HDPE with a 2 mm thickness, the first cracks appear only after 10 days of UV exposure. The formation of cracks results from chemicrystallization, and stress concentration induced by photo-degradation (Rabello and White 1997c).

Conversely, neat HDPE with a 3 mm thickness shows higher stability, remaining devoid of any visible cracks up to 15 days of UV exposure. Increased stability in the 3 mm thick sample may be attributed to the fact that, at an equivalent depth of photo-degradation, a greater proportion of the thinner sample, 2 mm, is susceptible to photo-degradation. Moreover, the appearance of cracks on the side surface provides an indicator of their depth. It is evident that, in HDPEUV15-2, the cracks extend throughout the entire thickness, Figure 4.4.

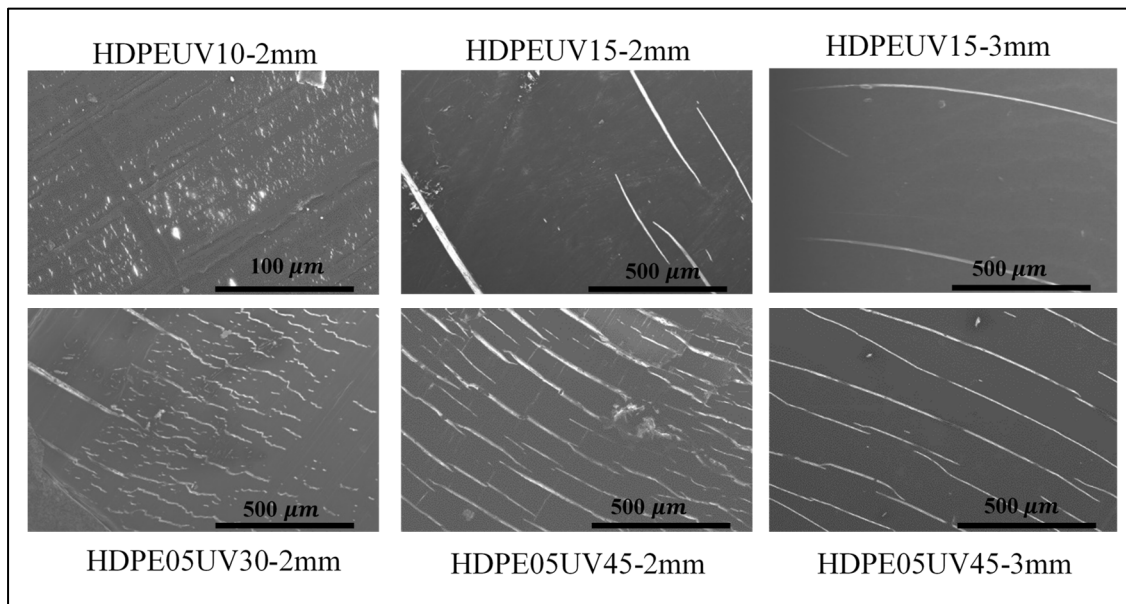


Figure 4.3. SEM images of the exposed surfaces of neat HDPE and HDPE05 with sample thicknesses of 2 and 3 mm.

In the case of HDPE05, a notable resistance to UV-induced cracks can be observed where the initial cracks with a depth of  $150\ \mu\text{m}$  become visible only after 30 days of UV exposure in 2 mm thick HDPE05. As UV exposure time increases to 45 days, both thicknesses of HDPE05 develop additional cracks, with greater depths. The crack depths are reported in Table 4.4.

Furthermore, the size of cracks is smaller in the composite material, HDPE05, compared to that of neat HDPE-2mm.

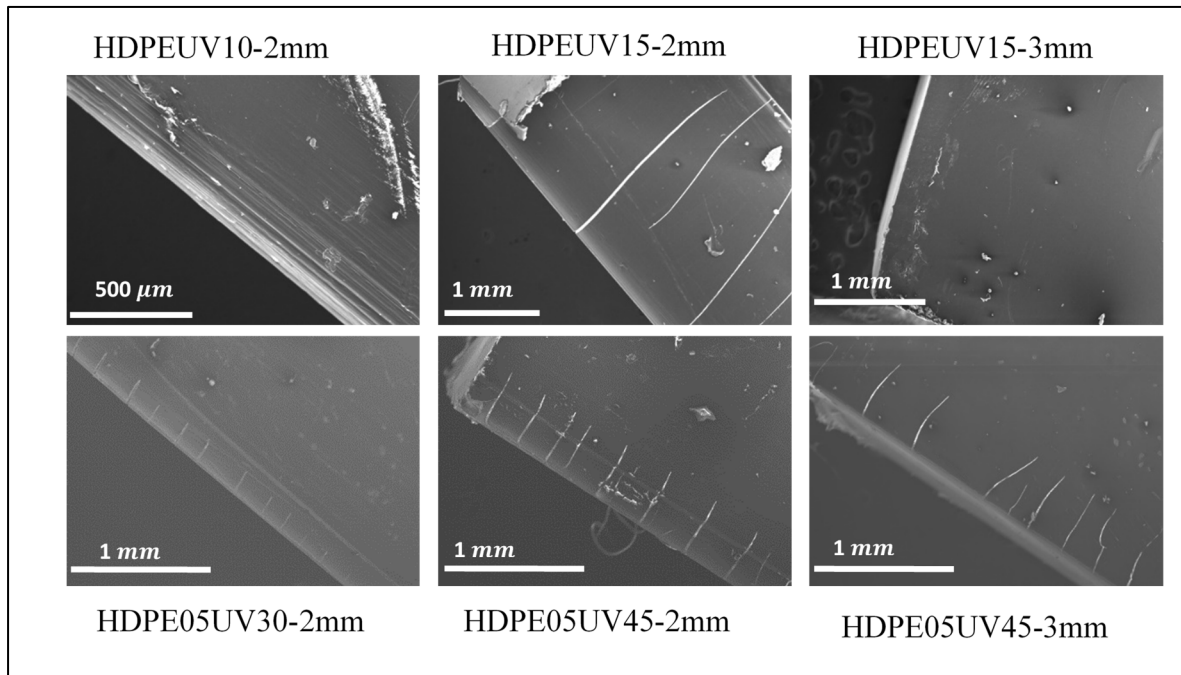


Figure 4.4. SEM images of the side surfaces of neat HDPE and HDPE05 with sample thicknesses of 2 and 3mm.

Table 4.4 The observed crack depth in HDPE and HDPE05

Sample	Crack Depth ( $\mu\text{m}$ )
HDPEUV10-2mm	-
HDPEUV15-2mm	Entire thickness (2000)
HDPEUV15-3mm	-
HDPE05UV30-2mm	150
HDPE05UV45-2mm	400
HDPE05UV45-3mm	410

### 4.3.3 Mechanical Properties

Figure 4.5 illustrates stress-strain curves of neat HDPE and HDPE05 specimens with two different thicknesses, 3 and 2 mm, subjected to different exposure times. The Figure is divided into four different zones, defined in Table 4.5, each aligned with specific microstructural

deformation. The initial segment is labeled as zone I or the elastic zone located before the first yield point. Zone II is reached as the strain falls between the first and second yield point. This zone corresponds to the onset of plastic deformation and lamella orientation (Brooks et al. 1995). Zone III starts after the second yield point corresponding to the onset of lamella fragmentation and continue with a necking development process (Séguéla 2007; Brooks et al. 1995). Finally, zone IV, beyond the hardening point, marks the hardening region (Nitta and Kuriyagawa 2012; Peterlin 1971).

Table 4.5. Different zones in stress-strain curves of HDPE

<b>Zones</b>	<b>location</b>
Zone I	Before first yield point
Zone II	Between first and second yield points
Zone III	Between second yield point and hardening points
Zone IV	Beyond hardening point

It can be seen from Figure 4.5(a) that as UV exposure time increases, the elongation at break consistently decreases which gradually promotes a shift in failure from zone IV to zone I. These observations are related to chain scission occurring in neat HDPE during photo-degradation (Grigoriadou et al. 2011; Hsueh et al. 2020; Fairbrother et al. 2019). Notably, shift in the failure zone and decrease in elongation at break occur at a considerably faster rate in the 2 mm thick sample. The same behavior was observed for HDPE01, and HDPE05 samples, where the thinner samples, 2 mm thick, are more affected by UV exposure.



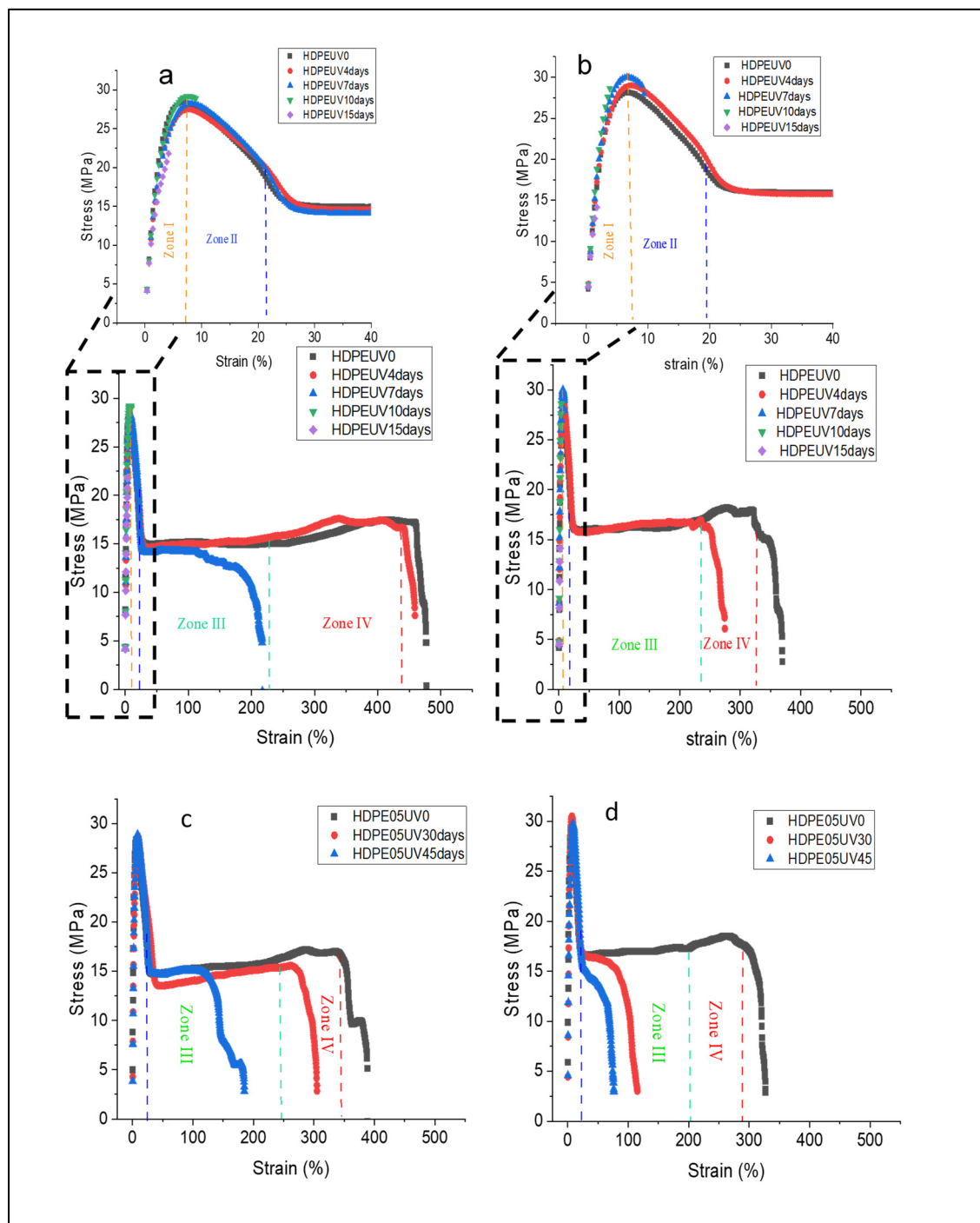


Figure 4.5. Stress-strain curves of neat HDPE with a thickness of: a) 3 mm and b) 2 mm and HDPE05 with a thickness of: c) 3 mm and d) 2 mm with different UV exposure times

The stress-strain curves were used to calculate retention of elongation at break for neat HDPE and its composites. Figure 4.6 shows retention of elongation at break as a function of UV exposure time and the corresponding effective UV dosage,  $D_{\text{eff}}$ , for neat HDPE, HDPE01, and HDPE05, for two different thicknesses.

It can be seen that the curves for all samples exhibit a reverse sigmoidal pattern which include an initial plateau followed by a steep fall, and eventually reach the second plateau. The first plateau indicates the initial resistance to UV degradation. Steep falling is an indication of the rate of degradation. The presence of FLG in composites, HDPE01 and HDPE05, not only extends the first plateau, but also decreases the slope of falling, indicating its effects on the initiation and propagation steps.

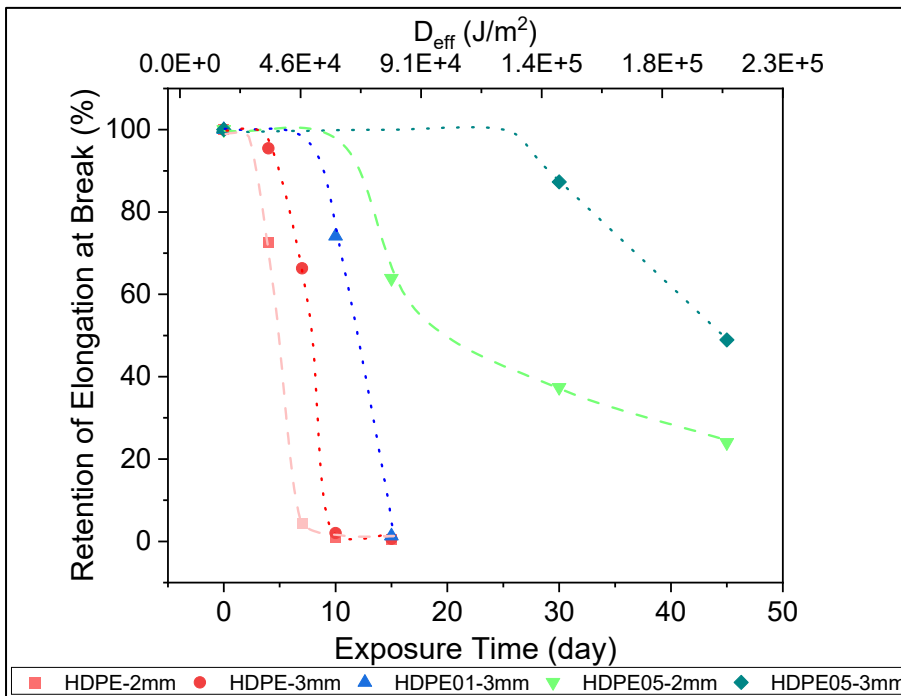


Figure 4.6 Retention of elongation at break of neat HDPE, HDPE01, and HDPE05 with thicknesses of 3 and 2 mm as a function of exposure time and corresponding "effective UV dosage"

Neat HDPE exhibits the fastest rate of loss in retained elongation compared to those of composites, reaching zero retention of elongation at break only after 10 days of UV exposure.

As expected, the thinner samples in each group display the least stability under UV exposure where the retained elongation curves shift to earlier UV exposure times. This can be related to the fact that in thinner samples, at the same degradation depth, a relatively larger portion of the sample experiences degradation.

Incorporating FLG into HDPE, HDPE01 and HDPE05, results in an increase in the length of the initial plateau and a more gradual decrease in retained elongation values. These comparative findings can be quantified by calculating the time it takes for a 50% reduction in the initial elongation value, denoted as  $t_{50}$ , presented in Table 4.6. Notably, the incorporation of 0.1 and 0.5 wt% FLG in 3 mm thick HDPE, increases  $t_{50}$  from 7 days for neat HDPE to 12 and 35 days, for HDPE01 and HDPE05, respectively. Similarly, for 2 mm thick samples,  $t_{50}$  is increased from 5 days to 20 days upon the addition of 0.5 wt% FLG.

Table 4.6. The calculated  $t_{50}$  for neat HDPE and its composites

Sample	$t_{50}$ (day)	
	3 mm thick	2 mm thick
Neat HDPE	7	5
HDPE01	12	-
HDPE05	35	20

The retained elongation values were considered to model lifetime of the samples, regardless of the sample thickness. Figure 4.7 shows retained elongation as a function of UV dosage per sample volume,  $D_{\text{eff}}/\text{Thickness}$ , for neat HDPE and HDPE05.

It can be seen from Figure 4.7 that in the case of neat HDPE, retained elongation values, for different thicknesses, merge into one single reverse sigmoidal curve, with a coefficient of determination,  $R^2$  being more than 0.99. These results indicate that in neat HDPE the interplay between the sample thickness and UV damage follows the superposition principle. However, in HDPE05, the curve deviates from this principle due to the incorporation of FLG into neat HDPE.

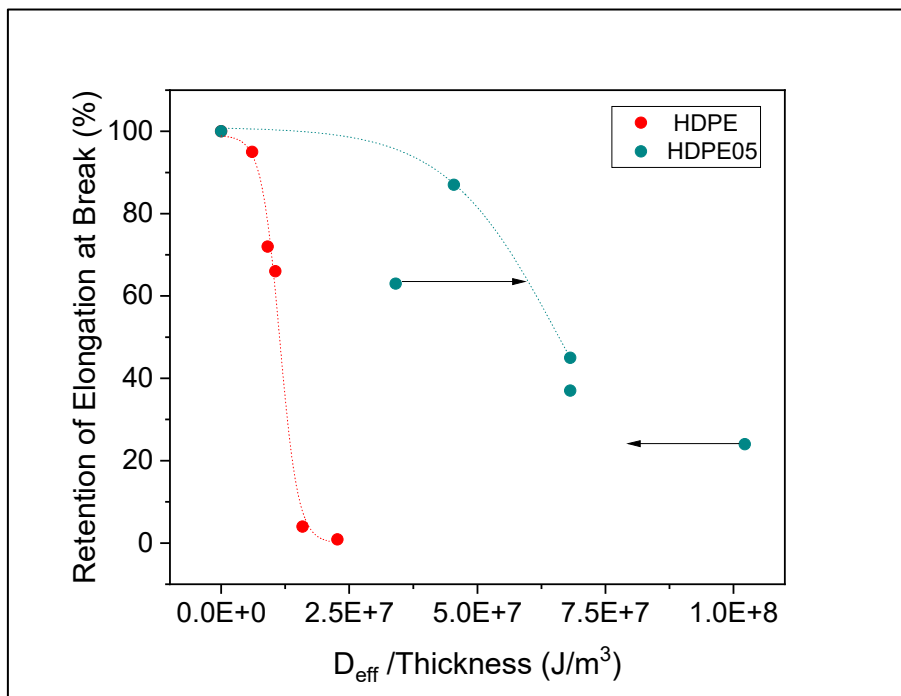


Figure 4.7. Retention of elongation at break of neat HDPE, and HDPE05 as a function of UV dosage per sample volume. The arrows indicate the deviation from the superposition principle.

The above-presented results show that the UV stability of HDPE composites strongly depends on FLG concentration, duration of UV exposure, and sample thickness. To establish a connection between changes in mechanical properties, photo-degradation depth and microstructural alteration, during UV exposure, an in-depth investigation of crystallinity is presented in the next section.

#### 4.3.4 Photo-Degradation Depth

Figure 4.8 shows a typical Raman spectrum of the UV exposed surface of neat HDPE for different exposure times. The Raman bands are normalized by the reference band located at  $1296\text{ cm}^{-1}$ . It can be seen that in neat HDPE, the orthorhombic crystal band intensity, located at  $1416\text{ cm}^{-1}$ , increases as a function of exposure time, suggesting that chemi-crystallization is taking place during UV degradation (Hiejima et al. 2018).

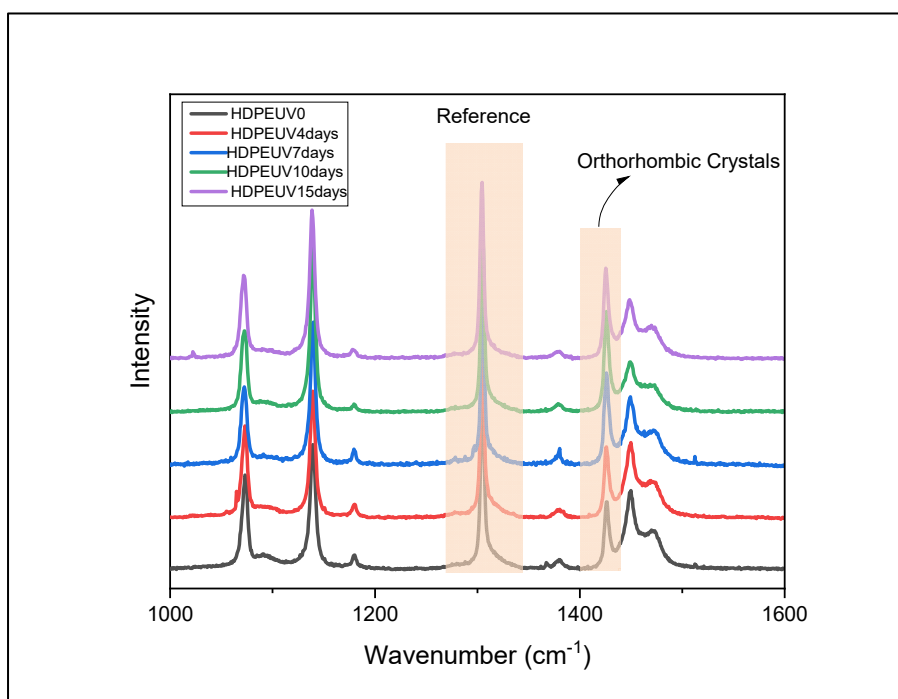


Figure 4.8. Raman spectrum of neat HDPE exposed surface with different UV exposure times

Figure 4.9 schematically shows the evolution of chemi-crystallization across the sample depth at different exposure times. In the context of chemi-crystallization during photo-degradation, the amorphous regions of the polymer undergo a process of reorganization and ordering into crystalline structures (Craig, White, and Kin 2005). Since chemi-crystallization is a result of chain scission during UV exposure, it was considered to represent the photo-degradation depth. For that Raman microscopy was performed on the samples cross-sections. The orthorhombic crystal band intensity was measured as a function of the sample depth. The affected depth, i.e.

the depth corresponding to change in crystallinity (chemi-crystallization), as shown in Figure 4.9, is considered as the photo-degradation depth.

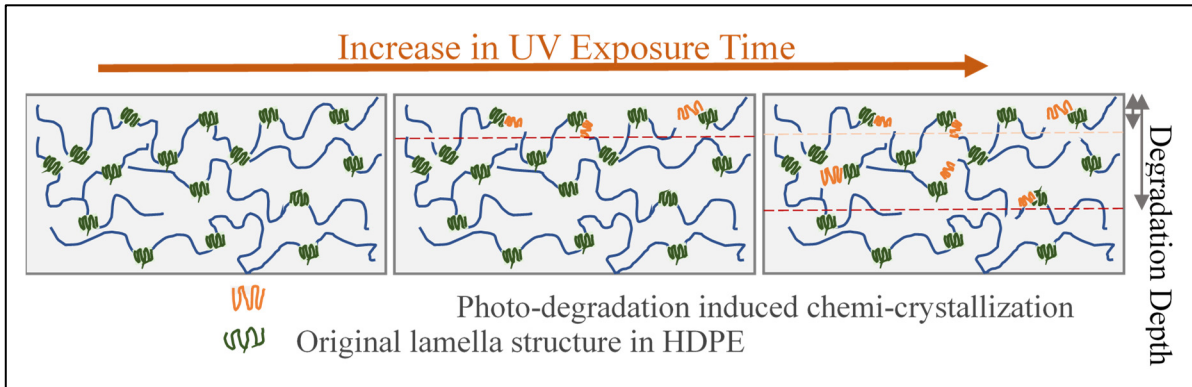


Figure 4.9. Schematic of chemi-crystallization evolution with UV exposure time

Figure 4.10 shows a typical crystal band intensity profile, as well as degree of crystallinity, along the depth of neat HDPE, and HDPE05, with thicknesses of 3 and 2 mm, for different UV exposure times. More detail data can be found in supplementary file. Figure 4.10 shows that prior to UV exposure, the intensity of the crystal band, and consequently the degree of crystallinity, in neat HDPE, and its composites, are quite consistent across the sample depth. Lower values are observed close to the mold surface due to the skin effect in which cooling rate and crystal morphology are different from bulk (Kamal and Moy 1983).

In neat HDPE, after 4 days of UV exposure, a slight increase in the crystal band intensity can be observed within the first 100-150  $\mu\text{m}$  of the depth, in both 3 and 2 mm thicknesses, pointing to chemi-crystallization in this region. However, the rest of the samples' depth remain unaffected. For a UV exposure time of 10 days, the affected depth increases to 300  $\mu\text{m}$  and 400  $\mu\text{m}$  in neat HDPE-3mm and neat HDPE-2mm, respectively. Subsequently, after 15 days of UV exposure, in neat HDPE-3mm, the affected depth is extended to 500  $\mu\text{m}$ , while in neat HDPE-2mm an increase in the crystal band intensity is observed throughout the entire sample depth.

In the case of HDPE01, the increase in the crystal band intensity is observed after 10 days of UV exposure. Further increase in UV exposure time, 15 days of UV exposure, leads to an increase in both the crystal band intensity and the affected depth to 300  $\mu\text{m}$ , while the remaining depth remains unaffected, indicating a limit to photo-degradation depth, within this range.

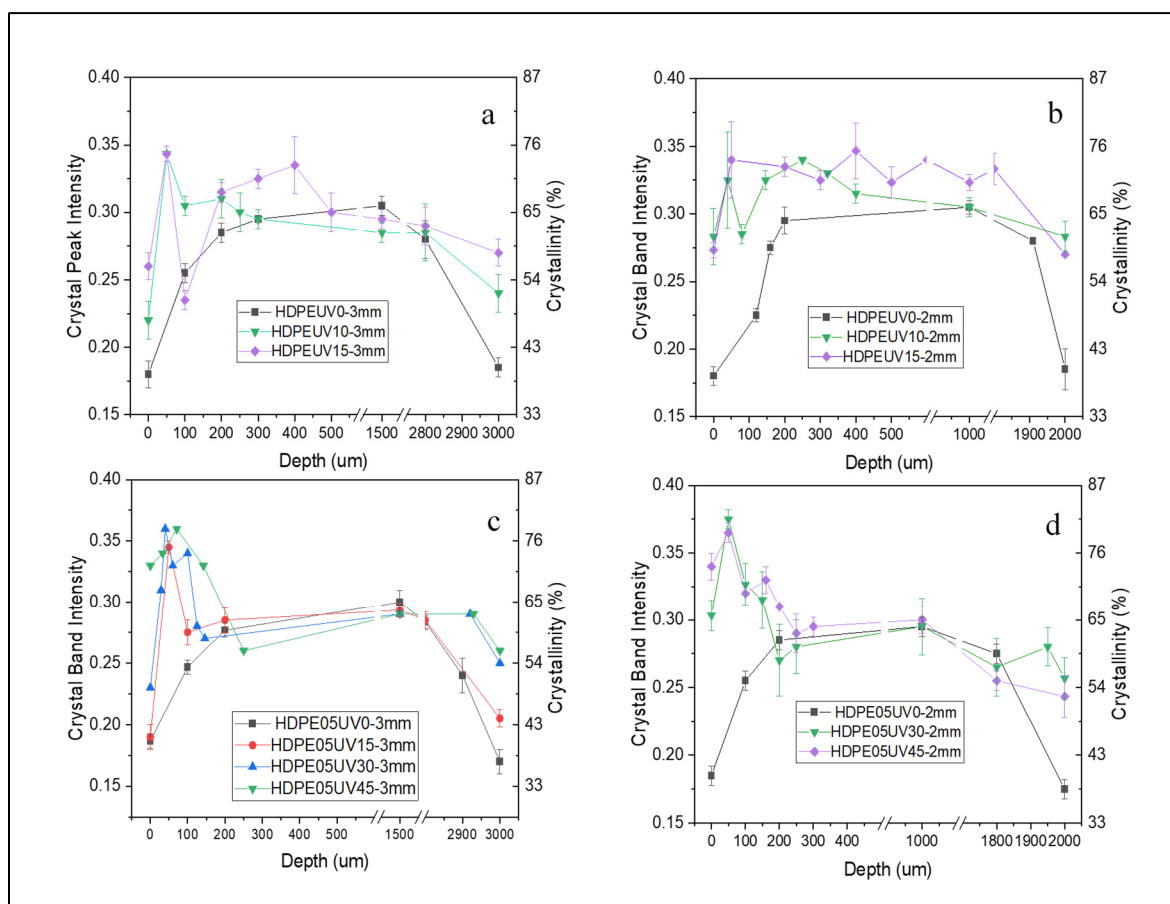


Figure 4.10. Crystal band intensity of: a-b) neat HDPE, c-d) HDPE05, with thicknesses of 3 and 2 mm as a function of sample depth, for different UV exposure times

In HDPE05, the alteration in the crystal band intensity and affected depth become apparent following a 15 and 10 days UV exposure period, in 3 and 2 mm thicknesses, revealing the remarkable stabilizing effect of FLG in preventing photo-degradation-induced microstructural changes.

The photo-degradation depth (D) can be evaluated from Figure 4.10 and presented in Table 4.7. It is important to note that the failure of a sample is intricately linked to the ratio of photo-degradation depth (D) and the sample's thickness- a characteristic parameter denoted as normalized photo-degradation depth, calculated according to equation (4.7), and reported in Table 4.7:

$$\text{Normalized photodegradation depth (\%)} = \frac{D}{T} \times 100 \quad (4.7)$$

Where T is the sample thickness.

Table 4.7. photo-degradation depth and normalized photo-degradation depth values of neat HDPE and its composites.

UV Exposure Time (day)	3 mm		2 mm		
	Photo-Degradation Depth (D) ( $\mu\text{m}$ )	D/T(%)	Photo-Degradation Depth (D) ( $\mu\text{m}$ )	D/T(%)	
Neat HDPE	4	100	3.3	165	8
	7	200	6.6	300	15
	10	300	10	400	20
	15	500	16.6	Entire Thickness	-
HDPE01	10	200	6.6	-	-
	15	300	10	-	-



UV Exposure Time (day)		3 mm		2 mm	
		Photo-Degradation Depth (D) ( $\mu m$ )	D/T(%)	Photo-Degradation Depth (D) ( $\mu m$ )	D/T(%)
HDPE05	10	-	-	80	4
	15	100	3.3	150	7.5
	30	150	5	200	10
	45	250	8	250	12.5

The normalized photo-degradation depth, D/T, was effectively employed to conduct an analysis of the samples' embrittlement. This analysis and its findings are detailed in the following section.

#### 4.3.5 Failure Zone based on "Normalized photodegradation depth", D/T

In Figure 4.11, the experimental failure behavior of neat HDPE, HDPE01, and HDPE05, based on the characteristic parameter, D/T, and UV dosage per sample volume, are presented. The ductile behavior (Zone III and IV) is shown in green color. The brittle behavior (Zone I and II) in red. The Figure shows that higher values of the normalized photo-degradation depth, D/T, corresponding to more profound alterations in microstructure, result in a shift towards brittle failure.

In neat HDPE, embrittlement happens at very low values of D/T, around 10 %, where the photo-degradation depth reaches only 10 % of the sample thickness. In HDPE01, the transition from ductile to brittle failure happen at the same value of D/T, but it requires higher value of UV dosage. The presence of FLG in HDPE01 allows for the extension of the exposure time, and correspondingly the UV dosage, which would result in microstructural change.

On the other hand, in HDPE05, even at much higher UV dosage (5 times higher than that of neat HDPE), the failure behavior is still ductile and the normalized photo-degradation depth is lower compared to neat HDPE. These results illustrate the FLG photo-stabilizing effect on HDPE, preventing brittle failure in the composite, even at higher UV dosage.

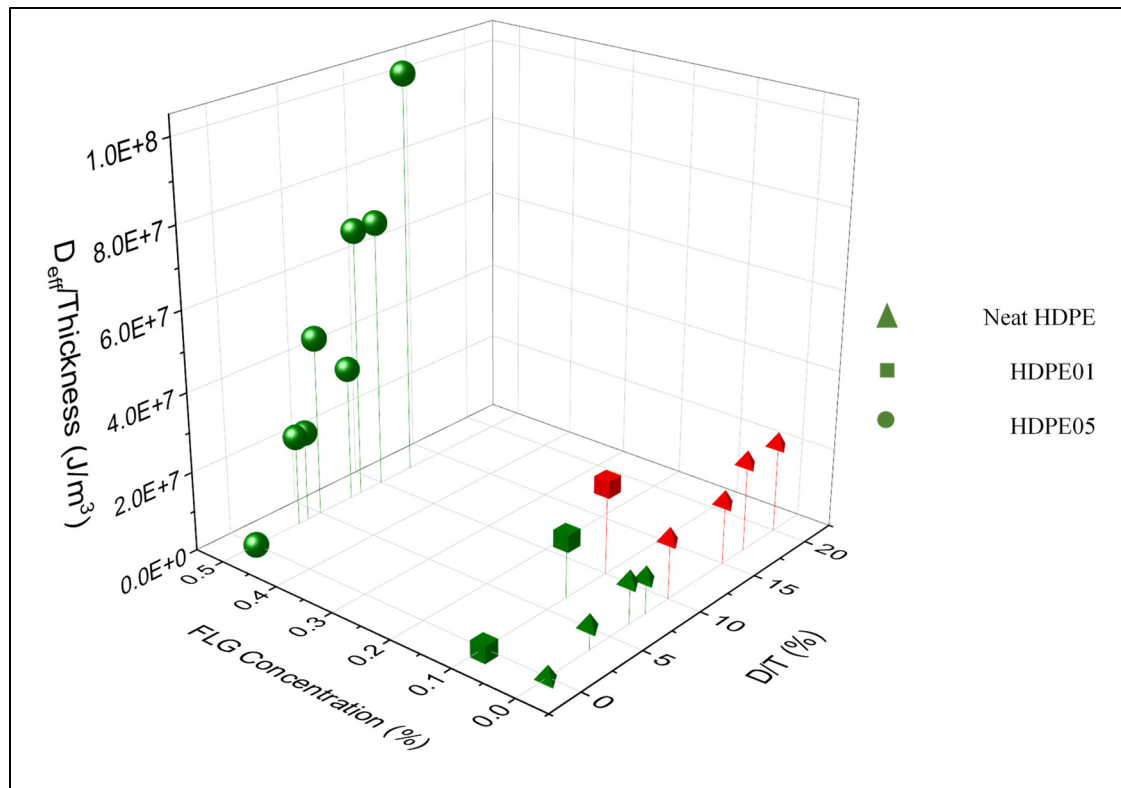


Figure 4.11. Failure behavior of neat HDPE and its composites as a function of UV dosage and normalized photo-degradation depth. The green color represents ductile behavior (Zone III and IV), and the red color indicates brittle behavior (Zone I and II).

#### 4.4 Discussion

In this study, a notable enhancement in the UV stability of HDPE composites was achieved through the incorporation of FLG. Retention of elongation at break was calculated for neat HDPE and its composites with thicknesses of 3 and 2 mm, as a function of exposure time and corresponding UV dosage. The retention curves exhibited a reverse sigmoidal shape for all the

samples, with significant changes in the presence of FLG. At low FLG concentration, corresponding to HDPE01, only the first plateau was extended to longer exposure time compared to that of neat HDPE, suggesting impeding the initiation step, while the falling slope remained nearly unchanged. Conversely, at higher concentration, HDPE05, not only the first plateau was extended, indicating impediment to the initiation step, but the falling slope of the curve also decreased significantly, demonstrating a deceleration in the propagation step. These results are in good alignment with our previous work which confirmed FLG can act as both UV absorber/reflector and free radical scavenger, effectively preventing both the initiation and propagation steps (Karimi et al. 2023). Moreover, the retention of elongation at break curves of HDPE05 display a tendency to reach a non zero plateau (a plateau above zero), even at higher exposure times. This result suggests a unique and promising potential of HDPE05 to maintain ductile behavior.

Furthermore, it was demonstrated that UV damage occurring in neat HDPE, during UV exposure, can be predicted based on evaluating the received UV dosage per sample volume. This analysis revealed a master curve for the retention of elongation at break of neat HDPE with different thicknesses as a function of UV dosage per sample volume, Figure 4.7. This finding demonstrates that the dependence of UV damage of neat HDPE on sample thickness and UV exposure time follows the superposition principle, indicating that reducing sample thickness is equivalent to increasing UV dosage/exposure time. However, this superposition principle was not observed in the presence of 0.5 wt% FLG.

A correlation between microstructural alteration and embrittlement (transition from ductile to brittle behavior), was established. In neat HDPE-3mm, chemi-crystallization primarily occurred within the first 500  $\mu\text{m}$  of the sample thickness, after 15 days of UV exposure indicating a photo-degradation depth an upper limit within this range. These results are in good agreement with previous studies on LDPE (Andrady et al. 2022) and HDPE (Moreno-Serna et al. 2023), where the amount of degradation species showed a sharp decrease with the sample thickness, suggesting an oxygen diffusion-controlled conditions during photo-degradation (Hsueh et al. 2020). Neat HDPE-2mm presented an oxygen diffusion-controlled degradation

behavior, only up to 10 days of UV exposure. After 15 days of UV exposure, chemi-crystallization extended throughout the entire thickness of neat HDPE-2mm, potentially facilitated by the created cracks in neat HDPE-2mm that exposed more surface to UV radiation (Yakimets, Lai, and Guigon 2004), and facilitated oxygen diffusion into deeper layers. In the case of HDPE05, chemi-crystallization took place only within the first 250  $\mu\text{m}$  of the sample thickness, for both 3 and 2 mm thick samples, even after 45 days of UV exposure. The more limited photo-degradation in HDPE05 compared to that of neat HDPE is attributed to the photo-stabilizing effect of FLG.

The photo-degradation depth was normalized by the sample thickness and correlated with the embrittlement behavior of neat HDPE and its composites as a function of UV dosage per sample volume, as illustrated in Figure 4.11. Notably, the embrittlement occurred in neat HDPE and HDPE01 when photo-degradation reached around 10% of the sample thickness, even before the appearance of visible cracks. This embrittlement was observed at a remarkably low value of UV dosage, below  $2 \times 10^7 \text{ J/m}^3$ , equivalent of 7 to 10 days of UV exposure. In fact, HDPE, characterized by plastic deformation under tension (Lin and Argon 1994; Brusselle-Dupend and Cangémi 2008; Peterlin 1971; Pawlak 2007), typically initiates plastic deformation after surpassing the second yield point. At the second yield point, tie molecules transfer the load to crystal structures and initiate plastic deformation through lamella slipping and fragmentation (Hsu et al. 2012; Rozanski and Galeski 2013). Embrittlement occurs when the sample fails to progress beyond the second yield point and effectively transfer the load to the crystal structures. Photo-degradation induces chemi-crystallization and chain scission, consequently disrupting the tie molecules from transferring the load to crystal structures, resulting in a reduction in elongation at break. At a critical point, the sample becomes incapable of efficiently transferring the load to crystal structures, ultimately leading to embrittlement. This study revealed that embrittlement occurs when photo-degradation induced chain scission reaches approximately 10% of the sample thickness in the case of neat HDPE. Notably, the incorporation of 0.5 wt% FLG into HDPE, HDPE05, demonstrated a remarkable resistance to embrittlement, at significantly higher UV dosage, reaching  $10^8 \text{ J/m}^3$ , equivalent of 45 days of UV exposure of 2 mm thick sample.

Interestingly, despite the formation of surface cracks, at extended exposure time, which are known as a crucial contributor to embrittlement, the composite maintained its ductile behavior. In the case of HDPE05 with a thickness of 2 mm, the photo-degradation depth, even exceeded 10% of sample thickness, yet the material retained its ductile behavior. Therefore, we believe that, the FLG photo-stabilizing effect alone may not account for the ductile behavior. To more adequately describe this behavior, one has to consider more closely the formation of surface cracks in the presence of FLG.

The formation of cracks during photo-degradation is known to originate from shrinkage and mechanical stress caused by chain scission and crosslinking (Awaja et al. 2016). When FLG is present in HDPE05, it increases sample heterogeneity, density, and mechanical stress (Al-Maqdasi et al. 2021), leading to promotion of surface cracks under UV exposure. In the composite samples, photo-degradation initiates, first, near the surface which is deprived of lower concentration of FLG as shown in Figure 4.2. Then, the formation of cracks takes place in the FLG induced weak regions at a higher density compared to neat HDPE, as shown in Figure 4.3. Interestingly, due to the photo-stabilizer role of FLG, these cracks remain local and arrested in this region near to the surface, preventing further propagation into the sample. Consequently, the degraded layer becomes isolated from the ductile core, allowing the composite to maintain a ductile behavior, even when degradation depth reached beyond 10 % of sample thickness. This is evident in the retained elongation curve of HDPE05-2mm, where a non-zero plateau indicates sustained ductility despite the effects of photo-degradation. This behavior was previously observed in photo-degradation of Polypropylene (PP)/talc system and contributed to the detachment of the degraded layer (Rabello and White 1996, 1997b, 1997c). Hence, the ability to maintain ductility and tendency to reach a non zero plateau, despite initial photo-degradation and cracks formation, achieved by isolating the degraded layer from the ductile core, correlates with the deviation from the superposition principle between the thickness of the exposed sample, UV exposure time when FLG containing composites compared to neat HDPE, as illustrated in Figure 4.7.

## 4.5 Conclusion

In this study, the effect of addition of FLG on photo-degradation depth of HDPE was investigated. Photo-degradation depth and chemi-crystallization that occurs across the sample was related to the tensile failure behavior, i.e. transition from ductile to brittle. The results showed that embrittlement occurred in 3 and 2 mm thick neat HDPE samples when photo-degradation depth reached 10% of the sample thickness, after 10 days of UV exposure. Notably, this embrittlement was observed in neat HDPE even before surface cracks formation. In contrast, HDPE containing 0.5 wt% FLG showed a ductile behavior, even at significantly higher UV dosage, up to 45 days of UV exposure. Interestingly, this sample maintained ductile behavior, even when photo-degradation depth reached beyond 10% of the sample thickness, and in the presence of surface cracks. This behaviour was attributed to the photo-stabilizing effect of FLG, as well as, to the fact that the degraded layer in this composite isolated from the remaining ductile core of the sample.

Additionally, a master curve was developed to predict retention at elongation at break of neat HDPE for different thicknesses as a function of UV dosage, normalized by the sample thickness. This result indicated that the superposition principle applies to the sample thickness, UV exposure time, and UV damage, meaning thinner samples undergo higher UV damage. However, incorporation of 0.5 wt% FLG resulted in a deviation from this principle. This deviation is most likely associated with FLG ability to preserve the ductility through localized surface damage and detachment of the degraded layer from the sample core.

In summary, incorporation of FLG into polymer composites promotes ductility retention, allowing the material to endure extended UV exposure without succumbing to embrittlement.

## CONCLUSION

In this section, the key findings of this PhD project are highlighted, and organized in the same sequence as their presentation in this thesis.

In the first part of this project, the FLG performance, as a photo-stabilizer for HDPE, was investigated. HDPE composites containing 0, 0.1, 0.25, and 0.5 wt% FLG were exposed to a UVA radiation in a QUV chamber, for different UV exposure times. The changes in chemical, rheological, and mechanical properties were tracked as a function of UV exposure time. It was found that:

- The addition of 0.25wt % and of higher concentrations of FLG into HDPE, effectively stabilized and inhibited HDPE photo-degradation. This led to an excellent retention in rheological and mechanical properties, even after 672 hours of UV exposure.

In order to separate identify the different photo-stabilizing mechanisms of graphene, its UV absorption/reflection ability and hydroxyl radical scavenging capacity, were investigated using UV-vis spectroscopy and EPR technique. A controlled procedure was employed to separate the contribution of these two mechanisms to FLG photo-stabilizing effect. It was found that:

- FLG incorporation into HDPE increased the composite's UV absorbance in entire range of 200-800 nm.
- UV transmittance showed a decrease with increasing FLG concentration. This was attributed to UV shielding properties of FLG, resulting from combination of FLG's UV absorption and reflection. In particular, the presence of  $\pi$  bonds in FLG structure can absorb UV radiation, and its large surface area can serve as an UV barrier.
- Addition of FLG into hydrogen peroxide mixture, effectively, resulted in a reduction in the amount of created hydroxyl radicals during UV exposure, evident from

decrement in characteristic EPR signal intensity. This finding was attributed to the both FLG's UV absorption/reflection, and hydroxyl radical scavenging mechanisms.

- To separate UV absorption/reflection and hydroxyl radical scavenging mechanisms, FLG aqueous suspensions were isolated from the mixture of hydrogen peroxide ( $H_2O_2$ ), while placing in the pathway of UV irradiation. It was shown that 57% of the reduction in EPR signal intensity was due to UV absorption/reflection and 43% due to hydroxyl radical scavenging mechanism.

Finally, the effect of FLG addition on photo-degradation penetration into HDPE was investigated. HDPE composites containing 0, 0.1, and 0.5 wt% FLG, with two thicknesses of 3 and 2 mm, were exposed to UV for several durations. The effective UV dosage and UV dosage per sample volume, corresponding to UV exposure times, were calculated based on the "Cumulative Damage Model". Elongation at break and failure zone were tracked as a function of UV exposure time and corresponding UV dosage. Photo-degradation depth, in which chemi-crystallization occurs, was investigated using Raman microscopy, and correlated to embrittlement, transition from ductile to brittle behavior. It was found that:

- In 3 mm thick HDPE, photo-degradation was an oxygen diffusion-controlled process in which chemi-crystallization and photo-degradation depth was confined to the first 500  $\mu m$  of the thickness. While chemi-crystallization and photo-degradation extended to the entire thickness of 2 mm thick HDPE, due to the appearance of big surface cracks facilitating oxygen diffusion.
- Addition of 0.5 wt% FLG into HDPE limited photo-degradation within 250  $\mu m$ , for both 3 and 2 mm thick samples, even after 45 days of UV exposure, indicating FLG photo-stabilizing effect.



- In HDPE and HDPE containing 0.1 wt% FLG, embrittlement happened when photo-degradation depth reached around 10 % of the sample thickness. This embrittlement occurred at low UV dosage, and even with no visible surface cracks.
- HDPE containing 0.5 wt% FLG maintained ductile behavior even when photo-degradation reached beyond 10 % of the composite thickness. This sample showed ductility even at higher UV dosage and in the presence of surface cracks. This tendency to maintain ductile behavior, despite photo-degradation effects, was contributed to the detachment of the degraded layer from ductile core of the composite.
- A master curve was developed to predict retention of elongation at break for neat HDPE as a function of UV dosage per sample volume, indicating superposition principle between sample thickness, UV exposure time, and UV damage.
- Incorporating 0.5wt% FLG led to a deviation from this principle. This deviation was attributed to the ability of FLG composite in maintaining ductility through detachment of degraded layer from ductile core of the composite.



## RECOMMENDATIONS

Similar to many research projects, there remains many opportunities for future investigation and developments in this field. The perspectives originated from this work emphasize the importance of continuing this research to develop our understanding of graphene performance and optimizing its role as a photo-stabilizer. Further exploring in this area may lead to unlock new insights for potential graphene-based materials applications, contributing to enhance the stability and longevity of diverse products and materials. Considering this, we propose the following recommendation for future researches:

- Since performance of graphene has, primarily, been evaluated in liquid state, it might be useful to explore its free radical scavenging effect within polymer matrix, in solid state. Conducting EPR test on polymer samples is quite challenging. It requires incorporating spin trapper to stabilize the created free radicals during photo-degradation. Overcoming these challenges could shed light on graphene's performance as a stabilizer in solid-state polymer matrices.
- It would be relevant to investigate the effect of FLG alignment on its UV absorption effect when UV exposure is parallel to the alignment direction.
- In this project only the photo-stabilizing effect of FLG has been evaluated, it would be relevant to explore the photo stabilizing effects of GO, and compare their performance to the one of FLG. Additionally, examining the compatibility between FLG/GO and the polymer matrix, along with assessing the dispersion effect on their mechanisms of action and photo-degradation rate, would be essential areas for analysis.
- In this project it was assumed that degradation initiates, completely, from the exposed surface and penetrates across the sample thickness. However, it is worth considering that degradation may also commence from the side surfaces. Therefore, investigating

the effect of sample width and penetration of photo-degradation within the sample could provide valuable insights to model life-time of products.

- We considered chemi-crystallization as the measure of photo-degradation depth within HDPE, using Raman microscopy. However, investigating alternative techniques such as Fourier Transform Infrared Spectroscopy (FTIR), to measure chemical products, as an indicator of photo-degradation depth within the sample, may lead to valuable insights. Employing the additional methods can enhance our understanding of the degradation processes occurring within the material.
- We found that chemi-crystallization was more pronounced in thinner samples suggesting a greater photo-degradation in those samples. Further Investigation into the orientation of polymer chains and FLG, induced by the injection molded process, on photo-degradation would provide more insights into the context.
- The provided master curve was developed using photo-degradation data of two different thicknesses. It may be relevant to take into account the data from at least one more thickness of HDPE, for a more comprehensive analysis. Furthermore, it can be beneficial to investigate the effect of thickness on the samples containing 0.1wt % graphene where photo-stabilization has not been achieved yet.
- Since retention of elongation at break of samples containing 0.5 wt% graphene did not reach zero plateau, it is recommended to increase exposure time to observe when this sample begin to show embrittlement. This may enable us to detect the point at which the detaching mechanism of degraded layer becomes inactive. This insight is beneficial for optimizing the durability and performance of graphene-containing materials under extended exposure conditions.

## ANNEX I

### SUPPLEMENTARY INFORMATION FOR ARTICLE 3

#### **Effect of Few-Layer Graphene (FLG) and Thickness on the Photo-Degradation Behavior of High-Density Polyethylene**

Samira Karimi<sup>1</sup>, Emna Helal<sup>1,2</sup>, Giovanna Gutierrez<sup>2</sup>, Nima Moghimian<sup>2</sup>, Eric David<sup>1</sup>, Tatiana Parra Vello<sup>3,4</sup>, Guilhermino José Macêdo Fechine<sup>3,4</sup> and Nicole Demarquette<sup>1\*</sup>

<sup>1</sup> Mechanical Engineering Department, École de Technologie Supérieure, 1100 Notre-Dame St W, Montréal, QC, Canada H3C 1K3

<sup>2</sup> NanoXplore Inc., 4500 Thimens Boulevard, Saint-Laurent, QC, Canada H4R 2P2

<sup>3</sup> Engineering School, Mackenzie Presbyterian University, São Paulo, SP, Brazil

<sup>4</sup> Mackenzie Institute of Research in Graphene and Nanotechnologies – MackGraphe, Mackenzie Presbyterian Institute, São Paulo, SP, Brazil

Paper submitted for publication, February 2024

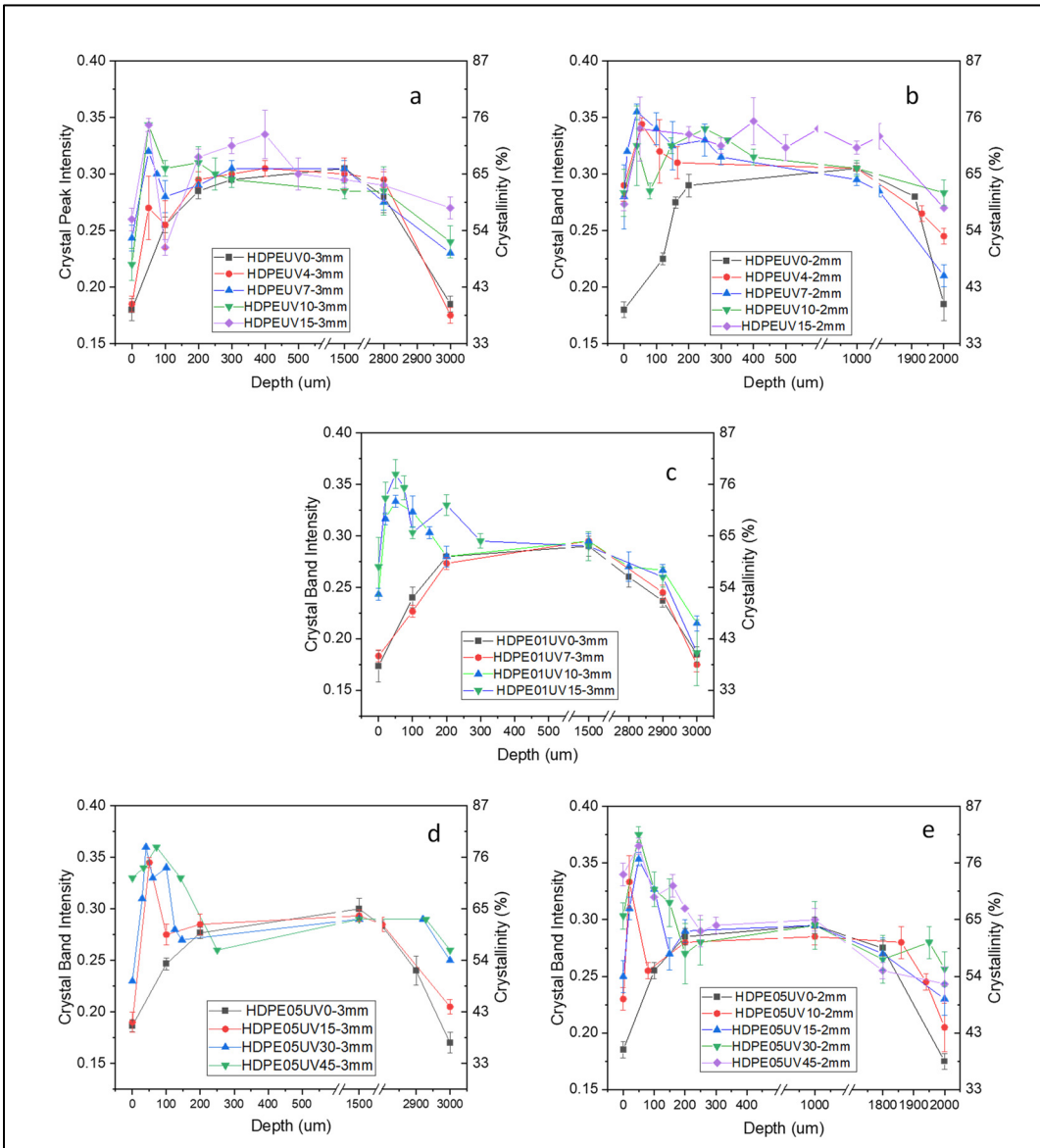


Figure A-I Crystal band intensity of: a-b) neat HDPE, c) HDPE01, d-e) HDPE05, with thicknesses of 3 and 2 mm as a function of sample depth, for different UV exposure times

## LIST OF BIBLIOGRAPHICAL REFERENCES

- Abdel-Bary, Elsayed M. 2003. *Handbook of plastic films* (iSmithers Rapra Publishing).
- Al-Maqdasi, Zainab, Liva Pupure, Guan Gong, Nazanin Emami, and Roberts Joffe. 2021. 'Time-dependent properties of graphene nanoplatelets reinforced high-density polyethylene', *Journal of applied polymer science*, 138: 50783.
- Allen, Matthew J, Vincent C Tung, and Richard B Kaner. 2010. 'Honeycomb carbon: a review of graphene', *Chemical reviews*, 110: 132-45.
- Allen, Norman S, Michele Edge, Amaya Ortega, Gonzalo Sandoval, Christopher M Liauw, Joanna Verran, John Stratton, and Robert B McIntyre. 2004. 'Degradation and stabilisation of polymers and coatings: nano versus pigmentary titania particles', *Polymer degradation and stability*, 85: 927-46.
- Allen, Norman S, and Alan Parkinson. 1982. 'Ultraviolet derivative absorption spectra of nylon 6, 6: Effect of photolysis versus photo-induced oxidation', *Polymer Degradation and Stability*, 4: 239-44.
- Allen, NS, and JF McKellar. 1975. 'Photodegradation and stabilization of commercial polyolefins', *Chemical Society Reviews*, 4: 533-47.
- Alotaibi, MD, AJ McKinley, BM Patterson, and AY Reeder. 2015a. 'Benzotriazoles in the aquatic environment: a review of their occurrence, toxicity, degradation and analysis', *Water, Air, & Soil Pollution*, 226: 226.
- Alotaibi, 2015. 'Benzotriazoles in the aquatic environment: a review of their occurrence, toxicity, degradation and analysis', *Water, Air, & Soil Pollution*, 226: 1-20.
- Amrollahi, S, B Ramezanzadeh, H Yari, M Ramezanzadeh, and M Mahdavian. 2019. 'In-situ growth of ceria nanoparticles on graphene oxide nanoplatelets to be used as a multifunctional (UV shield/radical scavenger/anticorrosive) hybrid compound for exterior coatings', *Progress in Organic Coatings*, 136: 105241.
- Andrady, Anthony L, Kara Lavender Law, Jessica Donohue, and Bimali Koongolla. 2022. 'Accelerated degradation of low-density polyethylene in air and in sea water', *Science of The Total Environment*, 811: 151368.
- Ashton, HE. 1970. 'Radiation and other weather factors.' in, *Canadian building digests 101-150*.

- Asimakopoulos, Alexandros G, Akinranti Ajibola, Kurunthachalam Kannan, and Nikolaos S Thomaidis. 2013. 'Occurrence and removal efficiencies of benzotriazoles and benzothiazoles in a wastewater treatment plant in Greece', *Science of The Total Environment*, 452: 163-71.
- Awaja, Firas, Shengnan Zhang, Manoj Tripathi, Anton Nikiforov, and Nicola Pugno. 2016. 'Cracks, microcracks and fracture in polymer structures: Formation, detection, autonomic repair', *Progress in Materials Science*, 83: 536-73.
- Bae, Sukang, Sang Jin Kim, Dolly Shin, Jong-Hyun Ahn, and Byung Hee Hong. 2012. 'Towards industrial applications of graphene electrodes', *Physica Scripta*, 2012: 014024.
- Bateman, L, and G Gee. 1948. 'A kinetic investigation of the photochemical oxidation of certain non-conjugated olefins', *Proceedings of the Royal Society of London. Series A. Mathematical and Physical Sciences*, 195: 376-91.
- Batista, Natassia L, Emna Helal, Rafael S Kurusu, Nima Moghimian, Eric David, Nicole R Demarquette, and Pascal Hubert. 2019. 'Mass-produced graphene—HDPE nanocomposites: thermal, rheological, electrical, and mechanical properties', *Polymer Engineering & Science*, 59: 675-82.
- Bertoldo, Monica, Simona Bronco, Chiara Cappelli, Tania Gragnoli, and Leonardo Andreotti. 2003. 'Combining theory and experiment to study the photooxidation of polyethylene and polypropylene', *The Journal of Physical Chemistry B*, 107: 11880-88.
- Bigger, Stephen W, and Oskar Delatycki. 1989a. 'The effect of hindered amine light stabilizers on the photooxidative stability of high-density polyethylene', *Journal of Polymer Science Part A: Polymer Chemistry*, 27: 63-73.
- Bigger, 1989. 'The effects of pigments on the photostability of polyethylene', *Journal of materials science*, 24: 1946-52.
- Bodur, Mehmet Safa, Mustafa Bakkal, and Hasret Ece Sonmez. 2018. 'A study on the photostabilizer additives on the textile fiber reinforced polymer composites: Mechanical, thermal, and physical analysis', *Polymer Engineering & Science*, 58: 1082-90.
- Brooks, NWJ, AP Unwin, RA Duckett, and IM Ward. 1995. 'Double yield points in polyethylene: Structural changes under tensile deformation', *Journal of Macromolecular Science, Part B: Physics*, 34: 29-54.
- Brusselle-Dupend, Nadège, and Laurent Cangémi. 2008. 'A two-phase model for the mechanical behaviour of semicrystalline polymers. Part I: Large strains multiaxial validation on HDPE', *Mechanics of Materials*, 40: 743-60.



- Bussière, Pierre-Olivier, Jérémy Peyroux, Geneviève Chadeyron, and Sandrine Therias. 2013. 'Influence of functional nanoparticles on the photostability of polymer materials: Recent progress and further applications', *Polymer Degradation and Stability*, 98: 2411-18.
- Chang, Kung-Chin, CH Hsu, HI Lu, WF Ji, CH Chang, WY Li, TL Chuang, JM Yeh, WR Liu, and MH Tsai. 2014. 'Advanced anticorrosive coatings prepared from electroactive polyimide/graphene nanocomposites with synergistic effects of redox catalytic capability and gas barrier properties', *Express Polymer Letters*, 8.
- Chaudhuri, Ishrat, Claudia Fruijtier-Pölloth, Yufanyi Ngiewih, and Len Levy. 2018. 'Evaluating the evidence on genotoxicity and reproductive toxicity of carbon black: a critical review', *Critical reviews in toxicology*, 48: 143-69.
- Choi, Wonbong, Indranil Lahiri, Raghunandan Seelaboyina, and Yong Soo Kang. 2010. 'Synthesis of graphene and its applications: a review', *Critical Reviews in Solid State and Materials Sciences*, 35: 52-71.
- Chowdhury, Indranil, Wen-Che Hou, David Goodwin, Matthew Henderson, Richard G Zepp, and Dermont Bouchard. 2015. 'Sunlight affects aggregation and deposition of graphene oxide in the aquatic environment', *Water research*, 78: 37-46.
- Çiplak, Zafer, Nuray Yildiz, and Ayla Çalimli. 2015. 'Investigation of graphene/Ag nanocomposites synthesis parameters for two different synthesis methods', *Fullerenes, Nanotubes and Carbon Nanostructures*, 23: 361-70.
- Claudé, B, L Gonon, V Verney, and JL Gardette. 2001. 'Consequences of photoageing on the durability of plastic glasses for automotive applications', *Polymer testing*, 20: 771-78.
- Craig, IH, and JR White. 2005. 'Crystallization and chemi-crystallization of recycled photodegraded polyethylenes', *Polymer Engineering & Science*, 45: 588-95.
- Craig, IH, JR White, and Phua Chai Kin. 2005. 'Crystallization and chemi-crystallization of recycled photo-degraded polypropylene', *Polymer*, 46: 505-12.
- Cui, Yanbin, SI Kundalwal, and S Kumar. 2016. 'Gas barrier performance of graphene/polymer nanocomposites', *Carbon*, 98: 313-33.
- Daglen, Bevin C, and David R Tyler. 2010. 'Photodegradable plastics: end-of-life design principles', *Green Chemistry Letters and Reviews*, 3: 69-82.
- Das, Subhasis, Tanmay Ghosh, Biswarup Satpati, Ambarish Sanyal, and Tanushree Bala. 2014. 'Keggin-lysine hybrid nanostructures in the shape modulation of gold', *Materials Research Express*, 1: 015007.

- Dash, GN, Satya R Pattanaik, and Sriyanka Behera. 2014. 'Graphene for electron devices: The panorama of a decade', *IEEE Journal of the Electron Devices Society*, 2: 77-104.
- de Moraes, Ana Carolina Mazarin, Patricia Fernanda Andrade, Andreia Fonseca de Faria, Mateus Batista Simões, Francisco Carlos Carneiro Soares Salomão, Eduardo Bedê Barros, Maria do Carmo Gonçalves, and Oswaldo Luiz Alves. 2015. 'Fabrication of transparent and ultraviolet shielding composite films based on graphene oxide and cellulose acetate', *Carbohydrate polymers*, 123: 217-27.
- de Oliveira, Yuri DC, Leice G Amurin, Fernanda CF Valim, Guilhermino JM Fachine, and Ricardo JE Andrade. 2019. 'The role of physical structure and morphology on the photodegradation behaviour of polypropylene-graphene oxide nanocomposites', *Polymer*, 176: 146-58.
- Demchenko, Alexander P. 2019. 'Excitons in Carbonic Nanostructures', *C—Journal of Carbon Research*, 5: 71.
- Deshoules, Quentin, Maelenn Le Gall, Catherine Dreanno, Mael Arhant, G Stoclet, Daniel Priour, and Pierre Yves Le Gac. 2021. 'Origin of embrittlement in Polyamide 6 induced by chemical degradations: Mechanisms and governing factors', *Polymer degradation and stability*, 191: 109657.
- Diallo, Abdou Khadri, Emna Helal, Giovanna Gutiérrez, Milad Madinehei, Éric David, Nicole Demarquette, and Nima Moghimian. 2022. 'Graphene: A multifunctional additive for sustainability', *Sustainable Materials and Technologies*: e00487.
- Du, Tingting, Adeyemi S Adeleye, Tong Zhang, Chuanjia Jiang, Min Zhang, Huihui Wang, Yao Li, Arturo A Keller, and Wei Chen. 2018. 'Influence of light wavelength on the photoactivity, physicochemical transformation, and fate of graphene oxide in aqueous media', *Environmental Science: Nano*, 5: 2590-603.
- Durmus, Haziret, Haluk Safak, H Zehra Akbas, and Gulnare Ahmetli. 2011. 'Optical properties of modified epoxy resin with various oxime derivatives in the UV-VIS spectral region', *Journal of applied polymer science*, 120: 1490-95.
- European chemicals agency. 2020. 'Candidate List of substances of very high concern for Authorisation'. <https://echa.europa.eu/candidate-list-table>
- Fadeel, Bengt, Cyrill Bussy, Sonia Merino, Ester Vázquez, Emmanuel Flahaut, Florence Mouchet, Lauris Evariste, Laury Gauthier, Antti J Koivisto, and Ulla Vogel. 2018. 'Safety assessment of graphene-based materials: focus on human health and the environment', *ACS nano*, 12: 10582-620.

- Fairbrother, Andrew, Hsiang-Chun Hsueh, Jae Hyun Kim, Deborah Jacobs, Lakesha Perry, David Goodwin, Christopher White, Stephanie Watson, and Li-Piin Sung. 2019. 'Temperature and light intensity effects on photodegradation of high-density polyethylene', *Polymer degradation and stability*, 165: 153-60.
- Fan, Xiaoqiang, and Liping Wang. 2015. 'Graphene with outstanding anti-irradiation capacity as multialkylated cyclopentanes additive toward space application', *Scientific reports*, 5: 12734.
- Fayolle, BCXALVJ, X Colin, L Audouin, and J Verdu. 2007. 'Mechanism of degradation induced embrittlement in polyethylene', *Polymer degradation and stability*, 92: 231-38.
- Fondriest Environmental. 2014. 'Solar Radiation & Photosynthetically Active Radiation'. <https://www.fondriest.com/environmental-measurements/parameters/weather/photosynthetically-active-radiation/>.
- Frasca, Daniele, Dietmar Schulze, Volker Wachtendorf, Bernd Krafft, Thomas Rybak, and Bernhard Schartel. 2016. 'Multilayer graphene/carbon black/chlorine isobutyl isoprene rubber nanocomposites', *Polymers*, 8: 95.
- Fu, Yanqing, Qiliang Wei, Gaixia Zhang, Yu Zhong, Nima Moghimian, Xin Tong, and Shuhui Sun. 2019. 'LiFePO<sub>4</sub>-graphene composites as high-performance cathodes for lithium-ion batteries: The impact of size and morphology of graphene', *Materials*, 12: 842.
- Gauthier, E, B Laycock, FJJ-M Cuoq, PJ Halley, and KA George. 2013. 'Correlation between chain microstructural changes and embrittlement of LLDPE-based films during photo- and thermo-oxidative degradation', *Polymer degradation and stability*, 98: 425-35.
- Geuskens, G. 1975. 'Photodegradation of polymers.' in, *Comprehensive Chemical Kinetics* (Elsevier).
- Ghasemi-Kahrizsangi, Ahmad, Jaber Neshati, Homeira Shariatpanahi, and Esmaeil Akbarinezhad. 2015. 'Improving the UV degradation resistance of epoxy coatings using modified carbon black nanoparticles', *Progress in Organic Coatings*, 85: 199-207.
- Gijsman, Pieter, Jan Hennekens, and Daan Tummers. 1993. 'The mechanism of action of hindered amine light stabilizers', *Polymer degradation and stability*, 39: 225-33.
- Goodwin Jr, David G, Trinny Lai, Yadong Lyu, Chen Yuan Lu, Alejandro Campos, Vytas Reipa, Tinh Nguyen, and Lipiin Sung. 2020. 'The impacts of moisture and ultraviolet light on the degradation of graphene oxide/polymer nanocomposites', *NanoImpact*, 19: 100249.

- Goodwin Jr, David G, Shih-Jia Shen, Yadong Lyu, Ronald Lankone, Ana C Barrios, Samir Kabir, François Perreault, Wendel Wohlleben, Tinh Nguyen, and Lipiin Sung. 2020. 'Graphene/polymer nanocomposite degradation by ultraviolet light: The effects of graphene nanofillers and their potential for release', *Polymer degradation and stability*, 182: 109365.
- Grause, Guido, Mei-Fang Chien, and Chihiro Inoue. 2020. 'Changes during the weathering of polyolefins', *Polymer degradation and stability*, 181: 109364.
- Grela, MA, MEJ Coronel, and AJ Colussi. 1996. 'Quantitative spin-trapping studies of weakly illuminated titanium dioxide sols. Implications for the mechanism of photocatalysis', *The Journal of Physical Chemistry*, 100: 16940-46.
- Grigoriadou, I, KM Paraskevopoulos, K Chrissafis, E Pavlidou, T-G Stamkopoulos, and D Bikiaris. 2011. 'Effect of different nanoparticles on HDPE UV stability', *Polymer degradation and stability*, 96: 151-63.
- Gulmine, JV, PR Janissek, HM Heise, and L Akcelrud. 2003. 'Degradation profile of polyethylene after artificial accelerated weathering', *Polymer degradation and stability*, 79: 385-97.
- Han, Dongxiao, Zhaoguo Meng, Daxiong Wu, Canying Zhang, and Haitao Zhu. 2011. 'Thermal properties of carbon black aqueous nanofluids for solar absorption', *Nanoscale research letters*, 6: 1-7.
- Hasan, Mudassir, Rajeev Kumar, MA Barakat, and Moonyong Lee. 2015. 'Synthesis of PVC/CNT nanocomposite fibers using a simple deposition technique for the application of Alizarin Red S (ARS) removal', *RSC Advances*, 5: 14393-99.
- Hasani, M, M Mahdavian, H Yari, and B Ramezanzadeh. 2018. 'Versatile protection of exterior coatings by the aid of graphene oxide nano-sheets; comparison with conventional UV absorbers', *Progress in Organic Coatings*, 116: 90-101.
- Helal, Emna, Rafael S Kurusu, Nima Moghimian, Giovanna Gutierrez, Eric David, and Nicole R Demarquette. 2019. 'Correlation between morphology, rheological behavior, and electrical behavior of conductive cocontinuous LLDPE/EVA blends containing commercial graphene nanoplatelets', *Journal of Rheology*, 63: 961-76.
- Hiejima, Yusuke, Takumitsu Kida, Kento Takeda, Toshio Igarashi, and Koh-hei Nitta. 2018. 'Microscopic structural changes during photodegradation of low-density polyethylene detected by Raman spectroscopy', *Polymer degradation and stability*, 150: 67-72.
- Horrocks, A Richard, and Mingguang Liu. 2003. "UV stabilising synergies between carbon black and hindered light stabilisers in linear low density polyethylene films." In *Macromolecular Symposia*, 199-220. Wiley Online Library.

- Horrocks, AR, J Mwila, M Mirafteb, M Liu, and SS Chohan. 1999. 'The influence of carbon black on properties of orientated polypropylene 2. Thermal and photodegradation', *Polymer degradation and stability*, 65: 25-36.
- Hsu, Yu-Chieh, Michael P Weir, Rowan W Truss, Christopher J Garvey, Timothy M Nicholson, and Peter J Halley. 2012. 'A fundamental study on photo-oxidative degradation of linear low density polyethylene films at embrittlement', *Polymer*, 53: 2385-93.
- Hsueh, Hsiang-Chun, Jae Hyun Kim, Sara Orski, Andrew Fairbrother, Deborah Jacobs, Lakesha Perry, Donald Hunston, Christopher White, and Lipiin Sung. 2020. 'Micro and macroscopic mechanical behaviors of high-density polyethylene under UV irradiation and temperature', *Polymer degradation and stability*, 174: 109098.
- Hussein, Ibelwaleed A. 2007. 'Rheological investigation of the influence of molecular structure on natural and accelerated UV degradation of linear low density polyethylene', *Polymer degradation and stability*, 92: 2026-32.
- Jan.F. Rabek. 1995. *Polymer photodegradation: mechanisms and experimental methods* (Chapman & Hall).
- Javadi, Younes, Mahdi Salami Hosseini, and Mir Karim Razavi Aghjeh. 2014. 'The effect of carbon black and HALS hybrid systems on the UV stability of high-density polyethylene (HDPE)', *Iranian Polymer Journal*, 23: 793-99.
- Johra, Fatima Tuz, Jee-Wook Lee, and Woo-Gwang Jung. 2014. 'Facile and safe graphene preparation on solution based platform', *Journal of Industrial and Engineering Chemistry*, 20: 2883-87.
- Junior, José Carlos Ferreira, Nima Moghimian, Giovanna Gutiérrez, Emna Helal, Abdellah Ajjji, Guilherme Mariz de Oliveira Barra, and Nicole R Demarquette. 2022. 'Effects of an industrial graphene grade and surface finishing on water and oxygen permeability, electrical conductivity, and mechanical properties of high-density polyethylene (HDPE) multilayered cast films', *Materials Today Communications*, 31: 103470.
- Kalaitzidou, Kyriaki, Hiroyuki Fukushima, and Lawrence T Drzal. 2007. 'Multifunctional polypropylene composites produced by incorporation of exfoliated graphite nanoplatelets', *Carbon*, 45: 1446-52.
- Kamal, Musa R, and Francis H Moy. 1983. 'Microstructural characterization of injection-molded articles', *Journal of applied polymer science*, 28: 1787-804.

- Kamweru, P Kuria, F Gichuki Ndiritu, T Kinyanjui, Z Wanjiku Muthui, R Gichuki Ngumbu, and P Migunde Odhiambo. 2014. 'UV absorption and dynamic mechanical analysis of polyethylene films', *International Journal of Physical Sciences*, 9: 545-55.
- Karimi, Samira, Ismaeil Ghasemi, and Foroud Abbassi-Sourki. 2019. 'A study on the crystallization kinetics of PLLA in the presence of Graphene Oxide and PEG-grafted-Graphene Oxide: Effects on the nucleation and chain mobility', *Composites Part B: Engineering*, 158: 302-10.
- Karimi, Samira, Ismaeil Ghasemi, Foroud Abbassi-Sourki, Mazen Samara, and Nicole R Demarquette. 2022. 'PEG-Grafted graphene/PLLA nanocomposites: Effect of PEG chain length on crystallization kinetics of PLLA', *ACS omega*, 7: 31197-204.
- Karimi, Samira, Emna Helal, Giovanna Gutierrez, Nima Moghimian, Eric David, Mazen Samara, and Nicole Demarquette. 2023. 'Photo-stabilization mechanisms of High-Density Polyethylene (HDPE) by a commercial few-layer graphene', *Polymer Engineering & Science*, 63: 3879-90.
- Karimi, Samira, Emna Helal, Giovanna Gutierrez, Nima Moghimian, Milad Madinehei, Eric David, Mazen Samara, and Nicole Demarquette. 2020. 'A review on graphene's light stabilizing effects for reduced photodegradation of polymers', *Crystals*, 11: 3.
- Klonos, Panagiotis, Sotiria Kriptomou, Apostolos Kyritsis, George Z Papageorgiou, Dimitrios Bikiaris, Dimitrios Gournis, and Polycarpos Pissis. 2015. 'Glass transition and segmental dynamics in poly (l-lactic acid)/graphene oxide nanocomposites', *Thermochimica Acta*, 617: 44-53.
- Kockler, Jutta, Michael Oelgemöller, Sherryl Robertson, and Beverley D Glass. 2014. 'Influence of titanium dioxide particle size on the photostability of the chemical UV-filters butyl methoxy dibenzoylmethane and octocrylene in a microemulsion', *Cosmetics*, 1: 128-39.
- Kolanthai, Elayaraja, Suryasarathi Bose, KS Bhagyashree, SV Bhat, K Asokan, D Kanjilal, and Kaushik Chatterjee. 2015. 'Graphene scavenges free radicals to synergistically enhance structural properties in a gamma-irradiated polyethylene composite through enhanced interfacial interactions', *Physical Chemistry Chemical Physics*, 17: 22900-10.
- Krishnamoorthy, Karthikeyan, Gui-Shik Kim, and Sang Jae Kim. 2013. 'Graphene nanosheets: Ultrasound assisted synthesis and characterization', *Ultrasonics sonochemistry*, 20: 644-49.
- Kumar, Annamalai Pratheep, Dilip Depan, Namrata Singh Tomer, and Raj Pal Singh. 2009. 'Nanoscale particles for polymer degradation and stabilization—trends and future perspectives', *Progress in polymer science*, 34: 479-515.

- Kusk, Kresten Ole, Manola Avdolli, and Leah Wollenberger. 2011. 'Effect of 2, 4-dihydroxybenzophenone (BP1) on early life-stage development of the marine copepod *Acartia tonsa* at different temperatures and salinities', *Environmental toxicology and chemistry*, 30: 959-66.
- Lee, Changgu, Xiaoding Wei, Jeffrey W Kysar, and James Hone. 2008. 'Measurement of the elastic properties and intrinsic strength of monolayer graphene', *science*, 321: 385-88.
- Lee, Seungae, Jin-Yong Hong, and Jyongsik Jang. 2013. 'The effect of graphene nanofiller on the crystallization behavior and mechanical properties of poly (vinyl alcohol)', *Polymer international*, 62: 901-08.
- Li, Tong, Chunlin Zhou, and Ming Jiang. 1991. 'UV absorption spectra of polystyrene', *Polymer Bulletin*, 25: 211-16.
- Lin, L, and AS Argon. 1994. 'Structure and plastic deformation of polyethylene', *Journal of materials science*, 29: 294-323.
- Lin, W, M Cossar, V Dang, and J Teh. 2007. 'The application of Raman spectroscopy to three-phase characterization of polyethylene crystallinity', *Polymer testing*, 26: 814-21.
- Liu, M, and AR Horrocks. 2002. 'Effect of carbon black on UV stability of LLDPE films under artificial weathering conditions', *Polymer Degradation and Stability*, 75: 485-99.
- Lu, T, E Solis-Ramos, Y Yi, and M Kumosa. 2018. 'UV degradation model for polymers and polymer matrix composites', *Polymer degradation and stability*, 154: 203-10.
- Mahendia, Suman, Geeta Kandhol, Uday P Deshpande, and Shyam Kumar. 2016. 'Determination of glass transition temperature of reduced graphene oxide-poly (vinyl alcohol) composites using temperature dependent Fourier transform infrared spectroscopy', *Journal of Molecular Structure*, 1111: 46-54.
- Mak, Kin Fai, Long Ju, Feng Wang, and Tony F Heinz. 2012. 'Optical spectroscopy of graphene: From the far infrared to the ultraviolet', *Solid State Communications*, 152: 1341-49.
- Martin, Jonathan W. 1993. 'Quantitative characterization of spectral ultraviolet radiation-induced photodegradation in coating systems exposed in the laboratory and the field', *Progress in Organic Coatings*, 23: 49-70.
- Martin, Jonathan W, Tinh Nguyen, Eric Byrd, Brian Dickens, and Ned Embree. 2002. 'Relating laboratory and outdoor exposures of acrylic melamine coatings: I. Cumulative damage model and laboratory exposure apparatus', *Polymer degradation and stability*, 75: 193-210.

- Martínez, Ana, and Annia Galano. 2010. 'Free radical scavenging activity of ultrashort single-walled carbon nanotubes with different structures through electron transfer reactions', *The Journal of Physical Chemistry C*, 114: 8184-91.
- Mistretta, MC, L Botta, AD Vinci, M Ceraulo, and FP La Mantia. 2019. 'Photo-oxidation of polypropylene/graphene nanoplatelets composites', *Polymer degradation and stability*, 160: 35-43.
- Mittal, Vikas, and Fakhruddin Patwary. 2016. 'Polypropylene nanocomposites with oxo-degradable pro-oxidant: Mechanical, thermal, rheological, and photo-degradation performance', *Polymer Engineering & Science*, 56: 1229-39.
- Moghimian, Nima, and Soroush Nazarpour. 2020. 'The future of carbon: an update on graphene's dermal, inhalation, and gene toxicity', *Crystals*, 10: 718.
- Moghimian, Nima, Sajjad Saeidlou, Helen Lentzakis, Gian Flippo Rosi, Naiheng Song, and Éric David. 2017. "Electrical conductivity of commercial graphene polyethylene nanocomposites." In *2017 IEEE 17th International Conference on Nanotechnology (IEEE-NANO)*, 757-61. IEEE.
- Mohamed, Riham R. 2015. 'Photostabilization of Polymers'.
- Moon, Young-E, Ju-Mi Yun, Hyung-II Kim, and Young-Seak Lee. 2011. 'Effect of graphite oxide on photodegradation behavior of poly (vinyl alcohol)/graphite oxide composite hydrogels', *Carbon letters*, 12: 138-42.
- Moreno-Serna, Viviana, Matias Ubilla, Lissette Montoille, Marcela Saavedra, Teresa Corrales, Lisa Muñoz, and Paula A Zapata. 2023. 'Influence of Modified SiO<sub>2</sub> Nanoparticles on the Photostability of Recycled HDPE', *Journal of Polymers and the Environment*: 1-14.
- Morlat-Therias, Sandrine, Elisabeth Fanton, Jean-Luc Gardette, Sophie Peeterbroeck, Michael Alexandre, and Philippe Dubois. 2007. 'Polymer/carbon nanotube nanocomposites: influence of carbon nanotubes on EVA photodegradation', *Polymer degradation and stability*, 92: 1873-82.
- Najafi, Ebrahim, and Kwanwoo Shin. 2005. 'Radiation resistant polymer-carbon nanotube nanocomposite thin films', *Colloids and Surfaces A: Physicochemical and Engineering Aspects*, 257: 333-37.
- Nikafshar, Saeid, Omid Zabihi, Mojtaba Ahmadi, Abdolreza Mirmohseni, Mojtaba Taseidifar, and Mino Naebe. 2017. 'The effects of UV light on the chemical and mechanical properties of a transparent epoxy-diamine system in the presence of an organic UV absorber', *Materials*, 10: 180.



- Nikolov, S, RA Lebensohn, and D Raabe. 2006. 'Self-consistent modeling of large plastic deformation, texture and morphology evolution in semi-crystalline polymers', *Journal of the Mechanics and Physics of Solids*, 54: 1350-75.
- Nitta, Koh-hei, and Mizue Kuriyagawa. 2012. 'Application of catastrophe theory to neck initiation of metallocene-catalyzed high-density polyethylene', *Polymer journal*, 44: 245-51.
- Nuraje, Nurxat, Shifath I Khan, Heath Misak, and Ramazan Asmatulu. 2013a. 'The addition of graphene to polymer coatings for improved weathering', *ISRN Polymer Science*, 2013.
- Ouchi, Isume, Ryo Miyamura, Makoto Sakaguchi, Shuuhei Hosaka, and Masahiko Kitagawa. 1999. 'Excitation and emission spectra of polyethylene terephthalate and polyethylene 2, 6-naphthalate films', *Polymers for Advanced Technologies*, 10: 195-98.
- Padrón, Alfonso J Chirinos. 1989. 'Mechanistic aspects of polymer photostabilization', *Journal of Photochemistry and Photobiology A: Chemistry*, 49: 1-39.
- Pascal Xanthopoulos. 2019. 'Light Stabilizers/UV Absorbers for Polymers '. <https://polymer-additives.specialchem.com/selection-guide/light-uv-stabilizers-selection-for-polymers>.
- Pawlak, Andrzej. 2007. 'Cavitation during tensile deformation of high-density polyethylene', *Polymer*, 48: 1397-409.
- Peña, JM, NS Allen, M Edge, CM Liauw, I Roberts, and B Valange. 2000. 'Triplet quenching and antioxidant effect of several carbon black grades in the photodegradation of LDPE doped with benzophenone as a photosensitiser', *Polymer degradation and stability*, 70: 437-54.
- Peterlin, A. 1971. 'Molecular model of drawing polyethylene and polypropylene', *Journal of materials science*, 6: 490-508.
- Prosheva, Marija, Mohammad Ali Aboudzadeh, Gracia Patricia Leal, Jadranka Blazhevskia Gilev, and Radmila Tomovska. 2019. 'High-Performance UV Protective Waterborne Polymer Coatings Based on Hybrid Graphene/Carbon Nanotube Radicals Scavenging Filler', *Particle & Particle Systems Characterization*, 36: 1800555.
- Qiu, Yang, Zhongying Wang, Alisa CE Owens, Indrek Kulaots, Yantao Chen, Agnes B Kane, and Robert H Hurt. 2014. 'Antioxidant chemistry of graphene-based materials and its role in oxidation protection technology', *Nanoscale*, 6: 11744-55.

- Qu, Lijun, Mingwei Tian, Xili Hu, Yujiao Wang, Shifeng Zhu, Xiaoqing Guo, Guangting Han, Xiansheng Zhang, Kaikai Sun, and Xiaoning Tang. 2014. 'Functionalization of cotton fabric at low graphene nanoplate content for ultrastrong ultraviolet blocking', *Carbon*, 80: 565-74.
- Raad, Ruqaya, and Mustafa Abdallah. 2022. 'Surface modification to enhance photo-stability of polymers', *GSC Advanced Research and Reviews*, 11: 080-88.
- Rabek, Jan F. 2012. *Polymer photodegradation: mechanisms and experimental methods* (Springer Science & Business Media).
- Rabello, MS, and JR White. 1996. 'Photodegradation of talc-filled polypropylene', *Polymer composites*, 17: 691-704.
- Rabello, J. White. 1997. 'Crystallization and melting behaviour of photodegraded polypropylene—I. Chemi-crystallization', *Polymer*, 38: 6379-87.
- Rabello, J. White. 1997. 'Photodegradation of polypropylene containing a nucleating agent', *Journal of applied polymer science*, 64: 2505-17.
- Rabello, J. White. 1997. 'The role of physical structure and morphology in the photodegradation behaviour of polypropylene', *Polymer degradation and stability*, 56: 55-73.
- Ran, Chenxin, Minqiang Wang, Weiyin Gao, Jijun Ding, Yanhua Shi, Xiaohui Song, Haowei Chen, and Zhaoyu Ren. 2012. 'Study on photoluminescence quenching and photostability enhancement of MEH-PPV by reduced graphene oxide', *The Journal of Physical Chemistry C*, 116: 23053-60.
- Rånby, Bengt. 1989. 'Photodegradation and photo-oxidation of synthetic polymers', *Journal of Analytical and Applied Pyrolysis*, 15: 237-47.
- Randviir, Edward P, Dale AC Brownson, and Craig E Banks. 2014. 'A decade of graphene research: production, applications and outlook', *Materials Today*, 17: 426-32.
- Reano, Armando F, Alain Guinault, Emmanuel Richaud, and Bruno Fayolle. 2018. 'Polyethylene loss of ductility during oxidation: Effect of initial molar mass distribution', *Polymer degradation and stability*, 149: 78-84.
- Reiß, Thomas, Kari Hjelt, and Andrea C Ferrari. 2019. 'Graphene is on track to deliver on its promises', *Nature nanotechnology*, 14: 907-10.
- Rodriguez, Ana K, Bilal Mansoor, Georges Ayoub, Xavier Colin, and Amine A Benzerga. 2020. 'Effect of UV-aging on the mechanical and fracture behavior of low density polyethylene', *Polymer degradation and stability*, 180: 109185.

- Rozanski, Artur, and Andrzej Galeski. 2013. 'Plastic yielding of semicrystalline polymers affected by amorphous phase', *International journal of plasticity*, 41: 14-29.
- Sanchez, Vanesa C, Ashish Jachak, Robert H Hurt, and Agnes B Kane. 2012. 'Biological interactions of graphene-family nanomaterials: an interdisciplinary review', *Chemical research in toxicology*, 25: 15-34.
- Séguéla, Roland. 2007. 'On the natural draw ratio of semi-crystalline polymers: review of the mechanical, physical and molecular aspects', *Macromolecular Materials and Engineering*, 292: 235-44.
- Serenari, Federico, Milad Madinehei, Nima Moghimian, Davide Fabiani, and Eric David. 2020. 'Development of reinforced polyester/graphene nanocomposite showing tailored electrical conductivity', *Polymers*, 12: 2358.
- Shams, Mehnaz, Linda M Guiney, Lijuan Huang, Mani Ramesh, Xiaoning Yang, Mark C Hersam, and Indranil Chowdhury. 2019. 'Influence of functional groups on the degradation of graphene oxide nanomaterials', *Environmental Science: Nano*, 6: 2203-14.
- Shehzad, F, MI Ahmad, and MA Al-Harhi. 2019. 'Photooxidative degradation of graphene-reinforced high-density polyethylene nanocomposites', *Journal of Applied Polymer Science*, 136: 47030.
- Shyichuk, AV, JR White, IH Craig, and ID Syrotynska. 2005. 'Comparison of UV-degradation depth-profiles in polyethylene, polypropylene and an ethylene-propylene copolymer', *Polymer degradation and stability*, 88: 415-19.
- Smijs, Threes G, and Stanislav Pavel. 2011. 'Titanium dioxide and zinc oxide nanoparticles in sunscreens: focus on their safety and effectiveness', *Nanotechnology, science and applications*, 4: 95.
- So, Ying-Hung. 2006. 'Photodegradation mechanism and stabilization of polyphenylene oxide and rigid-rod polymers', *Polymer international*, 55: 127-38.
- Soldano, Caterina, Ather Mahmood, and Erik Dujardin. 2010. 'Production, properties and potential of graphene', *Carbon*, 48: 2127-50.
- Stark, Nicole M, and Laurent M Matuana. 2004. 'Surface chemistry changes of weathered HDPE/wood-flour composites studied by XPS and FTIR spectroscopy', *Polymer degradation and stability*, 86: 1-9.

- Strobel, AF, and SC Catino. 1962. 'Relationship between ultraviolet absorber structural types and photostabilization of plastics', *Industrial & Engineering Chemistry Product Research and Development*, 1: 241-48.
- Tarcan, Raluca, Otto Todor-Boer, Ioan Petrovai, Cosmin Leordean, Simion Astilean, and Ioan Botiz. 2020. 'Reduced graphene oxide today', *Journal of Materials Chemistry C*, 8: 1198-224.
- Tayouri, Mohammad Iman, Sara Estaji, Seyed Rasoul Mousavi, Samaneh Salkhi Khasraghi, Reza Jahanmardi, Sasan Nouranian, Mohammad Arjmand, and Hossein Ali Khonakdar. 2022. 'Degradation of polymer nanocomposites filled with graphene oxide and reduced graphene oxide nanoparticles: A review of current status', *Polymer degradation and stability*: 110179.
- Terrones, Mauricio, Olga Martín, María González, Javier Pozuelo, Berna Serrano, Juan C Cabanelas, Sofia M Vega-Díaz, and Juan Baselga. 2011. 'Interphases in graphene polymer-based nanocomposites: achievements and challenges', *Advanced Materials*, 23: 5302-10.
- Tian, Mingwei, Zongqian Wang, Lijun Qu, Ke Wang, Shifeng Zhu, Xiansheng Zhang, and Ruichao Liu. 2018. 'Enhanced UV photo-stabilization of Nylon 6 filament with reduced graphene oxide/polyurethane nanocomposite Inks', *International Journal of Clothing Science and Technology*.
- Tipton, David A, and J West Lewis. 2008. 'Effects of a hindered amine light stabilizer and a UV light absorber used in maxillofacial elastomers on human gingival epithelial cells and fibroblasts', *The Journal of prosthetic dentistry*, 100: 220-31.
- Tsai, Perng-Jy, Hong-Yong Shieh, Lien-Te Hsieh, and Wen-Jhy Lee. 2001. 'The fate of PAHs in the carbon black manufacturing process', *Atmospheric Environment*, 35: 3495-501.
- Turton, TJ, and JR White. 2001. 'Effect of stabilizer and pigment on photo-degradation depth profiles in polypropylene', *Polymer degradation and stability*, 74: 559-68.
- Uran, S, A Alhani, and C Silva. 2017. 'Study of ultraviolet-visible light absorbance of exfoliated graphite forms', *AIP Advances*, 7.
- Wagner, Manfred Hermann, Wang Zheng, Peng Wang, Sebastián Ramos Talamante, and Esmaeil Narimissa. 2017. "Shear and elongational rheology of photo-oxidative degraded HDPE and LLDPE." In *AIP Conference Proceedings*, 030005. AIP Publishing LLC.
- Wang, Yingmin, Wenhui Kong, Lifeng Wang, Jin Zhong Zhang, Yan Li, Xiaoguang Liu, and Yong Li. 2019. 'Optimizing oxygen functional groups in graphene quantum dots for improved antioxidant mechanism', *Physical Chemistry Chemical Physics*, 21: 1336-43.

- White, JR, and A Turnbull. 1994. 'Weathering of polymers: mechanisms of degradation and stabilization, testing strategies and modelling', *Journal of materials science*, 29: 584-613.
- Wiles, DM, and DJ Carlsson. 1980. 'Photostabilisation mechanisms in polymers: A review', *Polymer degradation and stability*, 3: 61-72.
- Wu, HW, A Emadi, G De Graaf, Johan Leijtens, and RF Wolffenbuttel. 2011. 'Design and fabrication of an albedo insensitive analog sun sensor', *Procedia Engineering*, 25: 527-30.
- Xue, Qingzhong, Cheng Lv, Meixia Shan, Hongxin Zhang, Cuicui Ling, Xiaoyan Zhou, and Zhiyong Jiao. 2013. 'Glass transition temperature of functionalized graphene-polymer composites', *Computational materials science*, 71: 66-71.
- Yakimets, Iryna, Dawei Lai, and Michèle Guigon. 2004. 'Effect of photo-oxidation cracks on behaviour of thick polypropylene samples', *Polymer degradation and stability*, 86: 59-67.
- Yoo, Byung Min, Hye Jin Shin, Hee Wook Yoon, and Ho Bum Park. 2014. 'Graphene and graphene oxide and their uses in barrier polymers', *Journal of applied polymer science*, 131.
- Yousif, Emad, and Raghad Haddad. 2013. 'Photodegradation and photostabilization of polymers, especially polystyrene', *SpringerPlus*, 2: 1-32.
- Yousif, Emad, and Ali Hasan. 2015. 'Photostabilization of poly (vinyl chloride)-Still on the run', *Journal of Taibah University for Science*, 9: 421-48.
- Zepp, Richard, Emmanuel Ruggiero, Brad Acrey, Mary JB Davis, Changseok Han, Hsin-Se Hsieh, Klaus Vilsmeier, Wendel Wohlleben, and Endalkachew Sahle-Demessie. 2020. 'Fragmentation of polymer nanocomposites: modulation by dry and wet weathering, fractionation, and nanomaterial filler', *Environmental Science: Nano*.
- Zhao, Songmei, Fenghua Chen, Yingjuan Huang, Jin-Yong Dong, and Charles C Han. 2014. 'Crystallization behaviors in the isotactic polypropylene/graphene composites', *Polymer*, 55: 4125-35.
- Zweifel, Hans. 1999. "Stabilization of polymeric materials." In *Annales de chimie-Sciences des matériaux*, 401.